UNIVERSITÀ DEGLI STUDI DELL'AQUILA

DIPARTIMENTO DI SCIENZE FISICHE E CHIMICHE

Dottorato di Ricerca in Scienze fisiche e chimiche

XXXV ciclo

Titolo della tesi

New Catalysts for the Synthesis of Green Diesel by Deoxygenation of Vegetable oils

SSD CHIM/07

Dottorando

Di Vito Nolfi Giuseppe

Coordinatore del corso

Prof. Aschi Massimiliano

Tutor

Prof. Rossi Leucio

a.a. 2021/2022

Summary

List of acronyms

AC	Activated Carbon
AOAC	Association of Official Agricultural Chemists
ASTM	American Society for testing and materials
ATR	Attenuated Total Reflection
BEA	Beta Zeolite
BET	Brunauer-Emmett-Teller
BJH	Barrett-Joyner-Halenda
CDO	Catalytic Deoxygenation
CFA	Coal Fly Ash
COP	Conference of the Parties
DCO	Decarbonilation
DCO_2	Decarboxylation
DFT	Density Functional Theory
EN	European norm
EU	European Union
FAC	Fly Ash Cenosphere
FAME	Fatty Acid Methyl Ester
FT-IR	Fourier-transform infrared spectroscopy
GHGs	Greenhouse gases
HC	Unburned Carbon
HDO	Hydrodeoxygenation
HDS	Hydrodesulfurization
HVO	Hydrotreated Vegetable Oil

ICP-MS	Inductively Coupled Plasma-Mass Spectrometry
IUPAC	International Union of Pure and Applied Chemistry
LDH	Layered Double Hydroxides
LHV	Lower Heating Value
MCM	Mobil Composition of Matter
OECD	Organization for Economic Co-operation and Development
OLP	Organic Liquid Product
OMA	Organized Mesoporous Alumina
PM	Particulate matter
SAPO	Silicoaluminophosphate
SBA	Santa Barbara Amorphous
TOF	Turnover Frequency
UNFCCC	United Nations Framework Convention on Climate Change
USY	Ultrastable Zeolite Y
VOCs	Volatile Organic Compound
XRD	X-Ray Diffraction
ZSM-5	Zeolite Socony-Mobil

Abstract of the PhD thesis.

As part of the Ph.D. research work, the project presented in this Thesis is focused on the topic of renewable energy, in particular on the development of new catalysts for the catalytic deoxygenation reaction of vegetable oils for green diesel synthesis (a biofuel with the potential to replace mineral diesel).

One of the greatest challenges of the modern era is global warming, mostly related to the increase in the atmospheric concentration of greenhouse gases (mainly CO_2) caused by the overexploitation of fossil fuels by mankind. To avoid the further worsening of global warming, one of the major worldwide goals is to achieve carbon neutrality (i.e., net-zero carbon dioxide emissions) as soon as possible; to do so, the energy transition from non-renewable to renewable energy must first prioritized.

The transportation sector is one of the sectors with the highest fossil fuel consumption, contributing significantly to CO_2 emissions. In this sense, to help achieving carbon neutrality, newer and greener alternatives to be used as fuels must be found. Biofuels, defined as fuels which are environmentally friendly, biodegradable, non-toxic, and biomass-derived, are a valuable alternative to fossil fuels, especially because they are renewable, carbon neutral in nature, and prone to a lesser generation of emissions, including other pollutants such as SO_x and NO_x.

One of the most widely used fuels is biodiesel, also called FAME (fatty acid methyl esters), which is obtained from the transesterification reaction of vegetable oils. It is widely used commercially but cannot fully replace mineral diesel as it has several disadvantages, such as high oxygen, low heating value, lower cloud point, high corrosivity, and poor thermal and chemical stability. A better alternative to biodiesel is green diesel, a biofuel consisting

exclusively of hydrocarbons (mainly in the C_{15}-C_{18} range) and thus chemically similar to petroleum derivatives.

Green diesel is obtained by catalytic deoxygenation (CDO) reaction of vegetable oils, a thermal process performed mainly in a hydrogen atmosphere and with heterogeneous catalysts. During the reaction, fatty acid triglycerides are converted to hydrocarbons (having either the same number or one carbon atom less than the starting fatty acid) through three main reaction pathways: hydrodeoxygenation (HDO), decarbonylation (DCO), and decarboxylation (DCO_2). Once obtained, the hydrocarbons mixture undergoes hydroisomerization processes to improve the cold properties of the biofuel. After this, green diesel is suitable to be used as a fuel.

Compared to biodiesel, green diesel can be mixed in any proportion with petroleum-derived diesel, has higher heating value and cetane number, and lower cloud point; in addition, it can be produced using existing infrastructure (Figure 1).

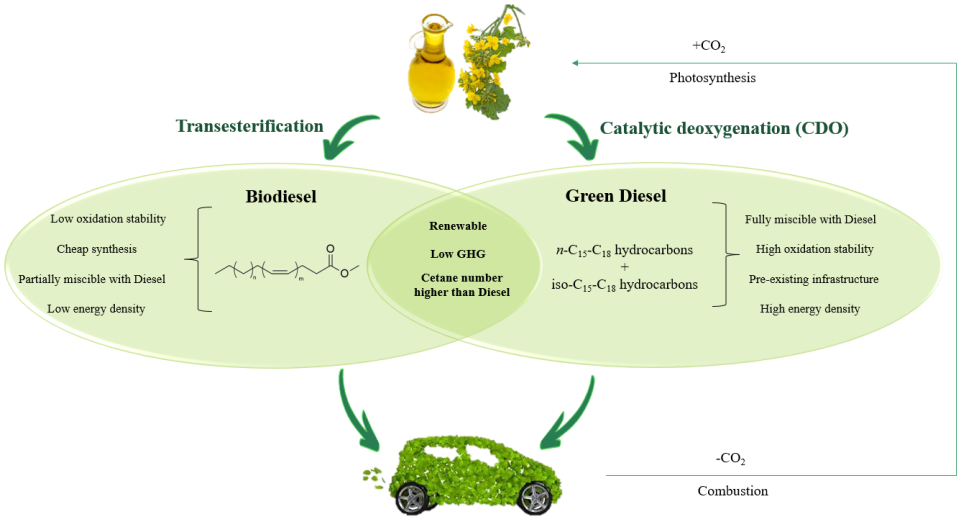

Figure 1. Schematic comparison between biodiesel and green diesel.

Currently, the synthesis of green diesel involves high temperatures and pressures; in addition, uses noble metal-based catalysts (expensive) or sulfided catalysts, which have the disadvantage of polluting the green diesel produced with sulfur. Therefore, the challenge set in this research work was to synthesize and test inexpensive and green catalysts to promote the catalytic deoxygenation reaction as efficiently as possible (thus active at the mildest possible conditions). In addition, as stated before, the industrial production of green diesel involves two reaction steps, a hydrotreating step that leads to the formation of linear hydrocarbons (producing a biofuel with a high cloud point) and a second hydroisomerization step that produces branching hydrocarbons resulting in a biofuel with better cold properties. With this in mind, another goal of this project was to find a catalyst that could promote in a one-step process both the hydrotreating and hydroisomerization reactions, reducing the cost and waste associated with the typical green diesel synthesis process. Therefore, two different catalytic systems were studied: fly ash cenosphere (FACs) supported catalysts (or Zeolite-supported catalysts where the zeolites are synthesized from FACs) and layered double hydroxide (LDH) based catalysts (figure 2).

FACs are a byproduct of coal combustion and have been chosen as a support for catalyst synthesis to add value to a waste material; LDHs instead are synthetic layered anionic clays and are chosen for their green synthesis and their catalytic properties that are suitable for the catalytic deoxygenation reaction. FACs-supported catalysts were synthesized by the wet impregnation method followed by calcination and activation via reduction in fixed bed reactor (figure 2); eleven FACs-supported catalysts were synthesized, six supported on FACs and five supported on zeolites (synthesized from FAC). The LDHs catalysts are synthesized with the co-precipitation method followed by ion exchange (adding another metal into the

catalyst), calcination, and reduction in a batch reactor (Figure 2). Twelve different LDHs catalysts were synthesized.

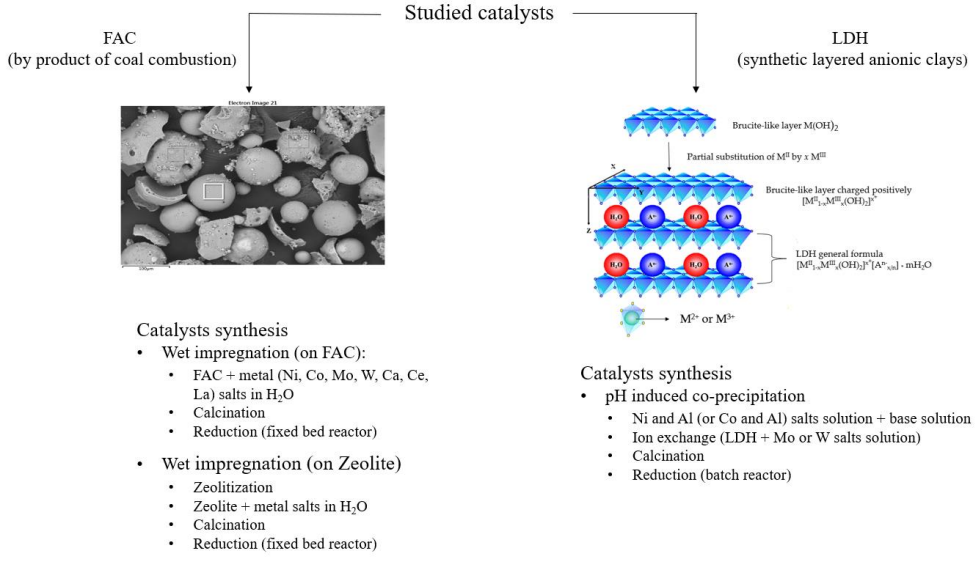

Figure 2. Catalyst used in the current research.

FACs-supported catalysts were firstly investigated.

- **FACs-supported catalysts**: a catalytic screening was firstly performed, by testing the catalysts in a batch reactor for 6h of reaction time at 320°C, 40bar H_2, 10wt% catalyst (g/g oil to catalyst), sunflower oil as feedstock, and hexane as solvent. From the catalytic screening, bimetallic catalysts demonstrated to be more efficient than trimetallic catalyst and the most efficient catalyst was found to be a Ni- and Mo-based catalyst (5wt% NiO and 15wt% MoO_3 respectively) supported on FACs (NiMo(5/15)/FAC). A conversion of 100% and a product yield of 72.2 wt% (consisting of 91.7% of *n*-C_{15}-C_{18} hydrocarbons) were obtained with this catalyst. Given the good results obtained with NiMo (5/15)/FAC, this catalyst was chosen

as a candidate to perform further investigations on recycling stability, solvent effect, and oil effect. Unfortunately, the recycling test shows that the catalyst quickly loses its activity leading to 19.7% conversion after three reaction cycles; this is ascribed to Mo leaching from the catalyst and coke deposition on the catalyst. Concerning the solvent effect, we observed that the solventless reaction led to low conversion, and by using dodecane instead of hexane, the catalyst showed lower catalytic activity. On the other hand, at the reaction condition used (320°C and 40bar H_2) hexane is in a supercritical state that shows a beneficial effect on the reaction promoting hydrogen solubility. From the oils screening, NiMo (5/15)/FAC shows 100% conversion for all the oils tested. Finally, another catalyst was synthesized slightly differently (wet impregnation followed by the zeolitization process). The catalyst was named NiMo (5/15)/FAC-Zeo and was tested under the same reaction conditions used for catalytic screening but activating the catalyst by batch reduction. The catalyst shows high activity leading to a conversion of 99.8%. To make a more accurate comparison, NiMo (5/15)/FAC was also tested after activation by batch reduction, and the comparison between the two catalysts shows that under these conditions, the NiMo (5/15)/FAC-Zeo catalyst is more efficient (99.8% vs. 94.8%). NiMo (5/15)/FAC-Zeo has shown interesting catalytic activities and will be the subject of future studies. The NiMo (5/15)/FAC catalyst was then characterized by ICP-MS, XRD, BET-BJH and FT-IR.

After having explored different aspects of FACs-supported catalysts, LDH-based catalysts were studied.

- **LDH based catalysts**: Initially, the catalytic activity of a Ni-, Mo- and Al- LDH catalyst (named NiMoAl (0.6) R.)(Ni/Al molar ratio = 0.6) was evaluated by

studying different aspects of the catalytic deoxygenation reaction of rapeseed oil, such as temperature, pressure, catalyst percentage and reaction time. From the reaction condition screening, temperature and pressure play a crucial role in the conversion degree; indeed, higher temperature and pressure promote the full conversion of the starting material, even when using the catalysts at 320°C, 40bar H_2 and 4wt% of catalyst, NiMoAl (0.6) R. resulted in 100% conversion and 73.6wt% of green diesel yield after only 2h of reaction time. Also, the reduction time effect of the catalyst was evaluated, showing the existence of a correlation between the effect of reaction time and the effect of reduction time. This interesting result suggests that the catalyst undergoes an in-situ reduction reaction. Thus, NiMoAl (0.6) R. activity without pre-activation by reduction was also investigated. The results showed that at 320°C, 40bar H_2, 10wt% of catalyst and 6h of reaction time, 100% conversion, and 60.6wt% of green diesel yield could be obtained. The high efficiency showed by this catalyst prompted the investigation of its stability in multiple catalytic cycles. The catalyst activity did not change for at least 5 reaction cycles (always showing a 100% conversion and~93% hydrocarbon in the *n*-C_{15}-C_{18} range), confirming the high activity of this catalyst. The LDH-based catalyst has shown great potential, so eleven other LDH-based catalysts have been synthesized by varying the metals and molar ratios between them. These catalysts were tested, in both reduced and oxidized states, at 320°C, 40bar H_2, 6h reaction time and 4wt% (for the reduced state) or 10wt% (for the oxidized state) of catalyst. In reduced state, trimetallic catalysts shows high activity than bimetallic ones, and among them, the most active are Mo-based catalysts (100% conversion and *n*-C_{15}-C_{18} hydrocarbons >85%). W-based trimetallic catalysts display lower activity but at the same time show a moderate hydroisomerization activity. The NiAl bimetallic catalysts have

high cracking activity (~ 15% hydrocarbon in the *n*-C_8-C_{14} range), and, among them, the catalyst with a higher Ni amount showed the best performance. In the oxidized state, these catalysts show different catalytic activity. The bimetallic NiAl catalysts showed lower cracking activity, but the effect of the Ni amount is more evident. Also in the oxidized state, trimetallic catalysts were more efficient than the bimetallic catalysts but, in this case, also W based catalyst showed 100% conversion. In addition, W-based catalysts retained their hydroisomerization activity, especially the NiWAl (2.33) catalyst (Ni/Al molar ratio = 2.33), resulting in 100% conversion, 72.4wt% green diesel yield, and 14.4% of branched hydrocarbons in the C_{15}-C_{18} range.

Chapter 1. Introduction to the research subject.

1.1. Correlation between humans and energy.

Energy, in all its forms, is crucial for the human species. Humans utilize energy sources for their sustenance, whether for food, work, or heating; in addition, discovering new energy sources and technologies always results in social and economic evolution[1]. The perfect example is represented by the “discovery” of fire, a fundamental event that allowed mankind to cook food and to be warm even during winter, thus enabling an important evolutionary step [2].

The most important energy transition, from which the modern era derives, is the Industrial Revolution (which began around 1750). During the Industrial Revolution, fossil fuels (mainly coal) became the world's primary energy resource. Prior to the industrial revolution, the main energy sources used were biomass (mainly wood for heating) and human and animal labor (agriculture and pastoral farming for food); in this era, development was constrained by the accessibility of these energy sources and their limited efficiency [3]. The industrial revolution can be dated to the invention of the coal-fueled steam engine; Thomas Newcomen invented the first prototype in 1712, but it was thanks to James Watt, who improved its efficiency, that in 1776 it was commercialized[4]. The invention of the steam engine allowed rapid industrial development as it was cheaper and considerably more efficient than animal labor, so it soon spread throughout Europe. Being a coal-fueled machine, the demand for coal also grew over time so that it remained the primary energy source until the mid-20th century when it was gradually replaced by oil (it was cheaper, more easily stored, and had a higher energy density than coal, thus ensuring greater efficiency)[5].

With the beginning of industrialization, there was also a significant increase in human welfare, which inevitably translated into an increase in the world population (Figure 3)[6].

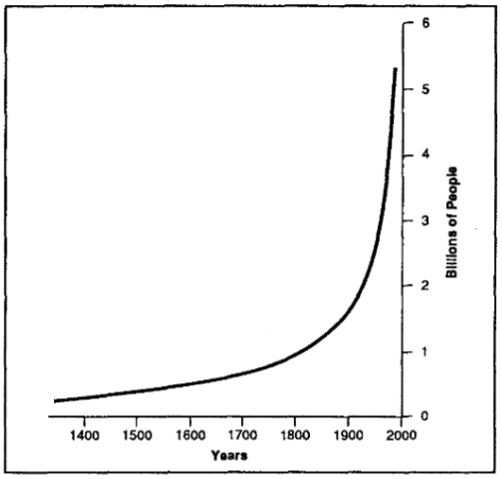

Figure 3. World population increase between the years 1400 and 2000[6]

In 1815, the world's population reached 1 billion and has grown sevenfold to date; it is estimated that it could reach 9.7 billion in 2050[7]. Population growth necessarily means an increase in energy demand; from 1971 to 2010, global energy demand increased from 5000 million of barrel oil equivalent (Mboe) to 11700[8]. Therefore, it is not surprising that, today fossil fuels meet 82% of the world's energy needs (including 31% oil, 24% natural gas, and 27% coal)[9]. In addition, their consumption is estimated to grow; the 2020 World Oil Outlook estimates, distinguishing between OECD (Organization for Economic Co-operation and Development) and non-OECD countries, an increase in energy demand of 72 Mboe/d (million barrels of oil equivalent a day) and this increase is given exclusively by non-OECD countries (Table 1)[10].

Table 1. Increase in global energy demand from 2019 to 2045 [10].

	Mboe/d[1]						Growth (Mboe/d)	Share of Global energy demand (%)	
	2019	**2025**	**2030**	**2035**	**2040**	**2045**	**2019-2045**	**2019**	**2045**
OECD[2] Countries	111.1	108.7	109.0	108.4	107.4	106.7	-4.4	38.4	29.5
Non-OECD Countries	178.1	194.3	212.9	229.8	244.9	254.6	+76.5	61.6	70.5
World	289.1	303.0	321.9	338.1	352.3	361.3	72.1	100	100

[1] Mboe/d: millions of barrel oil equivalent; [2] OECD: Organization for Economic Co-operation and Development.

In the cases of the transport sector, high oil consumption is reported; in 2015 accounted for 19% of the global energy demand (of which 92% from oil and 8% for natural gas, electricity, and other fuels)[11]. In addition, demand for oil and its derivatives is estimated to grow between 2019 and 2045 (Table 2 and Figure 4)[10]. The reduction in demand in 2020 should not be surprising as it is closely related to the restrictive policies imposed by nations worldwide to fight the COVID-19 pandemic[12].

Table 2. Increase in global oil demand from 2019 to 2045.

	Mboe/d							Growth (Mboe/d)
	2019	**2020**	**2025**	**2030**	**2035**	**2040**	**2045**	**2019-2045**
OECD Countries	23.6	20.9	22.9	20.6	18.4	16.4	14.6	-9
Non-OECD Countries	20.4	19.2	23.5	26.3	28.6	30.7	32.4	11.6
World	44.4	40.1	46.3	46.9	47.1	47.1	47.0	2.6

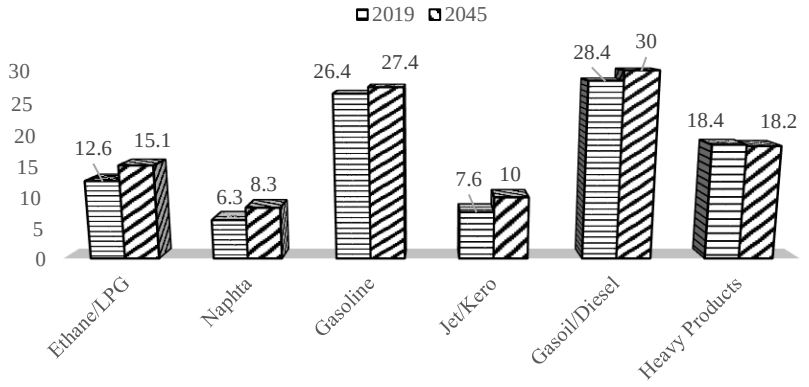

Figure 4. Increase in global oil derivates from 2019 to 2045.

From the above, the world's dependence on fossil fuels is evident, but this considerable consumption leads to numerous problems, the main ones concerning environmental pollution and global warming.

1.1.1. Fossil fuel issues.

Fossil fuel combustion leads to the emission of several environmentally hazardous pollutants:

- CO and CO_2: Partial combustion of hydrocarbons results in CO formation, a known toxic gas, while total combustion results in CO_2 formation, which is the main cause of global warming[13].
- SO_x: Although petroleum undergoes a desulfurization process, its derivatives still contain high amounts of sulfur; therefore, their combustion results in the formation of sulfur oxides, which are responsible for acid rain[14].
- NO_x: In addition to sulfur oxide formation, the combustion of petroleum and its derivatives produces nitrogen oxides also responsible for acid rain[14].

- VOCs (Volatile Organic Compounds): Hydrocarbons generated by incomplete combustion; they are related to several human diseases and contribute to the greenhouse effect[15, 16]
- Particulate matter (PM) and fine dust: Unburned particles that escape from the capture of machine filters; can cause pulmonary diseases and carcinomas[17]

All these pollutants are extremely hazardous to the environment and human health. Among them, extreme attention is paid to the emission of CO_2 and its effect on climate change; therefore, the reduction of atmospheric CO_2 and carbon neutrality are considered the major challenges of our century.

In earth history, climate change is a natural phenomenon; in fact, there are at least seven major ice ages that have occurred over the millennia[18]. The greenhouse effect is also a natural phenomenon, and it is crucial for life on earth because the presence of greenhouse gases (GHGs) has allowed the planet to reach temperatures suitable for life (15°C instead of – 18°C)[19]. When solar radiation hits the earth, some radiations are re-emitted from the earth (radiations in the range 4-100 μm); the presence of GHGs blocks this radiation in the atmosphere, allowing the earth to be warmed[19]. However, the rate at which global warming has been observed since the 20th century is not a natural phenomenon but depends strictly on anthropogenic activity[20-22]. Humans' activity significantly increases GHGs concentration in the atmosphere causing non-natural warming, and the main responsible are CO_2 emissions.

As can be seen from Figure 5, the atmospheric concentration of CO_2 remained almost constant before industrialization, but a significant increase in concentration occurred starting from the years of the industrial revolution (the detail highlighted in the figure is aimed at

stressing the correlation between the increase in CO_2 concentration with the invention of the steam engine by James Watt (1769))[23].

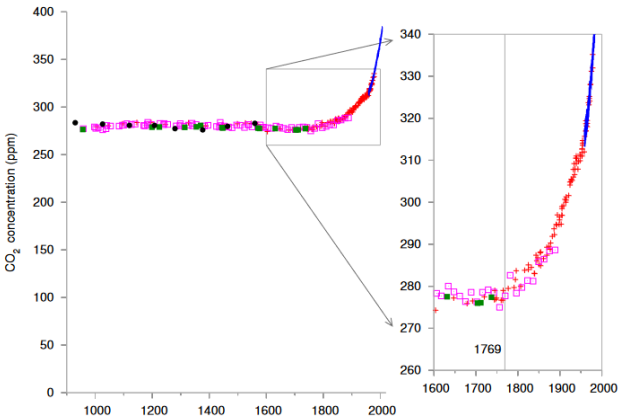

Figure 5. CO_2 concentration over years[23].

In 1850 the atmospheric concentration of CO_2 was 285ppm; in 2020, this value increased significantly to reach a concentration of 415ppm[24].

The transportation sector greatly contributes to the rise in atmospheric CO_2 concentrations; to date, it is reported that only road transport accounts for over 15% of total energy-related CO_2 emissions[25]. In the EU, the transport sector stands for 27% of total EU GHGs emissions in 2017, of which 72% is due from the road transport sector, and in 2020 is responsible for the emission of 2.54 billion metric tons of carbon dioxide [26, 27]. As previously noted, an excessive amount of GHGs in the atmosphere results in rising planet temperatures; compared to 1880, the earth's average temperature has increased by about 1.1°C and is expected to increase further over time[28]. The worst scenario reported by COP 26 (Conference of the Parties attended by the countries that signed the United Nations

Framework Convention on Climate Change (UNFCCC)) predicts a temperature increase in 2100 of about 2.6°C with devastating consequences for the planet[29, 30].

Given the catastrophic consequences of global warming, worldwide nations have begun to introduce reforms and policies to reach net-zero carbon dioxide emissions (i.e., balance between CO_2 emitted and CO_2 removed from the atmosphere)[24].

1.1.2. Global efforts against global warming.

According to the Intergovernmental Panel on Climate Change (IPCC), to avoid catastrophic consequences, CO_2 emissions must be reduced by 50-80% by 2050[31]. In this context, one of the most critical events against global warming is the COP21 that took place in Paris in 2015; on this occasion, the participating nations agreed (known as the Paris agreement) to work toward limiting the planet's temperature well below 2°C by 2100, with a more ambitious goal of no more than 1.5°C[32-34]. The European Union has been very focused on achieving carbon neutrality; in 2019 EU presented the European Green Deal, which in concordance with the Paris Agreement, presents a legislative plan that commits the European Union to achieve carbon neutrality by 2050[35]. As part of the Green Deal, in 2021 the European Union established the "Fit for 55" package that includes a set of legislation committing Europe to reduce emissions by at least 55% by 2030 compared to 1990 by helping to achieve carbon neutrality by 2050[26, 36]. The need for quick and decisive action to achieve carbon neutrality was also reiterated at COP26, emphasizing that there is little time left to achieve the Paris Agreement goals[37, 38]. As of February 2022, 198 nations are committing to achieving carbon neutrality, of which 60.6% are committed to achieving carbon neutrality by 2050-2070, but further efforts are needed to succeed in limiting global warming to 1.5°C[33].

To overcome the problems related to global warming, one of the strategies to be implemented

is the development of renewable and eco-friendly energy. Therefore, the development of biofuels is essential to achieve carbon neutrality; in addition, the production process must also be as sustainable as possible, and to do this, Green Chemistry must be used.

1.1.3. Green Chemistry and sustainability.

Green Chemistry has a very recent history; probably the first to mention Green Chemistry in a scientific paper was Cathcart in 1990, but it was in 1996, with the publication of "*Green Chemistry: An Overview"* by Anastas and Williams, that the foundations for the current "philosophy" of green chemistry were established[39]. Two years later Anastas and Werner published the book *"Green chemistry: theory and Practice"* which is still considered the keystone of Green Chemistry; in this text, the authors provide the first definition of Green chemistry *"Green Chemistry is based on the use of a set of principles that reduces or eliminates the use or formation of hazardous substances at the level of the design, manufacture and application of chemicals"* and introduce the *"12 Principles of Green Chemistry"* that one must always refer to in order to carry out sustainable chemistry[39, 40]. Figure 6 summarizes the 12 principles of green chemistry.

Figure 6. The 12 principles of green chemistry[39]

Applying all the 12 principles is very difficult but represents a goal that should always be aimed when a chemical synthesis or process is developed. With this objective, we tried to apply the 12 principles of Green Chemistry in this research work, in particular:

- *Energy Efficiency:* minimizing the energy input for a chemical process (e.g., temperature and pressure). In this regard, reaction conditions were explored to maximize the product and minimize energy consumption.
- *Catalysis*: The use of catalysts enables reactions to be performed under milder conditions (thus favoring the principle of energy efficiency). In addition, catalysts avoid reagents in stoichiometric amounts, thus minimizing waste generation; furthermore, the use of heterogeneous catalysts also allows them to be recycled, further minimizing waste. In this thesis, the use of heterogeneous catalysts is to observe this principle.

- *Safer chemical design:* The synthesized chemical must selectively exert its function and must not be toxic to humans and the environment. The synthesis of non-toxic biofuels fulfills this principle.
- *Degradation products design:* The synthesized compounds must adhere to the principle of "safer chemical design" but must also be designed in order that, after exerting their action, they are easily degraded into non-toxic substances. Compared with fossil fuels, biofuels produce lower amounts of pollutant gases.
- *Use of renewable raw materials*: Use of renewable materials should always be preferred over non-renewable materials. Examples of renewable materials are biomass (lignocellulosic feedstock, starch, vegetable oils, etc.). Biofuels are synthesized from biomass, and in this thesis, the use of vegetable oils feedstock fully respects this principle.
- *Atom economy*: A synthetic process must be designed so that all atoms of the reactants involved in the reaction are incorporated into the final product.

Green chemistry should not be regarded as a separate branch of chemistry but should be a "philosophy" fully integrated into the various branches of existing chemistry. It is hoped that over the years, Green Chemistry will be absorbed into every scientific discipline. Green chemistry is the guideline on which this thesis is based.

1.2. Biofuels.

Biofuels are defined as fuels, solid, liquid, and gaseous, that are environmentally friendly, biodegradable, and non-toxic and obtained by the treatment of biomass[41]. They can be obtained from renewable sources, and biomasses (defined as any material of biological origin derived from wood, crops, livestock, marine waste, and man-made waste) are the main renewable energy source to produce solid, liquid, and gaseous biofuels; in addition, biomass is a very cheap feedstock and is available in large quantities[42-44]. Biomass can mainly be divided into three categories:

- *Lignocellulosic feedstock*: This category includes carbohydrates such as starch, cellulose, hemicellulose, and lignin. Bioethanol can be obtained from the enzymatic digestion of complex carbohydrates followed by fermentation, while bio-oil is produced from lignin pyrolysis [45, 46].
- *Triglycerides feedstock*: This is the main component of vegetable and animal oils. Biodiesel is produced from the transesterification reaction of vegetable oils, while green diesel can be obtained from the catalytic deoxygenation reaction of vegetable oils.[47, 48].
- *Waste feedstock*: derives from human, animal, and industrial waste. The conversion of this waste is also environmentally friendly as it reuses waste that would otherwise have to be disposed of[49]. Several biofuels, such as biohydrogen, bioethanol, biodiesel, and green diesel, can be obtained from waste biomass[50-52].

Biofuels are an effective alternative to fossil fuels. Beyond the obvious advantage of renewability, biofuels are carbon neutral because the CO_2 emitted from their combustion is reused by plants and wood during their life cycle (thus not affecting atmospheric CO_2 levels); in addition, plants are sulfur-poor, so the combustion of derived vegetable oils biofuels

significantly reduce emissions of sulfur oxide[53, 54]. Biofuels can be produced biochemically (alcoholic fermentation, anaerobic digestion and enzymatic transesterification) or thermo-chemically (catalytic deoxygenation, pyrolysis, thermal and/or catalytic cracking and gasification of biomass) (Figure 7)[55, 56].

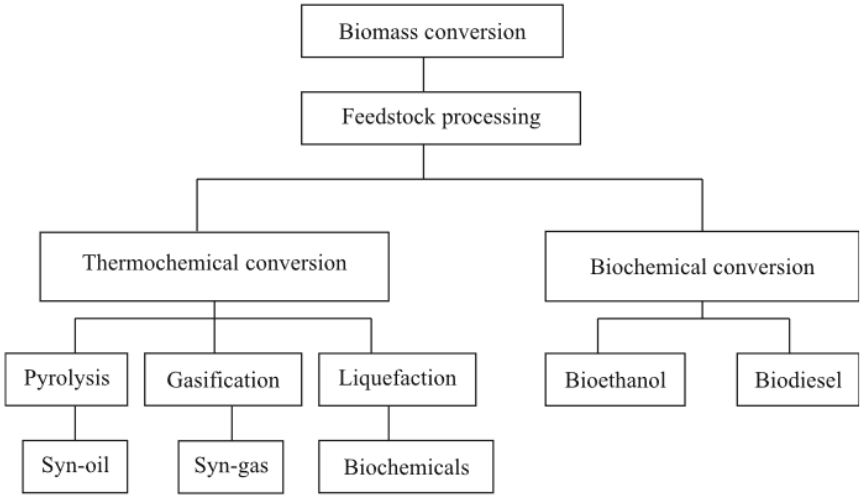

Figure 7. Process for biomass conversion [57].

The proper classification of biofuels depends on numerous factors, but for simplicity, they are classified according to the feedstock used for their production[58-60]

- *First-generation biofuels*: They are biofuels obtained from edible biomass such as sugar crops, starch, and edible vegetable oils[58, 59]. Examples of first-generation biofuels are biodiesel, bio-ethanol, and biogas. They are still the most commercially used biofuels, but they have an important drawback; edible feedstock causes competition between the food and biofuel industries[43].
- *Second-generation biofuels*: They were developed to overcome the drawbacks of first-generation biofuels; they are produced from non-edible feedstock such as

lignocellulose materials, waste, and non-edible vegetable oils. These biofuels also have a drawback and can lead to competition for available land[59].

- *Third-generation biofuels*: In this case, the biofuel is produced from oils derived from microalgae and cyanobacteria. Compared to many edible oils, higher growth rate and triglyceride yield make microalgae a promising alternative to edible vegetable oils. They do not require arable land and can grow even with wastewater [61]. The drawback of these biofuels is related to the low amount of oil produced by microalgae; in fact, the lipid content is about 20-50% of the weight of microalgae, which is less than other feedstock[62].
- *Fourth-generation biofuels*: These biofuels are produced from microalgae that are genetically modified to increase oil production and thus increase biofuel yield. Therefore, the aim is to use the benefits of microalgae and genetic engineering to increase biofuel production[63].

Only first- and second-generation biofuels are currently used commercially, as third- and fourth-generation biofuels still present problems related to low biomass production, high costs, and environmental issues[64].

Examples of first-generation biofuels are bioethanol, biogas, and biodiesel (fatty acid methyl esters, FAME), while second-generation biofuels obtained from edible and non-edible feedstock are hydrocarbon fuels obtained by catalytic deoxygenation or Fischer–Tropsch process[65]. Nowadays, the diesel engine is among the most widely used engines, and currently, the biofuels compatible with this engine are biodiesel and green diesel[66].

1.2.1 Vegetable oil as optimal feedstock for biofuels synthesis.

Vegetable oils are one of the most widely used feedstocks for biofuel production. Vegetable oils are the products obtained by chemical or mechanical extraction of seeds from plants such as sunflower, soybean, rapeseed, palm, etc.; they consist mainly of triglycerides, i.e., glycerol esters of mono- or polyunsaturated fatty acids (Figure 8, note that the configuration of the double bonds is *cis*-type) with an alkyl chain in the C_{14}-C_{18} range (and in smaller amounts also fatty acids up to 24 carbons atoms)[67-72].

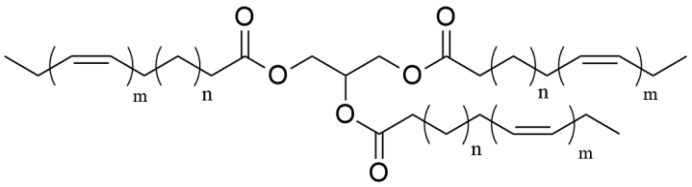

Figure 8. Triglyceride's structure.

The distribution of fatty acids in each type of oil is not constant but may vary depending on the crop, environmental conditions, harvesting, and processing[70]. Table 3 shows the typical composition of several vegetable oils[73, 74].

Table 3. Fatty acid composition of several vegetable oils[73, 74].

	Vegetable oil composition (wt%)								
Fatty acid	**Soybean**	**Rapeseed**	**Palm**	**Sunflower**	**Peanut**	**Corn**	**Jatropha**	**Canola**	**Microalgae**
Lauric (C12:0)	0.0	0.0	0.1	0.0	0.0	0.0	0.0	0.0	0.0
Myristic (C14:0)	0.0	0.0	0.7	0.0	0.1	0.0	0.0	0.1	0.6
Palmitic (C16:0)	11.3	4.9	36.7	6.2	8.0	6.5	15.9	5.1	27.8
Palmitoleic (C16:1)	0.1	0.0	0.1	0.1	0.0	0.6	0.9	0.0	0.0
Stearic (C18:0)	3.6	1.6	6.6	3.7	1.8	1.4	6.9	20.1	0.9
Oleic (C18:1)	24.9	33.0	46.1	25.2	53.3	65.6	41.1	57.9	28.2
Linoleic (C18:2)	53.0	20.4	8.6	63.1	28.4	25.2	34.7	24.7	9.3
Linolenic (C18:3)	6.1	7.9	0.3	0.2	0.3	0.1	0.3	7.9	23.9
C18:4	0.0	0.0	0.0	0.0	0.0	0.0	0.0	0.0	3.7
Arachidic (C20:0)	0.3	0.0	0.4	0.3	0.9	0.1	0.0	0.2	0.0
Eicosenoic (C20:1)	0.3	9.3	0.2	0.2	2.4	0.1	0.2	1.0	0.0
C20:5	0.0	0.0	0.0	0.0	0.0	0.0	0.0	0.0	3.4
Behenic (C22:0)	0.0	0.0	0.1	0.7	3.0	0.0	0.0	0.2	0.0
Erucic (C22:1)	0.3	23.0	0.0	0.1	0.0	0.1	0.0	0.2	0.0
Lignoceric (24:0)	0.1	0.0	0.1	0.2	1.8	0.1	0.0	0.0	0.0

[1]Cn:m: n is the number of carbon atoms and m is the number of double bonds.

Vegetable oils have a high energy density and similar chemical composition to petroleum derivatives, making them a perfect feedstock for biofuel production [75]. Given this similarity, it is possible to use vegetable oils directly as fuel and to prove this, Rudolf Diesel used peanut oil to run his engine; however, due to the high viscosity of vegetable oils, direct use causes several engine problems[45]. For this reason, it is necessary to convert vegetable

oils into a suitable fuel form. Some examples of the process used to convert oils in biofuels are transesterification, fermentation, thermal cracking, catalytic cracking, and hydroprocessing (that includes the CDO reaction)[76].

This thesis is focused on green diesel synthesis, a hydrocarbon biofuel derived from the catalytic deoxygenation reaction of vegetable oils, and it represents a technically innovative substitute for biodiesel. Before discussing the catalytic deoxygenation reaction for green diesel production, the advantages of green diesel over biodiesel will be discussed in the next section.

1.2.2 Biodiesel.

Biodiesel is defined as a biofuel for diesel engine use that meets the requirements of ASTM D 6751 (American Society for testing and materials) or EN 14214 (European norm)[57]. Biodiesel can be produced through several processes, including thermal cracking, ultrasonic and microwave techniques, but the most commercially used process is the transesterification of vegetable oils, acid or base-catalyzed (H_2SO_4 or NaOH/KOH), in the presence of methanol (or ethanol)[77]. Generally, methanol is preferred because it is inexpensive[45]. From the transesterification reaction in methanol (Scheme 1), the triglycerides of vegetable oils (1) are converted to fatty acid methyl esters (FAME) (2), whose trade name "Biodiesel", was coined by the National Soy diesel Development Board in 1992[47, 78].

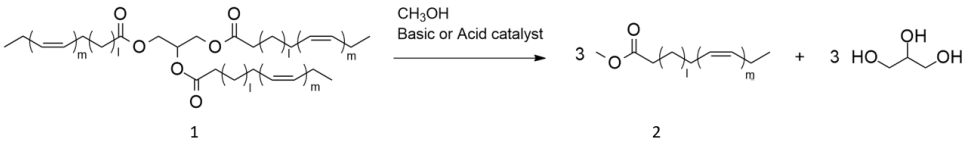

Scheme 1. Transesterification reaction.

Commercially, the main synthetic process uses basic homogeneous catalysts because, for the same yield, the acid-catalyzed reaction requires more severe reaction conditions and longer reaction times[59, 79]. Biodiesel is among the most commercially used first-generation biofuels and is mainly used in Europe, where there is the greatest use of diesel cars[59, 80]. Biodiesel can be used pure or blended with petroleum-derived diesel; when used pure, it is referred to as B100, but in this form, it has engine compatibility problems; in fact, biodiesel is mainly used in blends with petroleum-derived diesel at 7%v/v[66]. Biodiesel is an environmentally friendly alternative to petroleum-derived diesel; it is biodegradable, carbon neutral, and generates lower NO_x, SO_x, and PM emissions, especially when used in blends[81]. However, it has several drawbacks (which we will discuss later) that do not make it a suitable substitute for petroleum-derived diesel. These disadvantages are overcome by a more valuable biofuel, namely green diesel.

1.2.3 Green Diesel.

Green Diesel (trade name given by UOP/Eni), also known as Hydrotreated vegetable oil (HVO) or Renewable diesel, is a biofuel consisting exclusively of hydrocarbons and was first marketed by Neste oil in 2007 (under the trade name NExBTL)[82]. Green Diesel can be obtained from the catalytic deoxygenation reaction (CDO) of vegetable oil in which the

triglycerides are thermally treated, typically in a hydrogen atmosphere, with heterogeneous catalyst and converted in hydrocarbons in the C_{15}-C_{18} range[75].

Scheme 2 show a schematic view of the catalytic deoxygenation reaction. In the first step, triglycerides (1) are hydrogenated (4) and cleaved to obtain free fatty acids (5) and propane (6); after this, the free fatty acids (5) are converted into hydrocarbon by three main reactions: hydrodeoxygenation (HDO), in which fatty acid oxygen functionality is removed as H_2O to produce hydrocarbons with the same carbon atom number of the starting fatty acid (8), and decarbonylation (DCO) and decarboxylation (DCO_2), that producing hydrocarbons with one carbon atom less respect the starting fatty acids (7)[83-86]. During the reaction are possible many side reaction as isomerization (branched hydrocarbons formation), cracking (hydrocarbons and fatty acids are cleaved to form short-chain hydrocarbons), oligomerization via a Lewis acid-catalyzed Diels-Alder reaction (coke and heavy hydrocarbons formation) and gas-phase reaction as the water gas shift[83, 87-89].

The catalytic deoxygenation reaction then produces an exclusively hydrocarbon biofuel chemically analogous to petroleum-derived diesel, with similar chemical and physical characteristics. As with biodiesel, green diesel also has all the positive characteristics of biofuels: produced from renewable sources, is carbon neutral, and generates lower emissions of GHGs, VOCs, and PM[66]. In addition, as we will see in the next section, Green Diesel has characteristics that make it a better substitute for petroleum-derived diesel than biodiesel.

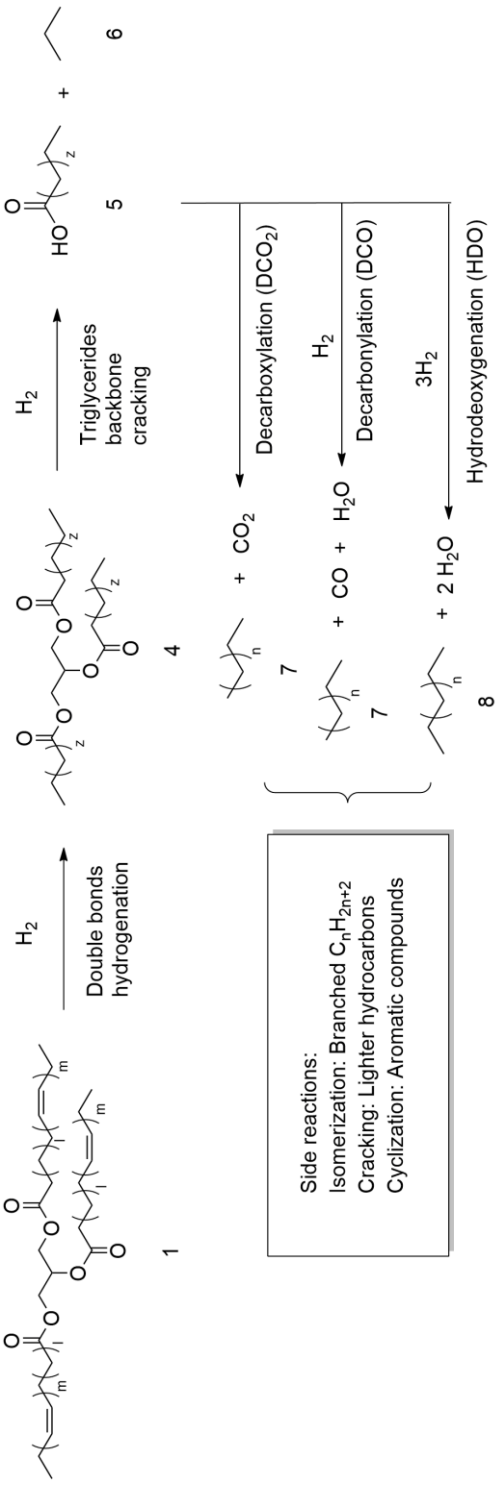

Scheme 2. Catalytic deoxygenation reaction[48].

1.2.4. Green Diesel vs Biodiesel.

Table 4 shows a comparison of the physicochemical properties of petroleum-derived diesel, biodiesel, and green diesel.

Table 4. Comparison between green diesel, petroleum-derived diesel and biodiesel[90, 91].

Properties	Petroleum-derived diesel	Biodiesel	Green Diesel
Carbon wt%	86.8	76.2	84.9
Hydrogen wt%	13.2	12.6	15.1
Oxygen wt%	0.0	11.2	0.0
Specific gravity	0.84	0.88	0.78
Cetane number	40-67	45-65	70-90
Lower Heating Value (LHV) MJ/Kg	42.3-43.1	37.2-38	43.7-44.5
Density at 15°C (Kg/m3)	796-841	880	770-790
Cloud point (°C)	-5 to 3	-5 to 15	-20 to 21
Sulfur content (ppm)	<10	<1	<1
NO_x emission	Baseline	+10	-10 to 0
Stability	good	medium	good

Looking at Table 4, the properties of green diesel are very similar to those of petroleum-derived diesel; this derives from the chemical similarity between the two fuels, which implies that green diesel marketing must necessarily be subject to the same ASTM and EN standards applied to petroleum-derived diesel[92]. On the other hand, biodiesel has a different composition than petroleum-derived diesel, so it has different characteristics and obeys different ASTM and EN standards. An adverse property of biodiesel is the high oxygen

content compared to green diesel and petroleum-derived diesel (due to the ester functionality of FAME); this results in lower carbon content and, therefore, lower LHV (lower heating value: is the amount of heat released during the combustion of a specified amount of substance, so higher LHV means better fuel combustion)[93, 94]. American and European specifications report a minimum cetane number of 40 (the cetane number measures the ignition quality of fuel in a diesel engine, so a higher cetane number results in better fuel) and, looking at Table 4, both biodiesel and green diesel have a higher cetane number than petroleum-derived diesel; moreover, between the two, green diesel has the higher cetane number [95]. In addition, biodiesel has other disadvantages compared with green diesel, such as a higher cloud point (the lower temperature at which wax (paraffin) begins to separate from the liquid of biofuel), higher corrosivity, and poor thermal and chemical stability[82, 93, 94, 96]. Concerning green diesel, from the typical catalytic deoxygenation reaction, linear hydrocarbons are formed; in this form, biofuel has a high cloud point. However, after proper treatment (hydroisomerization), some of the linear hydrocarbons are converted to branched hydrocarbons improving the cold properties of the biofuel[94, 97, 98].

Given the similar chemical nature, green diesel can be mixed in any proportion with petroleum-derived diesel and can even replace it completely; on the other hand, biodiesel can be mixed with petroleum-derived diesel only in specific proportions, and it can be used neat only after engine modification[99, 100].

From the emission perspective, both green diesel and biodiesel contribute to reducing CO_2, CO, NO_x, SO_x and PM emissions; moreover, given the higher combustion efficiency of green diesel, it produces fewer NO_x and CO emissions than biodiesel[94, 101, 102]. From a synthetic point of view, biodiesel has the advantage of simple synthesis with mild reaction conditions; however, the final product requires separation and purification processes to

remove the homogeneous catalyst and glycerol, and this implies a higher production cost[79, 80]. In addition, 95% of biodiesel production uses edible oils because non-edible oils (which generally contain more than 4wt% of H_2O) require acid esterification pretreatment before they can be used for biodiesel production[49, 78, 79, 91]. The use of edible oils results in a cost of about 75% of the total cost of biodiesel production, making it more expensive than petroleum-derived diesel. In addition, edible oils compete with the food industry generating raw material price increases[82, 103]. On the other hand, Green diesel is much more versatile and can be produced from both edible and non-edible oils and can be synthesized using the existing infrastructure used in the petroleum refinery[99].

1.3. Catalytic deoxygenation reaction for green diesel production.

After introducing the types of biofuels used in diesel engines and seeing the advantage of green diesel over biodiesel, this section will investigate the catalytic deoxygenation reaction to produce green diesel, which is the working scope of this thesis. Therefore, the reactions involved during the catalytic deoxygenation reaction and all factors affecting it will be discussed below.

1.3.1 Liquid phase reactions.

The catalytic deoxygenation reaction involves both liquid-phase and gas-phase reactions. There are several reactions that can occur in the liquid phase, and they will be addressed below to better understand the entire process.

1.3.1.1 Triglycerides cleavage.

In the CDO process, the first reaction that takes place in the liquid phase involves triglyceride double bonds hydrogenation. The hydrogenation reaction generally takes place at lower temperatures than those at which catalytic deoxygenation is conducted, so it already takes place during reactor heating[85, 104]. At this point, the triglyceride must be broken to be converted into hydrocarbons; four different mechanisms of triglyceride cleavage are reported in the literature (Scheme 3).

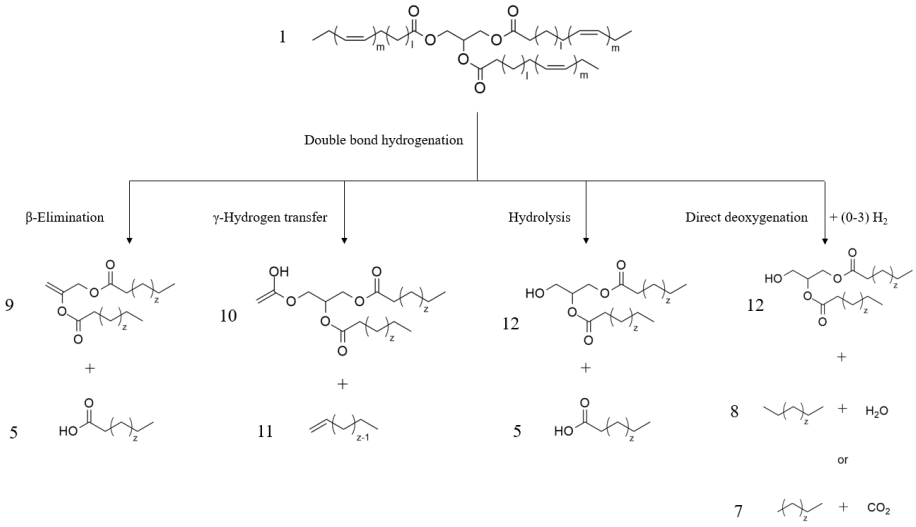

Scheme 3. Proposed mechanisms for triglyceride cleavage (adapted from[84]).

- *β-Elimination (Scheme 4):* Is the most widely accepted reaction mechanism and involves the removal of a fatty acid unit (5) and the formation of an unsaturated diglyceride (9)[105, 106].

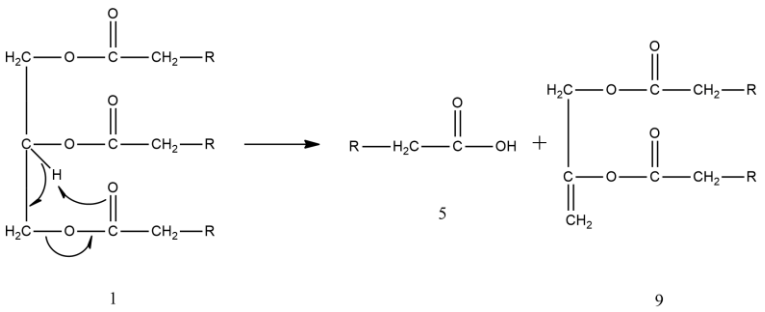

Scheme 4. β-Elimination reaction [106].

To release another molecule of fatty acid, the diglycerides undergo to double bond hydrogenation and now another β-Elimination can occur producing another mole of

free fatty acid. A further step of hydrogenation and β-elimination leads to the formation of the last unit of fatty acid and propane as a by-product. This mechanism was clearly observed by Boda et al studying the DO of tricaprylin over NiMoOx/γ-Al_2O_3 and Pd/C catalysts. The high concentrations of caprylic acid (70%) and the presence of propane confirm the hydrogenation of diglyceride and the β-elimination reactions mechanism (if diglyceride hydrogenation did not occur, the yield of caprylic acid would be lower since only one unit of fatty acid would be cleaved from the triglyceride)[107]. In addition, high caprilyc acid concentration seems to suggest that the β-elimination is a fast step, therefore the rate-determining step in the DO of tricaprylin must be the conversion of fatty acid in hydrocarbons[107]. This observation was also confirmed by Peng et al[108]. Therefore, since each step of β-Elimination also requires a mole of H_2, this reaction mechanism involves the consumption of 3 moles of H_2 [105, 109].

- *Hydrolysis*: In this case, the triglyceride is hydrolyzed and releases three fatty acids and one mole of glycerol. This reaction mechanism is observed in the case of hydrothermal reactions and with ester feedstock; this mechanism has never been observed for reactions using vegetable oils because they lack H_2O[75, 110].
- *γ-Hydrogen transfer (Scheme 5):* This reaction involves the cleavage of the triglyceride (1) to directly form an unsaturated hydrocarbon with two fewer carbon atoms than the starting fatty acid (11).

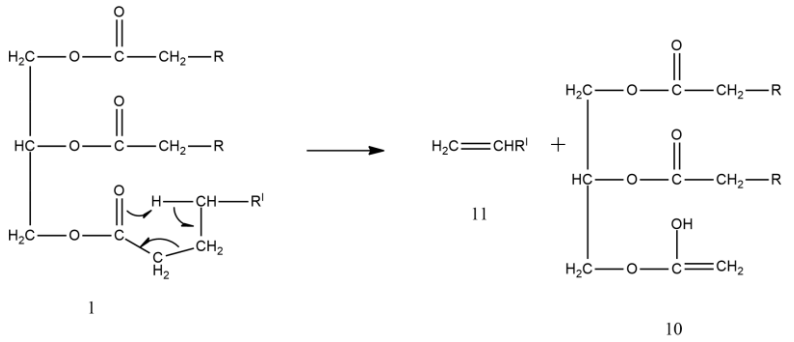

Scheme 5. γ-Hydrogen transfer reaction[106].

However, this mechanism is not observed at typical catalytic deoxygenation reaction conditions as it is more likely for processes performed at higher temperatures such as pyrolysis[84, 105, 106]. At the typical reaction conditions of CDO, fatty acids and propane are often observed as intermediates suggesting β-elimination as the main mechanism[109, 111-113].

- *Direct deoxygenation*: Direct deoxygenation refers to the reaction that, starting from triglycerides, leads directly to the formation of hydrocarbons and glycerol without observing fatty acids as intermediates in the mixture[75, 84, 111]. The resultant hydrocarbons will result from direct HDO or from direct DCO/DCO_2. The exact mechanism of direct HDO, DCO, and DCO_2 has yet to be well understood due to the absence of reaction intermediates. The proposed mechanisms are reviewed by Rogers et al[84]. For HDO, the proposed mechanism is similar to indirect HDO (which we will discuss in the next section); in this case, the formed reaction intermediates remain adsorbed on the catalyst surface and react rapidly to form C_n hydrocarbons. For direct DCO_2 and DCO, the authors report several mechanisms: 1) formation of formic acid as an intermediate that rapidly decomposes into CO. 2)

Cleavage of the C-COOH bond favored by a series of dehydrogenation reactions; this mechanism is proposed by Lu et al by DCO-DCO_2 DFT studying of propanoic acid[114]. 3) ketonization of fatty acid followed by deoxygenation[84].

Confirmed that β-elimination emerges as the most observed triglyceride cleavage mechanism, the successive observed deoxygenation reactions are indirect HDO, DCO, and DCO_2.

1.3.1.2 Indirect HDO, DCO and DCO_2.

The indirect HDO proposed mechanism is shown in Scheme 6.

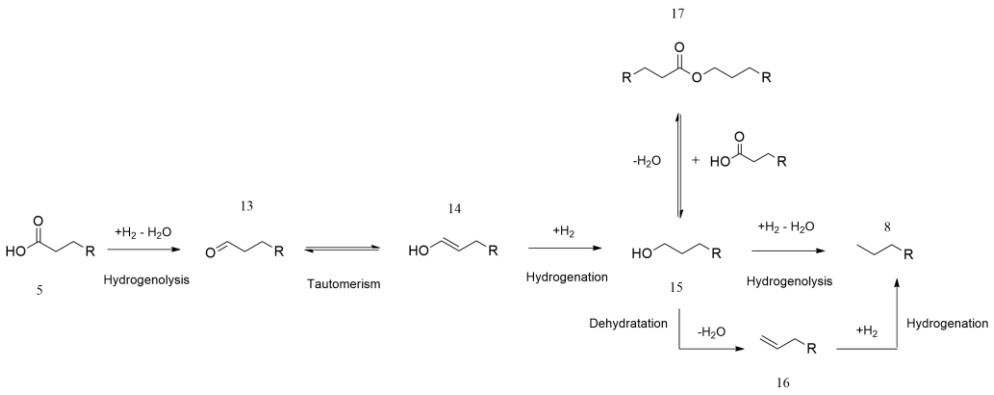

Scheme 6. HDO proposed mechanism (adapted from[75, 84]).

After the β-elimination the free fatty acids (5) undergo a hydrogenolysis reaction (breaking of a C-C or C-hetero-atom bond by H_2) to form an aldehyde (13). The aldehyde is in equilibrium with its tautomer (14), which after hydrogenation, converts to fatty alcohol (15). At this point, the alcohol can directly give a C_n hydrocarbon (8) via hydrogenolysis reaction,

or it can be dehydrated to an alkene (16) which in turn is hydrogenated to alkane (8). In addition, the alcohol can react with a free fatty acid to form an ester (17); this is an equilibrium, and the ester can be cleaved to reform the alcohol, which then proceeds to form the alkane. Several authors have observed experimental evidence of this reaction mechanism. Studying the DO of canola oil over CoMo/MCM-41 (MCM-41 = Mobil composition of Matter No 41), Kubicka et al. observed considerable amounts of oxygenated compounds (mainly fatty acids, fatty ester and smaller amounts of fatty alcohols) at low conversion degrees[112]. In contrast, at increasing conversion and hydrocarbon concentration (mainly C_{18} thus HDO reaction selectivity) they observe a significant decrease in oxygenated compounds, indicating that its represent reaction intermediates[112]. This evidence suggests that the reaction mechanism involves fatty acids formation followed by the formation of aldehyde/alcohols (rate-determining step) that react quickly to form esters or C_{18} hydrocarbons[112]. Furthermore, the esters' disappearance as the concentration of hydrocarbons increases suggests that they do not represent an end product of the reaction but only an intermediate from which alcohols can be reformed to obtain hydrocarbons[112]. This evidence has been further corroborated in their subsequent work[85]. Peng and co-workers have studied the reaction kinetics of 1-octadecanol deoxygenation, observing that the dehydration rate of 1-octadecanol is four times faster than the fatty acid hydrogenation reaction to alcohol/aldehyde, supporting the idea that the rate-determining step of the catalytic deoxygenation reaction is fatty acid hydrogenation[108].

The indirect DCO reaction has a similar reaction mechanism (Scheme 7).

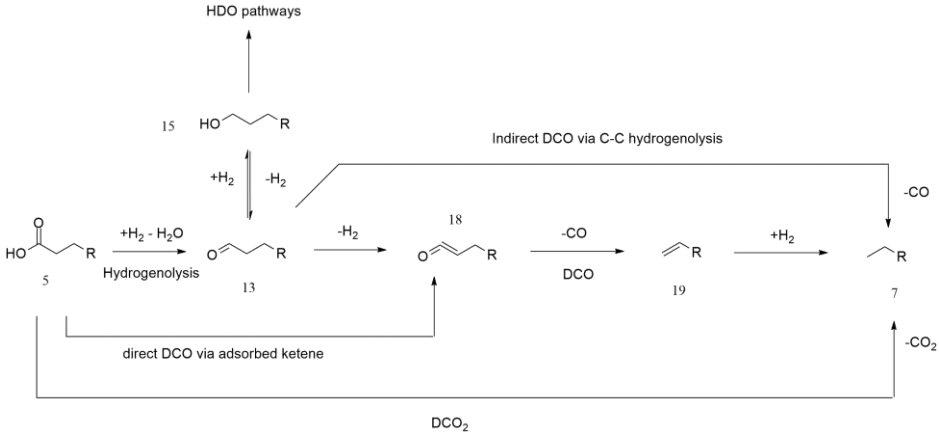

Scheme 7. DCO-DCO_2 proposed mechanism (adapted from[75, 84]).

Similar to HDO, also in DCO, the first reaction step involves hydrogenolysis of the fatty acid (5) to form the aldehyde (13). The aldehyde is always in equilibrium with its respective alcohol (15), and if the reaction selectivity favors HDO, then the reaction evolves in the manner described above for HDO. Conversely, if the reaction selectivity favors the DCO reaction, the alcohol participates as a spectator, and the aldehyde undergoes decarbonylation to obtain C_{n-1} hydrocarbons (7); in this case, the aldehyde/alcohol equilibrium shifts more toward the formation of the aldehyde promoting the formation of C_{n-1} hydrocarbons. Two main reaction mechanisms are proposed for the conversion of aldehyde to C_{n-1} hydrocarbon. Ruinart de Brimont et al., through DFT (density functional theory) studies of the DCO of heptanal, proposes that the first reaction step involves dehydrogenation of the aldehyde to form an alkanoyl intermediate[115]. This intermediate can then evolve through two different reaction pathways; the first pathway involves alkanoyl C-C bond hydrogenolysis (thus CO release) and formation of a C_{n-1} alkane; the second pathway, on the other hand, involves further dehydrogenation of the alkanoyl intermediate to obtain a ketene (18), which then loses CO converting to an alkene (19). The alkene must be hydrogenated to obtain the alkane C_{n-1}

(7) [115]. The presence of a ketene intermediate was confirmed by Peng et al. by studying the DO of palmitic acid and microalgae oil over Ni/ZrO_2 [116, 117]. Through in situ IR spectroscopy, the authors observed a band at 2050-2150 cm^{-1} attributable to C=C=O (ketene) bonding[116, 117].

The DCO_2 reaction is simple and directly involves the decarboxylation of fatty acid to form a C_{n-1} hydrocarbon.

From the C_n/C_{n-1} ratio, it is possible to determine the HDO/DCO-DCO_2 reaction selectivity. However, to discriminate between DCO and DCO_2 it is necessary to analyze the gas phase. When analyzing the gas phase in the CDO of lauric acid over Pd/C, Rozmyslowicz et al. observed a different DCO/DCO_2 reaction selectivity as the reaction atmosphere varies[118]. The main liquid hydrocarbon obtained is C_{11} (thus resulting from a DCO/DCO_2 reaction). However, they report that in argon atmosphere, the gas phase contains only CO_2 (thus DCO_2 selectivity), while in hydrogen-rich atmosphere, they observe CO in the gas phase, thus DCO selectivity[118]. The reactions exposed so far are the main reactions that occur in the liquid phase during the catalytic deoxygenation of vegetable oils, but as mentioned earlier, side reactions are also possible.

1.3.1.3 Side reactions.

One of the possible side reactions is hydroisomerization, through which alkanes are converted to branched hydrocarbons. In this case, the reaction occurs through a synergistic combination of an active metal (necessary for H_2 activation) and acid sites on the catalyst (necessary for isomerization to occur) (Scheme 8).

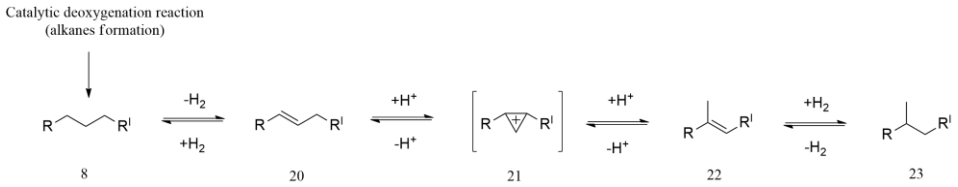

Scheme 8. Hydroisomerization reaction (adapted from [119]).

Hydroisomerization starts on double bond functionality so that it can occur either on an alkene derived from DCO or after the dehydrogenation of an alkane. Considering C_n (8) alkane (deriving from HDO), the first reaction involves metal-catalyzed dehydrogenation of the alkane; the resulting alkene (20) is protonated by a Brønsted acid forming an alkylcarbenium which, after rearrangement (through a cyclic transition state) (21), is deprotonated to reform an alkene (22). Finally, the alkene is hydrogenated to give rise to the branched hydrocarbon (23)[119, 120]. Green diesel obtained from the typical catalytic deoxygenation reaction has a high cloud point (about 20°C) because it consists exclusively of linear C_{15}-C_{18} hydrocarbons. However, an appropriate amount of branched hydrocarbons can significantly reduce the cloud point of the biofuel allowing its use[121]. Rabaev et al. obtained a hydrocarbon biofuel with high iso/normal hydrocarbon ratio and with cloud point <-35°C, performed the CDO of soybean oil in a trickle-bed reactor over Pt/SAPO-11-Al_2O_3 (SAPO-11 = silicoaluminophosphate No 11) at 375°C and 30bar H_2[122]. Another example is reported by Wang et al., who studied the DO of palm oil over NiMoW/γ-Al_2O_3-ZSM-5 (ZSM-5 = Zeolite Socony-Mobil No 5)[123]. The authors obtained at the appropriate reaction conditions (360°C, 50bar H_2, LHSV = 1.0h^{-1} and H_2/oil = 1000) a hydrocarbon biofuel containing 13wt% of isomerized hydrocarbons showing a cloud point of -5°C and cetane number of 66[123]. Typically, isomerization also leads to a reduction in the cetane number

of the biofuel, but it generally remains above the minimum value required by many countries' standards[95, 124].

Since the reaction mechanism is very similar, the hydroisomerization is often in combination with another side reaction, the hydrocracking reaction[95]. In the hydrocracking reaction, hydrocarbons in the diesel range (n-C_{15}-C_{18}) are converted to short-chain hydrocarbons (Scheme 9)[119].

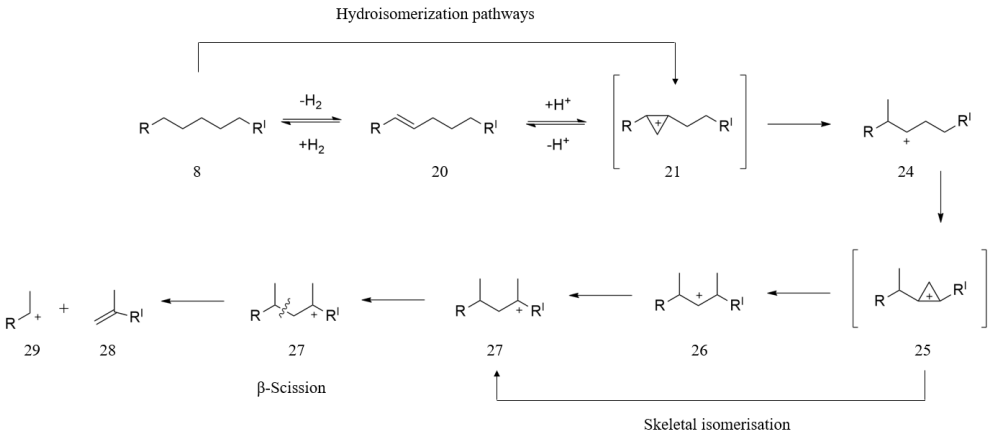

Scheme 9. Hydrocracking reaction. Readapted from [119].

The first part of the reaction is the same as hydroisomerization (8 to 21); when cracking takes place, the carbocation 21 undergoes skeletal isomerization (21 to 27), and after this, β-scission of the carbocation 27 produces an alkene (28), which is then hydrogenated, and a carbocation (29) which undergo to deprotonation.

This reaction is not desired to obtain high green diesel yields; on the other hand, if the goal is to obtain bio-jet or bio-gasoline biofuels the hydrocracking reaction should be promoted. Generally, hydrocracking and isomerization reactions are promoted by high temperatures, high pressure, and with catalysts having high acidity; therefore, in order to obtain a green

diesel-type biofuel with good cold properties, it is necessary to develop a process that can mainly promote the isomerization reaction[95, 108, 125-129]. A highly undesirable reaction is the oligomerization of fatty acids (that occurs via Lewis acid-catalyzed Diels-Alder reaction) to form heavy products (Scheme 10). These compounds act as coke precursors resulting in catalyst deactivation and lower diesel yields[87, 130].

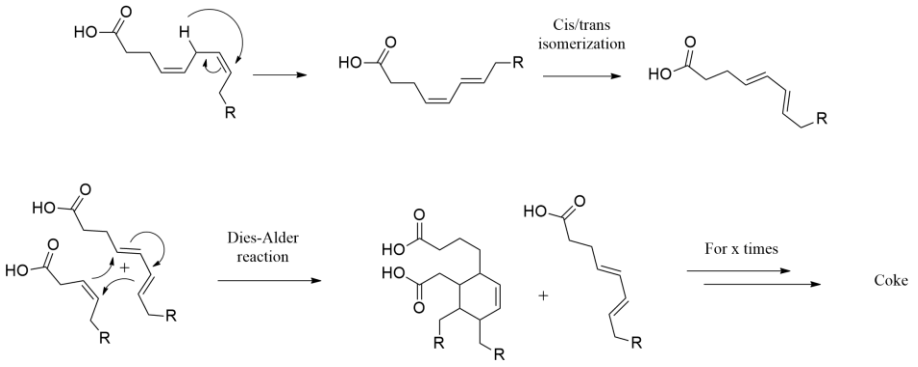

Scheme 10. Oligomerization reaction. Readapted from[87].

1.4.2 Gas phase reactions.

In addition to liquid-phase reactions, gas-phase reactions are possible. The CO and CO_2 produced by DCO and DCO_2 reactions can react with hydrogen via methanation reaction to form methane and water; in addition, the CO_2 produced is also involved in the water gas shift reaction (Scheme 11)[89].

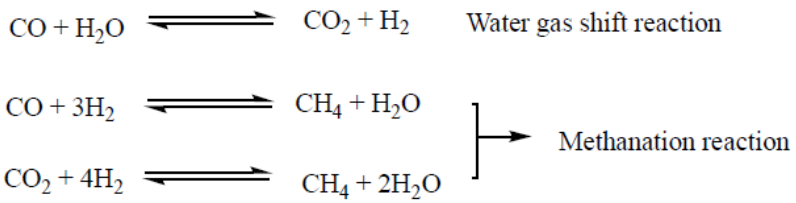

Scheme 11. Gas phase reaction

DCO and DCO_2 reactions are less environmentally friendly than HDO (they have a lower atom economy and generate pollutant gases) but consume less hydrogen and thus are preferred economically; however, looking at gas-phase reactions, we can see that the gases generated by DCO and DCO_2 can consume even more hydrogen than HDO making DCO and DCO_2 not as economically viable[131]. On the other hand, considering the water-gas shift reaction, driving the reaction towards H_2 production would be favorable from the point of view of H_2 consumption. Therefore, promoting DCO and favoring the water gas shift can be significantly positive from the economic point of view; this also means that it would be necessary to counteract methanation reactions that consume large quantities of hydrogen[84].

1.5 Factors affecting the catalytic deoxygenation reaction.

From what has been discussed, the catalytic deoxygenation reaction is a complex process. Biofuel yield, reaction selectivity (HDO, DCO, or DCO_2), hydrocarbon distribution in the biofuel as well as secondary and gas-phase reactions, can be affected by many factors such as catalyst (both active metal and support), temperature, pressure (and type of atmosphere), catalyst percentage, reactor type, solvent, and even feedstock type. Therefore, this section will show how all these parameters affect the catalytic deoxygenation reaction.

1.5.1 Effect of the active metal.

The catalytic deoxygenation reaction requires heterogeneous catalysts to occur. Typically, the catalysts used are sulfided transition metal catalysts, noble metal catalysts, reduced transition metal catalysts, and to a minor extent, nitride, phosphide, and carbide metal-based catalysts. Among the catalysts listed above, the most widely used are sulfided metal catalysts such as Mo and W doped with promoters such as Ni and Co; they are commonly used because, in addition to being very active in hydrodesulfurization (HDS) processes (similar process to CDO but involving the removal of sulfur from natural gas and petroleum refining products), they are also very active in the CDO reaction [44]. The main advantage of using these catalysts is the high activity they have toward HDS and HDO reactions which allows them to be used in the refinery industries in the co-processing of crude oil and vegetable oils; therefore, in this process, the same catalyst allows the removal of sulfur from crude oil and at the same time to produce biofuel via CDO [132, 133]. Catalyst sulfidation involves the thermal treatment of the catalyst in the presence of hydrogen sulfide or carbon disulfide that ensures the formation of active sites on the catalyst surface [134-136]. Kubicka et al.,

investigating the CDO of rapeseed oil over sulfided NiMo/γ-Al_2O_3, Ni/γ-Al_2O_3 and Mo/γ-Al_2O_3 observed that the bimetallic catalyst was more active than the monometallic ones; moreover, Ni is more selective towards DCO/DCO_2 and Mo towards HDO, while, with NiMo the products deriving from both reactions were obtained in the same amount [111]. In a comparative analysis of bimetallic sulfided NiMo, NiW, CoMo, CoW, supported on γ-Al_2O_3, SiO_2, TiO_2, SBA-15 (Santa Barbara Amorphous No 15), in rapeseed oil hydrotreatment, Horáček et al concluded that among the bimetallic catalysts the most active was NiMo/γ-Al_2O_3. NiMo/ γ-Al_2O_3 was also more active than NiCoMo and NiCoW trimetallic catalysts[137]. To better observe the effect of sulfided active metals, Zhang and collaborators have studied the different behaviors of unsupported CoMoS and NiMoS (excluding the effect of the support) in the CDO of rapeseed oil [138]. Both catalysts exhibit complete conversion, but NiMo has a higher conversion rate, higher diesel selectivity (less cracking), and a liquid product consisting of 90% n-alkanes [138]. On the other hand, CoMo leads to more cracking, and the liquid product is richer in olefins, indicating a lower hydrogenation capacity [138]. The lower hydrogenation capability agrees that CoMoS prefers DCO/DCO2 while NiMoS prefers HDO [138]. Toba et al. obtained a similar result by studying the CDO of waste oil over sulfided NiMo/Al_2O_3, CoMo/Al_2O_3 and NiW/Al_2O_3 [139]. The authors report that CoMo produces more olefine respect NiMo and NiW, thus is less suitable in the CDO of waste oils due to its lower hydrogenation capacity[139]. The molar ratio of metals used in the catalyst can also influence the reaction[139]. Simacek et al. evaluated the effect of different Ni/Mo ratios of sulfided NiMo/ γ-Al_2O_3 catalyst on the CDO of rapeseed oil. The authors observed that the catalyst with the highest Ni/Mo ratio is the one that leads to a higher amount of isomer hydrocarbons, especially at higher temperatures [140]. Sulfided catalysts are very active but also have the significant disadvantage of rapid deactivation via sulfur leaching. Kubička and Horáček, in the CDO of rapeseed oil over CoMo/Al_2O_3, have observed

that the catalyst's deactivation by leaching can be minimized by processing the oil with a sulfiding agent that reduces the leaching of the catalyst [113]. They also observed that deactivation of these catalysts via cooking could also occur due to oils with high concentrations of alkali and phospholipids [113].

Şenol et al. have also analyzed the effect of two sulfiding agents, H_2S and CS_2, observing that H_2S was more beneficial than CS_2 by also actively participating in promoting CDO by increasing the acidity of the catalyst and preventing catalyst deactivation, but this leads to the formation of pollutant gases and contamination of the biofuel with sulfur[141]. Because of these limitations, more attention has been paid to non-sulfided catalysts. Generally, these catalysts are based on noble metals because they are generally more active, although more expensive, than the corresponding reduced transition metals [89, 142]. Snåre et al. compared the activity of several noble metals (Pd, Pt, Ir, Ru, Os) and Ni supported on AC (activated carbon), γ-Al_2O_3, Cr_2O_3, and SiO_2 in the CDO of oleic acid. It was evident that the most active catalysts were based on Pd and Pt, followed by Ni [89]. In addition, they observed that Ni, Pt and Pd show marked selectivity toward DCO-DCO_2 (<2% C_{18} hydrocarbons), while Ru tends to prefer HDO[89, 143, 144]. Similar results are reported by Berenblyum et al. investigating the DO of stearic acid over M/γ-Al_2O_3 (where M = Ni, Pt, Pd and Cu)[145]. The authors report Pd as the most active catalyst and show that all the metals analyzed prefer DCO-DCO_2; among these, only Cu leads to the formation of olefins (recall that DCO can lead to the formation of alkenes) which indicates that among the catalysts analyzed, Cu is the one with the lowest hydrogenation capacity[145]. However, noble metal-based catalysts are expensive, so using cheaper catalysts is preferable. Morgan et al., investigating the hydrotreatment of tristearin, triolein, and soybean oil over 20wt% Ni/C, 5wt% Pd/C, and 1wt% Pt/C under nitrogen atmosphere, observed that a higher metal content makes the Ni-

based catalyst more active towards soybean oil CDO (leading to a 92% conversion) compared to noble metal catalysts (23% for Pt and 30% for Pd). On the other hand, 20wt %Ni/C was also the catalyst with the highest cracking and methanation activity[109]. Additionally, Veriansyah et al., comparing the activity of reduced monometallic Pd, Pt, and Ni-based catalysts with NiMo and CoMo sulfided bimetallic catalysts in the CDO of soybean oil, observed that, at catalyst-to-oil ratio = 0.088 and high Ni contents in the catalyst (66.0 3%), the Ni-based catalyst is among the most active, reporting a 96% conversion, deoxygenation > 90%, and a 99% in diesel selectivity[83]. At a lower catalyst-to-oil ratio (0.044), the best catalyst is sulfided NiMo. Sulfided CoMo was instead the catalyst with the highest degree of hydrocracking, as it leads to a lower yield of organic liquid product and a higher percentage of light hydrocarbons[83]. So, from what was reported by Veriensah et al., metal transition-based catalysts can also be an excellent alternative to typical sulfided catalysts. Similar results were reported by Harnos et al. by comparing the activity of reduced catalysts and sulfided catalysts on the CDO of sunflower oil[146]. Among the bimetallic catalysts, NiMo sulfided catalyst is the more active, resulting in a biofuel yield of 73% (98.9% conversion, *n*-C_{17} = 26.3% and *n*-C_{18} = 28.1%), while reduced NiMo leads to a biofuel yield of 66% (83.9% conversion, *n*-C_{17} = 5.1% and *n*-C_{18} = 45.9%)[146]. However, the authors show that reduced Ni/-Al_2O_3 with a 27 wt% Ni content has similar activity (91.1% conversion with 66.1 wt% of biofuel yield) as the sulfided NiMo and therefore represents an alternative to sulfided catalysts[146]. On the other hand, the reduced NiMo catalyst shows a higher degree of methanation (therefore higher H_2 consumption)[146]. Krár et al. evaluated the effect of reaction conditions in sunflower oil deoxygenation over reduced CoMo/γ-Al_2O_3 and, by comparing the activity between sulfided and reduced catalyst, they suggest that the reduced catalyst is more convenient because it does not require the addition of sulfur agents, which is necessary to maintain the sulfur catalysts activity (the yield of the diesel fraction is only 5%

lower)[147]. Srifa et al. have examined the activity of Ni/γ-Al_2O_3 and Co/γ-Al_2O_3 (both 10 wt%) reduced catalysts in the CDO of palm oil[148]. For both catalysts, they observed 100% conversion up to 150 h, but after 100 h, there was a decrease in the organic product yield from 92.2 to 75.6% for Ni and from 88.6 to 56.6% for Co[148]. The analysis of the recovered catalysts shows a certain degree of sintering; however, the deactivation after 100 h is attributed to the coke formation because, through proper treatment that leads to the removal of coke, the catalyst fully recovers its textural properties, which suggests a complete regeneration of catalytic performance[148]. In another work, Srifa and co-workers compared the activity of different M/γ-Al_2O_3 catalysts, where M = Co, Ni (5–10 wt%), Pd, and Pt (2–5 wt%), in the hydrotreatment of palm oil[149]. For higher metal loading (5–10 wt%), a conversion of 100% is observed, and at the same metal amount (5 wt%), the yield in terms of liquid organic products follows the trend Co (88.5%) > Pd (85.2%) > Pt (79.5%) > Ni (69.7%). Ni, Pd, and Pt prefer DCO/DCO_2, while Co prefers HDO[149]. Other alternatives to the above-mentioned catalysts, phosphide, carbide, and nitride catalysts, have also been developed[131].

1.5.2 Effect of catalyst's support.

Clearly, the active phase is crucial for the catalytic deoxygenation reaction; however, the support on which it is dispersed also plays an important role in the reaction. Figure 9 shows a schematic diagram of the most common supports used in the synthesis of heterogeneous catalysts for the CDO reaction.

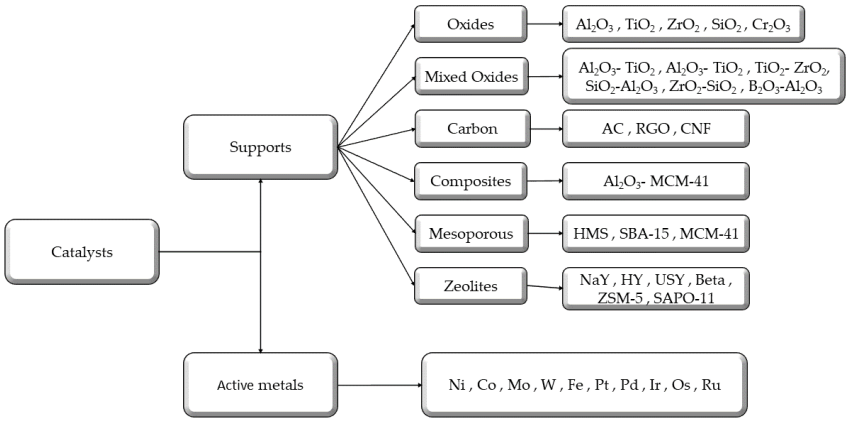

Figure 9. Main supports and active metals used in CDO reaction.

Acidity, surface area, and pore size are among the main characteristics that support must have to be effective in the catalytic deoxygenation reaction. Several authors report the importance of the surface area. Horáček et al., investigating the CDO of rapeseed oil over bimetallic sulfided NiMo, NiW, CoMo, and CoW catalysts, supported on γ-Al_2O_3, SiO_2, TiO_2, SBA-15, and hydrotalcite, have observed that the most active support was alumina together with SBA-15[137]. Compared to SiO_2, SBA-15 shows greater activity and different selectivity; with SBA-15, there is a greater prevalence of HDO, while SiO_2 prefers DCO/DCO_2[137]. This is due to the high surface area of SBA-15 (650 m^2/g) compared to SiO_2 (57 m^2/g), which improves the diffusion of the reagents inhibiting the breaking of the C–C bonds (and thus the DCO/DCO_2)[137]. The beneficial effect of support with a high surface area was also reported by Wang et al. in the hydrotreatment of soybean oil over NiMo carbide catalysts[150]. They observed that the best conversion (100%) and diesel selectivity (97%) were achieved with the lab-made NiMo/Al-SBA-15 (SBA-15 enriched with Al), which has the highest surface area and the largest porosity[150]. In addition, a catalyst with a high surface area ensures less

catalyst deactivation, as observed by Snare et al. in the CDO of oleic acid over Pd, Pt, Ir, Ru, Os, and Ni on AC , γ-Al_2O_3, Cr_2O_3, and SiO_2[89]. The higher activity of AC-supported catalysts is attributed to the high surface area of the support leading to lower deactivation via sintering and coking[89]. Similar results were reported by Kubicka et al. in the CDO of rapeseed oil over NiMo sulfided bimetallic catalysts supported on SiO_2, γ -Al_2O_3, and TiO_2 [151]. For all the tested catalysts, 100% conversion at 300°C was obtained; however, the highest degree of deoxygenation can be achieved with SiO_2, which has a larger surface area, higher acidity, and greater dispersion of the active phase[151]. Other evidence on the positive effect of supports with a high surface area is reported by other authors[152-155]. Support acidity is another parameter that can affect the deoxygenation reaction. Peng et al., in the CDO of palmitic acid over Pd, Pt, and Ni supported on ZrO_2, Al_2O_3, H-ZSM-5 (hydrogen form of Zeolite Socony Mobil-5), H-BEA (hydrogen form of β-zeolite) and C, reported that metal supported on supports with weak or medium acidity, such as ZrO_2 and zeolites, showed increased catalytic activity[116]. In another work, Peng et al. analyzed the CDO reaction of oil extracted from microalgae using two Ni-based catalysts supported on H-ZSM5 and H-β[108]. With Ni/H-ZSM5, the reaction shows a high degree of cracking (43%) and coke formation; the authors correlate these phenomena to the higher concentration of Brønsted acid sites of this catalyst that greatly favor cracking[108]. In addition, they found that by increasing zeolite's Si/Al ratio (as the Si/Al ratio increases, the zeolite's acidity decreases), cracking and coke formation decrease, but at the same time, the conversion decreases too[108]. The acidity–cooking correlation has also been reported by Ardiyanti et al. in the upgrading of fast pyrolysis oil using NiCu/γ-Al_2O_3 and NiCu/δ-Al_2O_3 [125]. Sotelo-Boyás et al., comparing the activity of Pt/zeolite catalysts (zeolite = HZSM-5 or HY typical hydrocracking catalysts), observed that HZSM-5 (more acidic than HY) gives a higher

gasoline yield (40% green gasoline) and a lower diesel yield, while with HY is the opposite making it a more suitable catalyst for the synthesis of green diesel with a certain degree of isomerization[129]. On the other hand, HZSM-5 is more suitable for green gasoline synthesis. Duan et al. have studied the effect of Al incorporation in Pd/Al-SBA in the CDO of sunflower oil[156]. The catalyst with the highest Al content is the most active, probably due to the enhanced acidity provided by the higher Al content[156]. The authors also observed that as acidity increased, selectivity towards HDO increased, suggesting a correlation between acidity and the HDO reaction[156]. The influence of support on HDO/DCO-DCO_2 reaction selectivity is also reported by Peng et al[108, 116, 117]. As observed by Twaiq et al., the size of support pores is also important[157]. By studying the cracking reaction of palm oil over various zeolites (HZSM-5, β-Zeolite, USY (Ultrastable Zeolite Y)), the authors suggest that the support pore size strongly affects the hydrocarbon distribution in the diesel mixture; USY zeolite, which has a larger pore size, leads to less cracking (gasoline range 4–17%) than HZSM-5 zeolite (gasoline range 17–28%)[157]. In addition, larger pore size also leads to a lower aromatic hydrocarbon content (20–38% for HZSM-5 versus 3–13% for USY)[157]. A sufficiently large pore size would tend to minimize cracking, thus leading to a greater diesel selectivity. For these reasons, mesoporous materials are experiencing increasing interest as the mesoporous pores of these materials allow for easier diffusion of the substrate, which implies less coking and cracking reactions[157, 158]. The efficiency of catalysts based on mesoporous supports was discussed in another work by Kubička and co-workers comparing the activity of sulfided CoMo/OMA (OMA = organized mesoporous alumina), CoMo/MCM-41, and CoMo/γ-Al_2O_3 (all CoMo catalysts have 3 wt% Co and 15 wt% Mo) in the DO of rapeseed oil[112]. Their study shows that OMA is more active than γ-Al_2O_3 catalysts. In contrast, the Si-based support (MCM-41) is the least active (OMA > γ-Al_2O_3 > MCM-41). The authors correlate the lower activity of MCM-41 compared

to OMA with a more unfavorable interaction between the active phase and the Si-based support than alumina-based support. The liquid product obtained is also free of light fractions and aromatics, and the authors related it to the higher diffusivity guaranteed by the mesoporous support.

1.5.3 Effect of the reaction temperature.

The reaction temperature is among the parameters that most influence the catalytic deoxygenation reaction and, thus, the biofuel produced. Snåre et al., studying the CDO of ethyl stearate over Pd/C, observed that an increase in temperature from 300 to 360°C leads to a fourfold increase in conversion[159]. Similar results were reported by Madsen et al. in the oleic acid/tripalmitin mixture (1:3) hydrotreating in an H_2 atmosphere over Pt/γ-Al_2O_3 [142]. The authors showed an increase in conversion from 6% at 250°C to 100% at 325°C [142]. An increase in conversion with temperature has also been observed by Mäki-Arvela et al., but more interestingly, they reported that an increase in temperature also leads to a higher degree of dehydrogenation as the n-heptadecane/n-heptadecene ratio decreases[160]. The effect of the reaction temperature on the dehydrogenation reaction was also observed by Cheng et al. in the hydrotreating of soybean oil over NiMo/HY (HY = hydrogen form of the zeolite Y) to produce jet biofuel[161]. Their work reported an increase in the formation of aromatic hydrocarbons as the temperature rises. In fact, at temperatures above 390°C, the aromatic content increased from 17.6% to 28.7%[161]. A similar trend was also observed by Li et al.[162]. The temperature also greatly influences the hydrocarbon distributions in biofuel. Verma et al. found that a temperature increase (375–450°C) leads to an increase in the distribution of hydrocarbons in the kerosene range (higher yield at 425°C), indicating an improved cracking reaction with the temperature and; as a consequence, they also observed

an increase in isomerization activity as the temperature increases[126]. Working at 375°C led to higher diesel selectivity (85–96%); if higher temperatures were used (450°C), cracking prevailed, leading to a decrease in the kerosene range in favor of gaseous products[126]. Similar results were observed by Srifa et al.[127]. The correlation between cracking and temperature has also been observed by Pinto et al. in the DO of pomace oil olives[163]. As the temperature increased, an increase in light hydrocarbons and a decrease in heavy fractions was observed; this phenomenon was improved with longer reaction times[163]. Moreover, analyzing the gas phase, they observed that as the temperature increases, the presence of gases such as methane, ethane, and other gaseous hydrocarbons increases, indicating a greater degree of cracking[163]. They also observed an increase in CO and CO_2 concentration, which seems to indicate that an increase in temperature leads to higher selectivity of reaction towards DCO/DCO_2, and this agrees with the endothermic nature of these reactions; on the other hand, HDO is exothermic and therefore favored at lower temperatures[164, 165]. Liu et al. investigated the isomerization of palm oil over Ni/SAPO-11, observing that low reaction temperatures (320 °C) yield low isomerization (in favor of a higher selectivity towards n-alkanes in the diesel range), while higher temperatures considerably increase isomerization activity, often accompanied by a significant cracking; isomerization selectivity greater than 80% and a liquid hydrocarbon yield of 70% were obtained[128]. Considering all the above reported, it is evident that temperature control is crucial to obtain the desired fuel type. Moreover, the temperature also plays an important role in the deactivation of the catalyst. Higher temperatures can lead to catalysts sintering, increasing the formation of aromatics and coke, which leads to rapid deactivation of the catalyst[166].

1.5.4 Pressure and reaction atmosphere effect.

The catalytic deoxygenation reaction can be performed in an inert atmosphere, typically He and Ar, in a hydrogen atmosphere, or even in an H_2/He or Ar mixture. The gas type and the pressure can significantly influence the CDO reaction. Snåre et al. performed the reaction on different feedstock (oleic acid, linoleic acid, and methyl oleate) over Pd/C, varying the reaction atmosphere[167]. Pure H_2, pure Ar, and H_2–Ar mixture were used. Working in an H_2-rich atmosphere, where the deoxygenation reaction is strongly promoted, they observed, for each feedstock used, a greater conversion of hydrocarbons[167]. Similar results were obtained by Santillan-Jimenez et al. in the hydrotreating of ethyl stearate over Pd/C[106]. The authors observed that an H_2-rich atmosphere promotes the hydrogenation of unsaturated species and therefore increases the concentration of saturated hydrocarbons in the biofuel[106]. Kubickova et al. showed lower amount of aromatic hydrocarbons and high concentration of saturated hydrocarbons in the H_2 atmosphere, but more interesting, they also reported better conversion and catalyst TOF (turnover frequency) in 5%H_2/Ar atmosphere[168]. In addition, the authors showed that H_2 partial pressure affects the reaction; higher pressure leads to a lesser amount of unsaturated hydrocarbon compound[168]. Particularly interesting results were reported by Santillan-Jimenez et al. in the CDO of stearic acid and tristearin over Pd(5%)/C and Ni(20%)/C in pure H_2, pure N_2, and 10% H_2/N_2 [169]. They observed different catalysts' activity depending on the used atmosphere; Ni/C is more active in pure H_2, while Pd/C is better in 10%H_2/N_2. In conjunction with the reaction atmosphere, pH_2 can greatly influence the catalytic deoxygenation reaction[169]. In methyl oleate hydrotreatment over Pd/SBA-15, Lee and co-workers reported that an increase in H_2 pressure from 25 to 60 bar leads to a significant improvement in conversion and C_{15}–C_{18} selectivity (up to 100% conversion and 70% selectivity C_{15}–C_{18})[170]. A further increase

from 60 to 80 bar leads to a decrease in conversion, and this is due to increased competition between the substrate and H_2 for the catalyst's active sites[170, 171]. The positive effect of partial hydrogen pressure has also been reported by Nimkarde et al. in the CDO of Karanja oil over NiMo and CoMo catalysts [172]. By increasing the pressure from 15 to 30 bar, the conversion increased from 62.1% to 88.4% over NiMo and from 60.1% to 85.6% over CoMo [172]. Sotelo-Boyás et al. observed a progressive increase in conversion and selectivity to HDO by increasing the pressure from 50 to 110 bar [129]. A decrease in concentration of heavy fractions in favor of light C_5–C_{12} fractions was also observed, indicating that high pressures seem to favor a higher cracking degree[129]. This seems to be in contrast to what was observed by Yang et al. studying the CDO of a mixture of C_{18} acids over sulfided NiW/SiO_2-Al_2O_3 [173]. Varying the pressure from 20–80 bar, the C_3–C_{11} light fraction yield decreased as the pressure increased, while the diesel yield increased up to 40 bar and then decreased at higher pressures; the authors suggested that high pressure restrains cracking reactions and explained this with the Le Chatelier Principle[173]. They also observed a decrease in DCO/DCO_2 selectivity and a higher prevalence of HDO at higher pressure due to the major amount of hydrogen available for HDO. Higher pressure also tends to inhibit isomerization due to a higher amount of H_2 adsorbed on the catalyst sites used for isomerization. Anand et al. studied the CDO of jatropha oil by varying the P from 20 to 90 bar[174]. Their work shows an increase in conversion from 91% to 98% by increasing the pressure from 40 to 90 bar and a drastic reduction in conversion (31%) by working at pressures of 20 bar. Despite the high conversion obtained at 40 bar, the biofuel has a high concentration of heavy product (20% > C_{18}), which decreases by increasing the pressure. The authors report that under their conditions the optimum pressure value is 80 bar of H_2 [174].

1.5.5 Other parameters.

The catalyst, temperature, and pressure are the main factors to consider; however, other parameters can also play a role in the catalytic deoxygenation reaction, such as the solvent, feedstock, and the reactor used. Mäki-Arvela et al. have observed a different reaction selectivity of their catalyst using free fatty acids or methyl esters as a feedstock[175]. With free fatty acid, the reaction proceeds via DCO_2, while with the corresponding methyl esters it appears that the reaction proceeds via DCO. In addition, the authors have also observed that compounds with longer chains tend to retard the reaction rate[175]. Morgan et al., studying the CDO of triolein and soybean oil under an inert atmosphere over a hydrotalcite-type catalyst, observed high cracking and coking activity only with soybean oil, which suggests that a higher degree of substrate unsaturation tends to favor cocking and cracking[176]. In addition, as observed by Kiatkittipong and co-workers in the DO of CPO (crude palm oil), DPO (degummed palm oil), and PFAD (palm fatty acids distillate), the degree of feedstock pre-treatment also seems to influence the reaction[177]. With PFAD, the reaction requires less severe conditions, and a better hydrocarbon yield is obtained. In addition, the authors also observed that Pd/C is more promising when working with PFAD, while sulfided $NiMo/\gamma\text{-}Al_2O_3$ is preferred with triglyceride-type substrates[177]. The catalytic deoxygenation reaction can be performed in batch, semi-batch, or continuous reactors. Compared to continuous reactors, batch reactors allow for preliminary studies to be made to optimize reaction conditions and generate kinetic data in an easy and economical manner[178]. The use of continuous and semi-batch reactors has the advantage of purging the reactor of CO_x formed during the reaction, and this has a dual advantage; one is to shift the balance of the reaction towards the products, and the other is to avoid poisoning of the catalysts by CO adsorption[171, 179]. By comparing the same reaction conditions with the

same catalyst (Pd/C), Snåre et al. observed higher productivity in the semi-batch mode compared to the continuous reactor by attributing the cause to the mass transfer limitations in the fixed-bed reactor[167]. The solvent used can also slightly influence the catalytic deoxygenation reaction. Gosselink et al. evaluated the effect of the solvent by comparing *n*-decane, *n*-dodecane, and mesitylene and reported that *n*-decane and mesitylene led to better catalytic activity than n-dodecane[75]. Low-boiling solvents guarantee better activity[125, 180]. The solvent can also modulate the activity of the catalysts, since Pt/C is more active than Pd/C in the CDO of free fatty acids in aqueous media while the opposite is the case in organic media[110, 181].

1.6 Emission characteristics of Green Diesel.

As mentioned earlier, green diesel brings significant benefits, including emission reduction. Neste Oil reported an exhaustive study on the emissions produced by their renewable diesel in several vehicles, both pure and blended formats[182]. In each case, a decrease in CO, CO_2, unburned carbon (HC), NO_x and PM emissions is reported compared to the EN 590 standard; there is a 27% decrease in CO in the case of trucks and buses, and 38% (neat renewable diesel) and 45% (blended) in the case of passenger's cars. In addition, emission reductions of 4-6% CO_2, 31-55% HC, 1-9% NO_x, and 13-30% PM were observed[182]. Similar results were obtained by Krumar et al.; in this case, the authors correlate the reduction in pollutant gas emissions to two reasons: 1) green diesel mixes better with air by promoting complete combustion (thus less CO and HC). 2) The higher cetane number of green diesel reduces the rate of heat release in the cylinder and reduces the maximum flame temperature in the cylinder, favoring lower pollutant gas emissions (lower temperatures inhibit dissociation of CO_2 to CO and formation of NO_x)[183]. Compared to petroleum-derived diesel, Pflaum et al. observed a 50% reduction of HC by using neat green diesel and correlated this with the lack of aromatic compounds in this biofuel[184]. Erkkila et al. have studied the effect on the emission of isomerized Green Diesel, and they report that neat renewable diesel reduces the emission of NO_x, PM, CO and HC of 10%, 30%, 29% and 39% respectively; In addition, by using a blend of green diesel and gasoline, emissions decrease as the green diesel content increases [185].

Chapter 2. Results and discussions.

The first part of the chapter provides an overview of the aim of the work and how we approached the research work. After that, a general description of the catalytic systems studied and how we tested them in the catalytic deoxygenation reaction is presented. In addition, a description of the catalyst characterization techniques and the analysis techniques of the reaction mixtures obtained after the catalytic tests are given. Finally, all the data obtained, and observations related to the results achieved after catalytic tests are reported.

2.1 Aim of the work.

In the introduction chapter, we have seen that the transport sector consumes large amounts of petroleum derivatives with a heavy impact on CO_2 atmospheric concentration; it is reported that road transport accounts for over 15% of total energy-related CO_2 emissions[25]. According to this, the research on renewable and environmentally friendly biofuels is part of the strategy to reach carbon neutrality. Mineral diesel is one of the most widely used fuels. Therefore, we believe that green diesel is a viable solution to limit fossil fuel consumption.

Another alternative to fossil fuels is electricity; from the environmental point of view, electricity in the transport sector greatly contributes to CO_2 emissions reduction. However, they have several drawbacks. like limited battery capacity, lack of charging infrastructure, and electricity production are still highly dependent on the use of fossil fuels. All this evidence does not make the electric engine a viable alternative in the short period. On the other hand, biofuels are produced from renewable resources, use existing infrastructure and are more efficient. For this reason, biofuels and green diesel represent a more valuable alternative for the short period.

Of course, to completely replace petroleum-derived diesel and thus contribute to carbon neutrality, the green diesel production process must be sustainable, starting from the raw materials to the final product. For this reason, research on green diesel synthesis must be implemented.

As stated in the opening chapter, the nature of the catalyst is one of the main parameters affecting the CDO reaction; therefore, this thesis work is focused on the development of new catalysts that are inexpensive, green, and active at the mildest possible reaction conditions.

2.1.1 Catalysts choice.

The first question we asked ourselves was about the choice of catalysts, and our goal was to synthesize economic and eco-friendly catalysts.

The first objective was to assess which metals might be most efficient. From the literature reviewed in the opening chapter, we saw that noble metals such as Pd and Pt are very active in the CDO reaction[89, 186-192].

Usually, these catalysts are effective after activation via reduction and often lead to high conversions and green diesel yields; however, noble metal-based catalysts are very expensive, reducing the economic viability of the whole process. For this reason, we opted to use less valuable metals. Metals such as Ni, Co, Mo and, W are often used in the CDO of vegetable oils, but unlike noble metals, they are activated via sulfidation; in this state, they have similar activities to those of noble metals[127, 138, 139, 193-197]. Despite this, these catalysts have a significant drawback; they produce biofuels with higher sulfur content and, thus, higher SO_x emissions from their combustion. Given the activity of these metals, we chose to use them for our catalysts, preferring activation via reduction (avoiding sulfur contamination).

In case of supported catalysts, the nature of the support is also essential for the activity of the catalyst. Generally, catalysts for DCO are supported-metal catalysts. The most used supports are metal oxides (Al_2O_3, TiO_2, ZrO_2, SiO_2), silicoaluminophosphate materials (SAPO), and zeolites; these materials are often obtained synthetically through more or less expensive syntheses and with the use of organic solvents[116, 117, 122, 128, 137, 145, 151]. Therefore, wanting to maintain a green approach, we have chosen supports representing a green and economical alternative to the supports commonly used for CDO catalysts' synthesis.

After making these considerations, we chose to study the following catalytic system:

- *Fly ash cenosphere (FACs) supported catalysts*: FACs are a by-product of coal combustion. FACs are a potentially polluting material, and their disposal involves high costs. Therefore, synthesizing supported catalysts on FACs is a sustainable way to use this waste material. In addition, FACs have chemical characteristics that make them a good support for the synthesis of heterogeneous catalysts; in particular, chemical inertia and thermal resistance make FACs an excellent material for catalyst's synthesis used in various reactions such as transesterification for biodiesel synthesis, condensation, oxidation, and reduction[198-203]. However, to the best of our knowledge, FACs have yet to be used in the catalytic deoxygenation reaction. In addition, being rich in SiO_2 and Al_2O_3, FACs are also used for zeolites synthesis. As seen in the opening chapter, several works report the use of zeolites in the catalytic deoxygenation reaction with excellent results, so we decided to use also zeolites derived from FACs as support for catalyst synthesis. In addition, the zeolitization of FACs enhances the surface area of the material, as well as the acidity, and this could be positive for the activity of the resulting catalyst. Thus, FACs and Zeolites are used as supports and several metals like Ni, Co, Mo, W, Ca, La, and Ce are chosen to impregnate the supports.

- *Layered double hydroxides (LDH) derived catalysts*: Layered double hydroxides are anionic clay with layered structure and with the general formula $[M(II)_{1-x}M(III)_x(OH)_2]^{x+}(A^{n-}_{x/n}) \cdot mH_2O$ where M(II) and M(III) are the bivalent and trivalent metal, respectively, A is the counterion needed to counterbalance the positive charge of the layers, and x = M(III)/(M(II)+M(III))[204]. LDH catalysts were chosen as they have several positive characteristics. They are highly versatile materials; by varying the bivalent and trivalent metals and the stoichiometric ratio between them, several catalysts can be synthesized for different applications [205-208]. In contrast, only a few papers report using of LDHs catalyst for the CDO of vegetable oil[209-211]. Moreover, LDHs have good ion-exchange capacities, which allowed us to synthesize a wider pool of catalysts by introducing a third metal, such as Mo, W, and V, through an ion-exchange reaction. In addition, we chose these catalysts because they have green characteristics; water is used as a solvent for their synthesis and they are also eco-friendly and nontoxic materials[212, 213].

2.1.2. Research guidelines.

Once we figured out the catalysts to study, we began to plan the work to be done. As a first step, we wanted to study FACs-supported catalysts attracted by the idea of using a waste material. Therefore, we synthesized a series of FACs and zeolites-supported catalysts through the wet impregnation method by impregnating on support different metals such as Ni, Mo, Co, W, La, Ce and Ca. After this, catalyst screening was performed to evaluate the most active catalyst; therefore, operating conditions were set, and all catalysts were tested. Found the most efficient catalyst, it was used to carry out further studies. Therefore, studies were

carried out on the effect of solvent and recycling stability of the catalyst for multiple catalytic cycles. In addition, since the starting feedstock can also play an important role in the green diesel synthesis process, we also studied the activity of the catalyst with different oils. After these catalytic studies, the catalyst was characterized to identify its physico-chemical characteristics. Finally, we have carried out a brief study on the activity of a differently synthesized and activated FACs-supported catalyst; this catalyst shows high activity, so we plan to perform further studies on this catalyst in the future.

After studying FACs-supported catalysts, we investigate LDHs catalysts. Initially, we synthesized a Ni, Mo Al-based LDH catalyst and evaluated its activity as a function of reaction conditions; the effects of temperature, pressure, and catalyst wt% were then investigated. Having found the best reaction conditions, other parameters, such as reaction time and the reduction time for catalyst activation, were also studied. In addition, we also tested the catalyst activity without the reduction activation, and the results showed high activity even without the reduction step. Observing the high activity of this catalyst, we synthesized other LDH-derived catalysts by varying the metals and the molar ratio between them. Two different catalytic screenings were carried out, one by analyzing the activity of the catalysts after reduction and one by studying the activity of the catalysts without the reduction step (i.e., in the oxidized state). These analyses provided interesting information on the effect of the different metals used and the effect of the catalyst activation method. As in the case of FACs-supported catalysts, the most efficient catalyst was characterized.

2.2 Synthesis of the catalysts.

As previously noted in this Ph.D. thesis research, different formulations of two classes of materials were studied:

- *Fly ash cenosphere (FACs) and Zeolites-supported catalysts.*
- *Layered double hydroxide (LDH) derived catalysts.*

FACs and Zeolite (obtained from FACs) are used as supporting material and are impregnated with different active metals, while layered double hydroxides are synthesized by varying their constituent metals. A brief introduction to these two classes of materials and the synthetic methodologies used for catalyst synthesis will be discussed below.

2.2.1. Fly Ash Cenosphere (FACs) and Zeolites-supported catalysts.

2.2.1.1 About FAC.

Fly Ash Cenosphere (FACs) are components of coal fly ash (CFA), a waste product derived from coal combustion in power plants. CFA accounts for 80% of the by-products generated by coal combustion. Considering that coal still accounts for 27% of global energy demand, large amounts of CFA are generated annually (about 750 Mt of fly ash)[9, 214, 215]. Currently, between 10 and 30% of the CFA produced is recycled while the rest is disposed of, implying costs, large landfill sites and thus environmental pollution (the presence of metal oxides and toxic organic substances make fly ash a highly polluting waste)[214, 216]. From the above, recycling fly ash, and thus FACs, leads to significant environmental benefits.

CFA are produced in coal-fired power plants between 1200°C and 1700°C and are composed of four components, namely unburned carbons, cenospheres (FACs), magnetite, and solid fraction [214]. The composition of FACs is highly variable and depends significantly on the

type of coal burned and the transformations that occur during combustion (to date, 316 individual minerals and 188 mineral groups have been found in different fly ash)[217, 218]. FACs consist mainly of aluminosilicates, SiO_2 (50-67wt%) and Al_2O_3 (20-36wt %), and the rest comprises oxides of various metals such as Fe, Ca, Mg, Na, Ti, and K. They are classified into two classes, class F and class C. Class F includes CFA and FACs in which the content of SiO_2, Al_2O_3, and Fe_2O_3 is greater than 70%, while, in class C, the content of these oxides is between 50 and 70%[219]. Morphologically, FACs are characterized by spherical particles ranging from 5 to 500 µm (Figure 10)[220, 221].

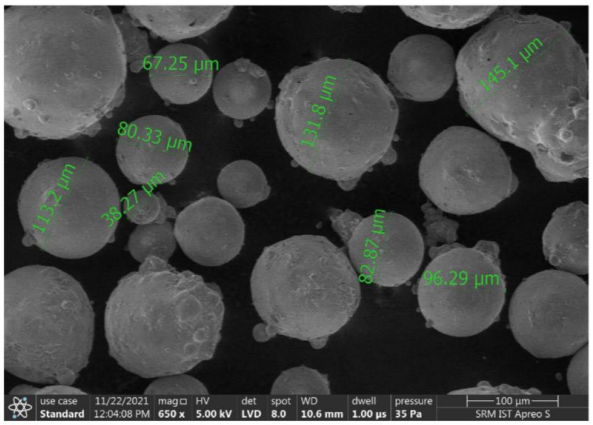

Figure 10. SEM image of fly ash cenosphere[221]

As previously stated, FACs are rich in Al_2O_3 and SiO_2, making it an excellent substrate for the synthesis of zeolites. Zeolites are synthetic aluminosilicate crystals with regular micropores (with a framework in which $[SiO_4]^{4-}$ and $[AlO_4]^{5-}$ tetrahedra are linked by sharing their oxygens) with excellent catalytic and ion exchange properties and widely used in the energy, chemical industry, and other fields[222].

There are two main methods for zeolite synthesis from CFA and FACs; the alkali dissolution method and the alkali fusion method[198, 219, 222, 223].

In this thesis work, zeolites were synthesized by the alkali fusion method, which involves mixing FACs with alkali, typically sodium hydroxide (NaOH), and fusing them (~550 ◦C). Sodium silicate (Na_2SiO_3), sodium aluminate ($NaAlO_2$), and sodium aluminosilicate ($NaAlSiO_4$) are formed, and the remaining unburned carbon gets oxidized to carbon dioxide. After that, the solid mixture is hydrothermally treated; at this stage, sodium silicate and sodium aluminate are dissolved in a hot alkaline solution and, the process of nucleation and crystallization to form zeolites begins[219].

2.2.1.2 Synthesis of FACs-supported catalysts.

The FACs used in this work were obtained from a coal-fired power plant located in Kolkata (India). Before being used, the FACs are treated with an acid solution to remove impurities and soluble metals [224]. Catalysts are then prepared via excess wet impregnation; this method is particularly attractive from the perspective of Green Chemistry because it is technically simple and safe, produces low amounts of waste, and is inexpensive[225]. This method involves dissolving the metal precursor within an aqueous or organic solution where the support is immersed[226]. The solution containing the precursors will penetrate inside the support by capillary action (the ability of a liquid to flow within small spaces without the assistance, and often even in opposition, of external forces such as gravity) [227]. The solubility of the precursor in the solution limits the maximum amount of metals that can be loaded. The concentration of metals in the support depends on the transfer conditions into the support pores during impregnation and drying [227].

Briefly, catalysts were prepared by dissolving the chosen quantities of metal salts in an aqueous suspension containing FACs. Metal nitrates were chosen as salts because they are

highly soluble in water, inexpensive, and easily decompose[225]. Once the impregnation step is completed, the water is removed by evaporation, and the solid is dried. We preferred to avoid filtration to prevent that some of the metal salts could be washed from the support during the washing steps used in filtration. The catalyst is then calcined (at the decomposition temperature of the metal salts used) to convert them into their corresponding oxides. Finally, to obtain the active form of the catalyst, it is reduced in a tubular fixed-bed reactor in a flow of H_2/N_2. The reduction conditions were chosen after H_2 consumption analysis with an ABB gas analyzer. Essentially, the ABB gas analyzer is an analyzer placed downstream of the tubular fixed-bed reactor that measures the H_2 consumption and, thus, the hydrogen used by the catalyst during reduction; therefore, when the temperature required for reduction is reached, the system will monitor a decrease in H_2 indicating the reduction temperature. After reduction, the catalysts are stored in containers where Ar is added to maintain an inert atmosphere and avoid possible oxidation. The catalysts are labeled as MNX (m/n/x)/FAC where M, N, and X are the metals impregnated on the supports, while m, n, and x are the nominal wt% (as oxides) of the corresponding metals.

Using the described synthetic process, we synthesized six catalysts, three bimetallic and three trimetallic, supported on cenospheres impregnating metals such as Ni, Mo, Co, W, Ca, Ce, and La (Table 5).

Table 5. FACs-supported catalysts synthesized.

Catalyst[1]	Calcination conditions[2]	Reduction conditions[3]
NiMo (5/15)/FAC	400°C (5°C/min), 4h	700°C (5°C/min), 3h
CoMo (6/15)/FAC	600°C (5°C/min), 4h	800°C (10°C/min) 3h
NiW (5/15)/FAC	600°C (5°C/min), 4h	800°C (10°C/min) 3h
NiMoCe (5/15/5)/FAC	400°C (5°C/min), 4h	820°C (5°C/min), 3h
NiMoCa (5/15/20)/FAC	800°C (20°C/min), 4h	700°C (5°C/min), 3h
NiMoLa (5/15/5)/FAC	800°C (10°C/min), 4h	800°C (10°C/min) 3h

[1]The wt% of the metals is referred to as the wt% of their oxide.
[2]Chosen after a literature review on the decomposition temperature of the used salts [228-232].
[3]Chosen after ABB analysis.

Ni, Mo, Co, and W were chosen because they were cheaper than the noble metals and because, as described in the introductory chapter, they are particularly active in CDO. We synthesized three bimetallic catalysts from the combination of these metals supported on FACs. On the other hand, trimetallic catalysts were synthesized by adding a third metal, Ca, Ce, and La, to the NiMo combination to evaluate how the third metal affects the catalytic activity.

As an example, let us consider NiMo (5/15)/FAC catalyst. The amounts of nitrates used for the wet impregnation were chosen to ensure that, after calcination, the resulting catalyst has a nominal weight% of NiO and MoO_3 of 5wt% and 15wt%, respectively. These quantities were chosen after preliminary studies performed on other FACs-supported catalysts with lower percentages (studies addressed during my master's thesis). From these studies, we have observed that smaller amounts of supported metals are insufficient for the complete conversion of vegetable oils. For the calcination step, the thermal conditions were chosen considering the decomposition temperature of $Ni(NO_3)_2 \cdot 6H_2O$ and $(NH_4)_6Mo_7O_{24} \cdot 4H_2O$. From a literature review, these salts decompose into NiO and MoO_3 around 350°C; therefore,

to ensure complete decomposition, we set the calcination conditions at 400°C for 4h [228, 229]. Finally, the reduction conditions were chosen after ABB analysis (as described above). From the ABB analysis of a small amount of NiMo (5/15)/FAC, we observed H_2 consumption between 450°C and 630°C; therefore, to ensure a complete reduction of Ni we have set the reduction conditions at 700°C for 3h. The same approach was adopted for the synthesis of all other catalysts.

2.2.1.3 Synthesis of FACs-derived Zeolites-supported catalysts.

Before synthesizing the Zeolites-supported catalysts, FACs were converted to zeolites by the alkali fusion method proposed by Sutarno and Arryanto[224]. FACs were fused with NaOH in a muffle furnace, and alumina and silica were converted into a soluble form namely sodium silicate (Na_2SiO_3), sodium aluminate ($NaAlO_2$), and sodium aluminosilicate ($NaAlSiO_4$). The resulting solid is suspended in H_2O milli-Q to solubilize the silicates and aluminates and then aged in H_2O overnight. At this point, the suspension is hydrotreated and then the resulting zeolites were filtered and dried. The metals are then impregnated in the zeolite support via excess wet impregnation in the same way described for FACs-supported catalysts. To evaluate the effect of the different support used, the catalysts were synthesized with the same metals and amounts used for the synthesis of the FACs-supported catalyst. The calcination conditions used are the same as those used for the corresponding FACs-supported catalysts. The reduction conditions have been evaluated with the ABB gas analyzer in the same way described above (the support can affect the reduction temperature of supported metals). The catalysts are labeled in the same way used for FAC-supported catalysts, namely MNX (m/n/x)/Zeo where M, N, and X are the metals impregnated on the supports, while m, n, and x are the nominal wt% of the corresponding metals oxides.

Another catalyst was prepared by a slightly different method. FACs are first impregnated with Ni and Mo to obtain NiMo (5/15)/FAC (in the same way described for FACs-supported catalysts). Before being calcined, the catalyst undergoes zeolitization treatment as described in this section. At this point the catalyst is calcined (under the same conditions used for the other Ni- and Mo-based catalysts) and then batch reduced (thus using a different reduction method than that used for the other catalysts). This catalyst is synthesized with the idea of growing zeolite around the metal (thus acting as a templating agent) to obtain a metal phase more intimately bonded to the support. This catalyst is labeled NiMo (5/15)/FAC-Zeo. All the zeolites-supported catalysts synthesized are presented in Table 6, and the calcination and reduction conditions reported in the table are the same used for the FACs-supported catalysts.

Table 6. Zeolites-supported catalysts synthesized.

Catalyst[1]	**Calcination conditions**[2]	**Reduction conditions**[3]
NiMo (5/15)/Zeo	400°C (5°C/min), 4h	700°C (5°C/min), 3h
NiW (5/15)/Zeo	600°C (5°C/min), 4h	750°C (5°C/min), 3h
NiMoCe (5/15/5)/Zeo	400°C (5°C/min), 4h	720°C (5°C/min), 3h
NiMoCa (5/15/20)/Zeo	800°C (20°C/min), 4h	780°C (5°C/min), 3h
NiMoLa (5/15/5)/Zeo	800°C (10°C/min), 4h	850°C (10°C/min) 3h
NiMo (5/15)/FAC-Zeo	400°C (5°C/min), 4h	320, 60bar H_2, 8h[4]

[1] The wt% of the metals is referred to as the wt% of their oxide.
[2]Chosen after a literature review on the decomposition temperature of the used salts[228-232].
[3]Chosen after ABB analysis.
[4] Catalyst reduced in batch.

2.2.2 Layered double hydroxides (LDH) based catalysts.

2.2.2.1 About LDH.

Layered double hydroxides are anionic clay with layered structure and with the general formula $[M(II)_{1-x}M(III)_x(OH)_2]^{x+}(A^{n-}_{x/n}) \cdot mH_2O$ where M(II) and M(III) are the bivalent and trivalent metal respectively, A is the counterion needed to counterbalance the positive charge of the layers, and x = M(III)/(M(II)+M(III))[204]. The sheet structure is very similar to $Mg(OH)_2$ layered brucite structure, but, in this case, the bivalent cations (Mg) are partially replaced by trivalent cations; the presence of the M(III) cations generates a positively charged layers that are counterbalanced by compensatory anions placed in the interlayer space. M(II) and M(III) metals are at the center of edge-sharing octahedra, and at the vertices of the octahedrons there are hydroxide ions that can interact via hydrogen bonds with ions in the interlayer[233, 234]. Figure 11 shows a schematic representation of the LDH structure.

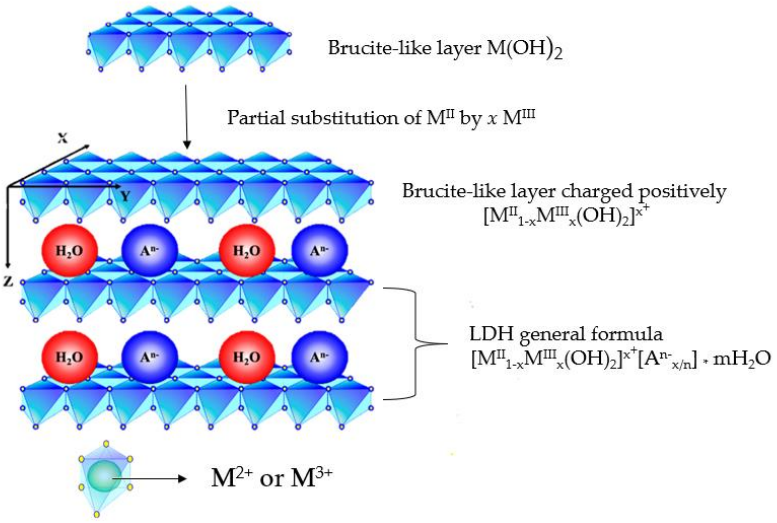

Figure 11. LDH structure (readapted from[235]).

Divalent metal ions commonly used in these structures include Mg^{2+}, Ni^{2+}, Zn^{2+}, Cu^{2+}, Mn^{2+}, Fe^{2+}, Co^{2+}, and Ca^{2+}; examples of trivalent cations include Al^{3+}, Fe^{3+}, Cr^{3+}, Mn^{3+}, Ga^{3+}, Co^{3+}, Eu^{3+} and V^{3+}(to replace the divalent metal, the atomic radii of M(III) must be similar to that of M(II))[213]. The most common compensating anion is CO_3^{2-} due to the high affinity of LDHs for this anion. However, it is possible to introduce other anions, such as inorganic anions (Cl^-, SO_4^{2-}, NO_3^-, etc.), organic ions (acetate, dodecyl sulfate, terephthalate, etc.), or polyoxometalates ions[236-238].

We have chosen this catalytic system because LDHs materials have several interesting properties:

- *Green catalyst*: LDHs are ecofriendly and nontoxic materials (in fact, they are used as carriers of biologically active molecules), and their synthesis uses water as a solvent [212, 213].
- *Tunability*: Many LDHs can be synthesized by varying bivalent and trivalent metals, and, therefore, they can be used for different applications[239].
- *Ion exchange capacity*: LDHs are materials with high ion exchange capacity, and, for this reason, they are used for wastewater treatment and pollutant removal. In addition, by exploiting this feature, it is possible to add another metal with catalytic properties of interest[213, 240, 241].
- *Suitable properties for catalysis*: after calcination, the LDHs are converted in homogeneous mixtures of oxides with high surface area and small crystal size (also stable to thermal treatments), which by reduction form small and thermally stable metal crystallites[234].
- *Memory effect*: The properties of LDHs that allows the reconstruction, under mild conditions, of the original LDHs structure when contacting the calcined LDHs with water solutions containing various anions[233].

For our purpose, LDHs represent an excellent subject to study. They are synthesized easily and greenly way since water is used as the solvent. In addition, their versatility allows us to synthesize LDHs with different metals so that we can evaluate the effect of metal type on the activity of the resulting catalysts.

There are several methods to synthesize LDHs, and the main ones involve pH-induced co-precipitation (precipitation at high supersaturation, precipitation at low supersaturation and urea hydrolysis)[242, 243].

In this thesis, LDHs were synthesized by the low supersaturation co-precipitation method; the solution containing the metals and the solution containing the base required for precipitation (usually NaOH) are slowly added to the reaction solvent (H_2O), and the pH of the solution is kept constant at the desired value by adjusting the addition of base to the solution containing the metals[244]. This method produces more crystalline LDHs than other pH-induced precipitation methods[244].

2.2.2.2 Synthesis of layered double hydroxides.

LDH catalysts were prepared in two steps. In the first step, four NiAl LDHs precursors and one CoAl precursor were prepared. Three NiAl LDHs precursors were prepared according to the co-precipitation method proposed by Arias et al.[245]. The quantities were used to synthesize LDHs having the formula $Ni_{(1-x)}Al_x(OH)_2(C_8H_6O_4)_{x/2} \cdot nH_2O$ with three different Ni/Al molar ratios (Ni/Al = 2.33, 0.63, 0.25 and x = 0.30, 0.61, 0.80).

Two solutions, one containing the Al and Ni salts (in the chosen Ni/Al molar ratios) and one containing NaOH and terephthalic acid, were dropped into a flask containing H_2O milli-Q. Precipitation is carried out by keeping the pH in the range of 6.3-6.8 and under continuous stirring. Carbonate ion is one of the most affine anions to LDHs therefore, to avoid carbonate formation and to ensure the intercalation of the terephthalate ion, the solution is kept under

continuous bubbling of Ar. Terephthalate was chosen as the intercalating ion to ensure an interlayer space large enough to allow subsequent ion exchange with large-sized ions such as polyoxometalates[246]. At the end of the co-precipitation step, the mixture was aged for 16h at room temperature; the resulting solid was then filtered and dried.

In this way, three NiAl LDHs precursors were synthesized and are named NiAl LDH (m) (where m is the nominal M(II)/M(III) ratio, m = 2.33, 0.63 or 0.25). At this point, a third metal (Mo or W) is introduced into the LDH structure via ion exchange between terephthalate and $(NH_4)_6Mo_7O_{24} \cdot 4H_2O$ or $(NH_4)_6W_{12}O_{39} \cdot xH_2O$[247]. To perform the ion exchange reaction, the LDH precursor was suspended in a solution containing $(NH_4)_6Mo_7O_{24} \cdot 4H_2O$ or $(NH_4)_6W_{12}O_{39} \cdot xH_2O$ (the amount was set to 50% excess with respect to the stoichiometric amount required) and hydrothermally treated under continuous stirring for 24h. After this, the solid was filtered and dried. At this stage, the catalyst is labeled NiMeAl LDH (m) where Me is the metal added via ion exchange, and m is the nominal M(II)/M(III) ratio (m = 2.33, 0.63 or 0.25). Once dried, the catalyst was calcinated in a muffle furnace at 450°C (10 °C/min) for 3h. After calcination, the catalyst is named NiMeAl (m) C., where C. means "calcined". Before the DCO reaction, the NiMoAl (m) C. catalyst was reduced in batch at 320°C, 60bar and for the desired reduction time; in this state, the catalyst is labeled NiMeAl (m) R. where R. means "reduced".

The CoAl precursor was synthesized according to Coelho et al[248]. Co-precipitation was carried out in a very similar way to that done for NiAl LDH precursors; The Co/Al molar ratio chosen is 0.63, and the co-precipitation was performed by continuous Ar bubbling and maintaining the pH in the range between 6.3-6.8; however, in this case, the precipitation was performed at a higher temperature while the aging step was conducted for 48h under continuous stirring. Work-up, ion exchange, calcination, and reduction were performed in

the same ways described above for the NiAl precursors. CoAl-based catalysts are labeled in the same way done for NiAl catalysts.

The fourth NiAl precursor was synthesized using the urea co-precipitation method proposed by Pancrecious et al[249]. Ni and Al nitrates, and urea (in a 2:1:7 ratio) were dissolved in H_2O milli-Q, and the solution was stirred and heated under reflux conditions for 24 hours in an Ar atmosphere. In this case, the pH was checked at the end of the reaction and must have a value of 7.4. After that, the solid was filtered and dried. The resulting material is named NiAl LDH (UR) (where UR means urea). The NiAl LDH (UR) precursor undergoes ion exchange with NH_4VO_3, and the reaction was performed by adding the NiAl (UR) precursor to a 0.02M solution of NH_4VO_3. Ion exchange was carried out under an Ar atmosphere and at room temperature for 24h. The catalyst was then dried, calcined (in this state, the catalyst is named NiVAl (UR) C.), and activated by reduction in batch (now the catalyst is labeled NiVAl (UR) R.).

Table 7 reports all the LDH-based catalysts synthesized in this thesis work.

Table 7. LDH-based catalysts synthesized.

Catalyst[1]	Me^{2+}	Me^{3+}	Me from the ion exchange	Me^{2+}/Me^{3+} (molar)	x[2]	Me^{2+}/Third metal
NiAl (0.25)	Ni	Al	-	0.25	0.80	-
NiAl (0.63)	Ni	Al	-	0.63	0.61	-
NiAl (2.33)	Ni	Al	-	2.33	0.30	-
NiAl (UR)	Ni	Al	-	2	0.33	-
CoAl (0.63)	Co	Al	-	0.63	0.33	-
NiMoAl (0.25)	Ni	Al	Mo	0.25	0.80	0.21
NiMoAl (0.63)	Ni	Al	Mo	0.63	0.61	0.57
NiMoAl (2.33)	Ni	Al	Mo	2.33	0.30	2.2
NiWAl (0.63)	Ni	Al	W	0.63	0.61	0.33
NiWAl (2.33)	Ni	Al	W	2.33	0.30	2
NiVAl (UR)	Ni	Al	V	2	0.33	2.3
CoMoAl (0.63)	Co	Al	Mo	0.63	0.33	0.57
CoWAl (0.63)	Co	Al	W	0.63	0.33	0.33

[1]All the catalysts were calcined at 450 (10°C/min) for 3h and reduced in batch at 320°C, 60bar H_2, and at the desired reduction time.

[2]x = Me (III)/(Me (III)+Me (II)).

2.3 Catalyst characterization techniques.

After synthesis, the catalysts that showed higher activity was characterized to identify the physico-chemical characteristics of the material.

The characterization techniques used are as follows.:

- *Inductively coupled plasma-mass spectrometry (ICP-MS).*
- *Surface area and porosity analysis (BET-BJH method).*
- *Powder X-ray diffraction (XRD)*
- *Fourier-transform infrared spectroscopy (FT-IR)*

This section will provide a short description of the fundamentals of these techniques and the purpose of their use.

2.3.1 Inductively coupled plasma-mass spectrometry (ICP-MS).

To assess the elemental composition of the catalysts and, thus, the effective concentration of the active metals, inductively coupled plasma-mass spectrometry (ICP-MS) was performed. From this analysis, we can then determine the real amount of metals in the catalyst.

Typical ICP-MS apparatus consists of six component: a system for sample introduction, a nebulization system, the inductively coupled plasma (ICP), an interface, a mass analyzer, and a detector (Figure 12)[250].

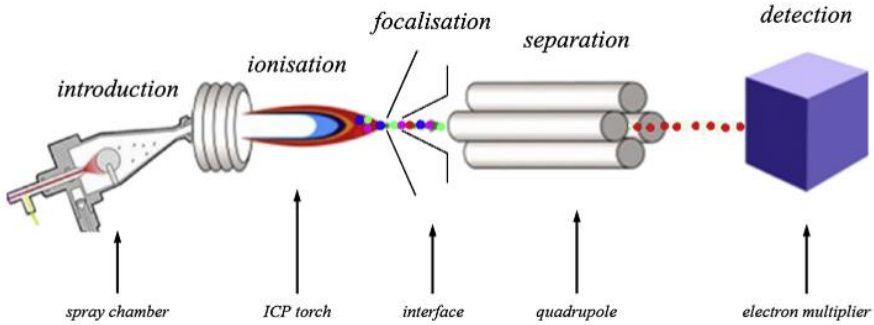

Figure 12. ICP-MS configuration[250].

The most common configuration for sample introduction uses an autosampler and a peristaltic pump to deliver the sample to the nebulizer. Now the nebulizer transforms the liquid sample into a spray. After being aerosolized, the sample enters the spray chamber that selectively filters out the larger aerosol droplets generated by the nebulizer and smooths out nebulization 'pulses' produced by the peristaltic pump. The nebulized sample is then sent to the ICP compartment in which is present the argon plasma (plasma is essentially an ionized gas consisting of positively charged ions and free electrons). The plasma is formed at the end of three concentric quartz tubes, collectively referred to as the torch. After reaching the high-temperature plasma, the sample is desolvated, vaporized, atomized, and ionized. Now Ar flow drives the ions in an interface system that focuses them toward the mass spectrometer. In the mass spectrometer, the ions are separated according to their m/z ratios and finally directed to the detection system in which an electron multiplier transforms ion signals into electric pulses that are computing with a computer.

2.3.2 Surface area and porosity analysis.

The textural properties, surface area, pore volume, pore diameter, and pore size distribution of the materials studied are determined via N_2 physisorption and BET-BJH analysis.

BET (Brunauer-Emmett-Teller) analysis is based on the phenomenon of the physisorption of an inert gas, usually N_2. Through the experimental measurement of the N_2 physisorption isotherms (the change in adsorptive capacity with respect to the partial pressure of the gas) at the boiling temperature of N_2 (77K), it is possible to determine when a statistical monolayer has been reached (i.e., when in the isotherm the amount of gas adsorbed is equivalent to covering a single layer). Knowing the number of gas molecules required to cover the surface of the solid with a monolayer and the area occupied by a single molecule, it is possible to calculate the surface area of the solid under consideration[251, 252]. The BET method is based on four assumptions:

- The heat adsorbed by the first layer is constant.
- The interaction between adsorbed molecules in the same layer can be neglected.
- The adsorbed molecule can form a new absorbing surface making the process continuous.
- The heat of adsorption for all other layers, after the first, is equal to the heat of liquefaction.

The BET isotherm can be expressed in its linear form as in Equation 1:

$$\frac{P/P_0}{n(1-P/P_0)} = \frac{1}{n_m C} + \frac{C-1}{n_m C}(P/P_0) \qquad \textit{Equation 1}$$

Where P and P_0 are the equilibrium and the saturation pressure of nitrogen at the temperature of adsorption, n is the quantity adsorbed, n_m is the amount of gas adsorbed on the monolayer, and C is the BET constant of the material expressed with Equation 2:

$$C = \exp\left(\frac{E_m - E_L}{RT}\right) \qquad \textit{Equation 2}$$

Where E_m is the heat of adsorption for the monolayer, E_L is the heat for the second and higher layers and is equal to the heat of liquefaction or heat of vaporization. The C expression can be applied only in the range $0.05<P/P_0<0.3$ of the BET isotherm (defined as linear BET plot) and finding the intercept and the slope in this range is possibly known C and thus n_m. Knowing these values, the surface area can be calculated utilizing Equation 3.

$$S_{BET} = \frac{n_m N_A \sigma_m}{m} \qquad \textit{Equation 3}$$

Where: σ_m is the molecular cross-sectional area (0.162 nm^2 for N_2), N_A is the Avogadro number, and m is the sample's mass.

From the BET isotherm is also possible to perform the BJH mesoporosity assessment. The BJH method is based on two assumptions:

- All the pores have a cylindrical shape.
- There are no interconnected pores.

Based on these assumptions, BJH (Barrett-Joyner-Halenda) method exploits the Kelvin equation (Equation 4) that correlates the pore radius with the partial pressure that causes N_2 adsorption and desorption in the pores.

$$\ln\frac{P}{P_0} = -\frac{2\gamma V_l}{r_k RT}$$ *Equation 4*

Where γ is the surface tension, V_l is the molar volume, R is the universal gas constant, T is the temperature of the adsorption/desorption measure, r_k is the Kelvin radius (radius of that pore having the most probable volume)[253]. By the Kelvin equation and BJH method, an integral (i.e., cumulative) V=f(d) results. This curve is then differentiated to get the correspondent diameter distribution curve.

2.3.3 X-ray diffraction.

The phase composition of catalysts has been determined with powder X-ray diffraction technique.

A typical XRD diffractometer is composed of six main components (Figure 13) [254]:

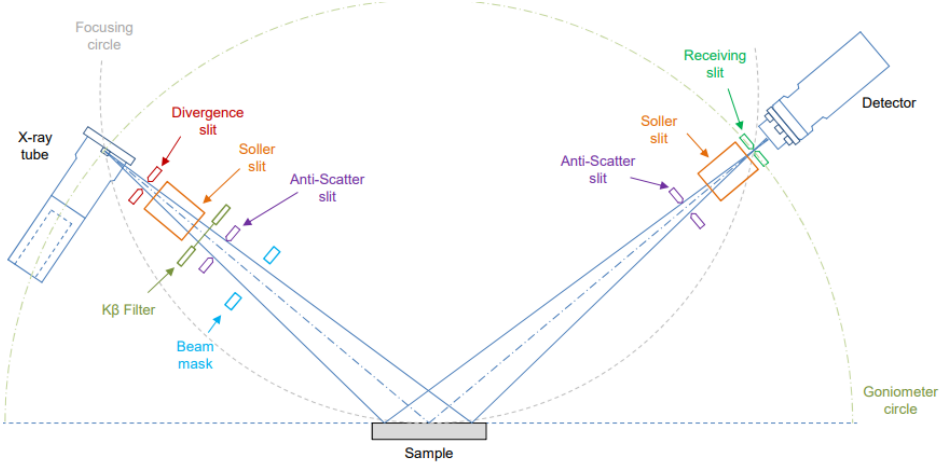

Figure 13- Schematic representation of an XRD with Bragg-Brentano geometry

- X-ray source: X-ray photons are generally produced via high-voltage acceleration (generally 20 and 60 kV) of the electrons emitted from a tungsten filament.
- Primary optics: once the X-rays are produced, they are directed to the primary optics that are designed to collimate the beam and select the desired wavelength that should impact the sample.
- Sample holder: this is the part of the instrument where the sample is placed.
- Secondary optics: are placed between the sample and the detector. They are used to collimate the diffracted beams from the sample and direct them to the detector.
- Detector: there are several types of detectors, but each is dedicated to converting incoming diffracted beams into an electrical signal that can be analyzed.
- Goniometer: allows the X-ray source, sample, and detector to be moved precisely so that the X-rays cover a wide θ range. In typical Bragg-Brentano geometry, the X-ray source and sample are fixed while the detector rotates at a velocity of 2θ relative to the sample.

XRD analysis is based on the diffraction phenomenon that occurs when X-ray photons impact a crystal structure[254]. When X-ray photons impact the atoms of the material, several interactions can occur; however, the diffraction phenomenon occurs only when a constructive interference between the incident beam and the beam elastically scattered by the material takes place [254]. The diffraction phenomenon obeys Bragg's law (Figure 14, Equation 5)

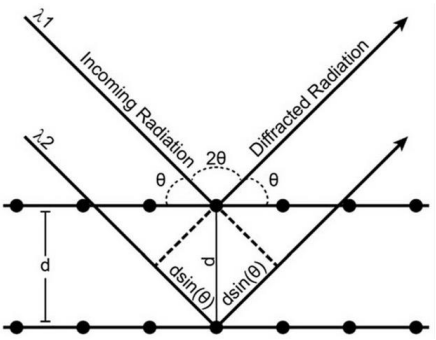

Figure 14. Bragg's Law Reflection.

$$2dsin\theta = n\lambda$$ *Equation 5*

Where d is the interplanar distance, θ is the scattering angle, λ is the wavelength of the incident wave, and n is a positive integer number.

By varying the angle θ, Bragg's law is satisfied for different distances d in crystalline materials. The result is a diffractogram that shows peaks related to the different crystalline phases of the sample. Each material has its characteristic diffractogram that can be identified by comparison with reference standards. Among the different XRD techniques, the catalysts studied in the present work were analyzed with the powder XRD (PXRD) technique. PXRD is a non-destructive technique that provides information about the crystal structure, phase composition, and other properties of a material. It is a relatively fast and simple technique, requiring minimal sample preparation. PXRD has high sensitivity to small changes in crystal structure, and it can analyze a wide range of sample types. However, it is less effective at analyzing samples with large unit cells or those containing heavy elements. Additionally, PXRD cannot provide information about the arrangement of atoms within a crystal[255].

2.3.4 Fourier-transform infrared spectroscopy (FT-IR).

The FT-IR measurements are performed with a PerkinElmer Spectrum instrument working in ATR (attenuated total reflection) mode.

When infrared radiation interacts with matter, it causes vibrational transitions at the molecular level; as a result, every chemical bond in the species under consideration will undergo a vibrational transition at its specific energy. The number of modes in which a molecule can vibrate depends on the number and type of bonds it contains, and the number of atoms in it. These modes are called normal modes and correspond to 3n-5 for diatomic molecules and 3n-6 for all remaining molecules, where n represents the number of atoms. The vibrational frequency (ν), and thus the energy required to occur, is related to the mass and bond strength of the atoms involved according to Equation 6.

$$\nu = \frac{1}{2\pi c}\sqrt{k\mu} \qquad \textit{Equation 6}$$

Where c is the speed of light in cm/s, k is the binding constant, and μ is the reduced mass of the atoms involved in the vibration. It is important to specify that only vibrational modes that generate a variation in dipole moment are IR active.

Fourier transform spectrometers have high sensitivity and resolution and require little acquisition time. In these instruments, the wavelengths of photons generated are not selected by a monochromator but are all transmitted to the sample through an interferometer. The interferometer is a device that divides the IR beam into two distinct paths and then recombines them after introducing a difference in the two paths. Under these conditions, interference between the beams can occur. The intensity variations of the output beam can

be measured with a detector and the result is an interferogram; after this, the Fourier transform converts the interferogram into a typical IR spectrum[256].

In ATR mode, the beam does not directly hit the sample but is directed towards a high refraction index crystal (quartz or diamond), over which the sample under analysis is placed. When the beam strikes the ATR crystal, it undergoes a theoretically infinite series of total internal reflections during which the radiation penetrates a few microns into the sample. If the sample absorbs at specific frequencies, the outgoing radiation will be selectively attenuated (Figure 15).

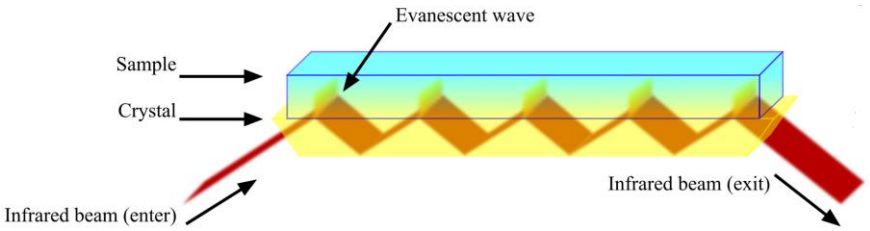

Figure 15. Schematic operation of the ATR.

The ATR technique provides short-time analyses and increased reproducibility; however, it is important to clarify that to use this technique, there must be direct contact between the sample and the ATR crystal; in addition, the refractive index of the crystal must be significantly different with respect to the one of the sample.

2.4 Catalytic tests.

After synthesis, the catalysts were tested towards the catalytic deoxygenation reaction of vegetable oils. The vegetable oils used were first characterized and then the catalysts were tested in a batch reactor; the resulting reaction mixtures were then worked up before the analysis.

A brief description of the procedures performed is given in this section.

2.4.1 Characterization of the vegetable oils used.

The innovative and renewable nature of the green diesel synthesis process is due to using of renewable substrates such as vegetable oils. Each vegetable oil has its own typical composition, which also affects the hydrocarbon distribution of the biofuel produced; therefore, before performing the catalytic tests, we characterized the oils used. Different vegetable oils were used as substrates for CDO, and each was characterized through transesterification reaction according to the standard AOAC 969.33 (AOAC = Association of Official Agricultural Chemists)[257]. This is a derivatization method in which the triglycerides of the oils are converted in FAME (similar to biodiesel production) which are more volatile and more easily analyzed via GC-FID.

During the transesterification reaction, the triglycerides are first saponified to produce free fatty acid; after this, adding a solution of BF_3 in methanol catalyzes the esterification reaction leading to the formation of fatty acid methyl ester.

The resulting FAMEs were then analyzed with a GC-FID equipped with a column suitable for separating of methyl ester isomers. In this way, we can identify the individual FAMEs and thus the fatty acids contained in oils. FAME identification was performed by comparing

the retention times of the sample with a C_{14}-C_{22} FAME reference standard. As an example, Figure 16 shows the comparison between the reference standard and the methyl esters obtained after the transesterification of sunflower oil.

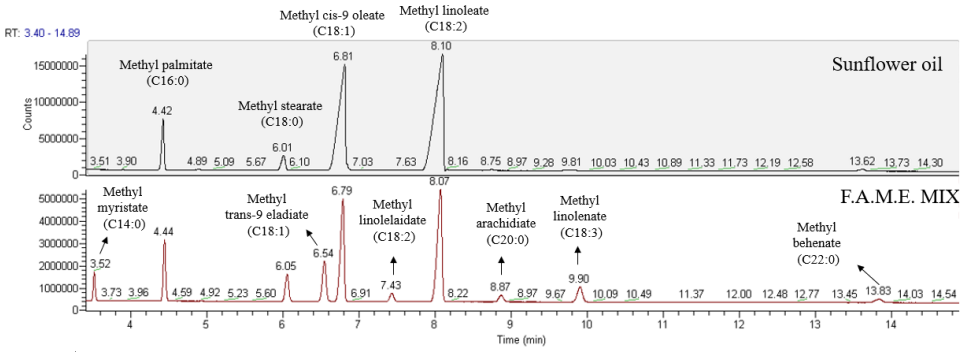

Figure 16. Comparison between transesterified sunflower oil and the FAME standard.

Performing the same procedure, the other oils used were characterized (table 8).

Table 8. Fatty acid composition of used vegetable oils.

	FAME (Area %)											
Oil	C14	C16	C18	C18:1*c*[1]	C_{18}:2*c*	C_{18}:3*c*	C20	C20:1 *c*	C22	Saturated	Unsaturated (mono)	Unsaturated (poly)
Sunflower	0.0	6.5	3.2	38.6	51.5	0.2	0.0	0.0	0.0	9.7	38.6	51.7
Rapeseed	0.0	4.9	1.7	64.5	19.5	7.3	0.6	1.2	0.3	7.5	65.7	26.8
Soybean	0.2	11.3	3.9	21.4	55.3	7.2	0.3	0.0	0.4	16.1	21.4	62.5
Peanut	0.0	7.4	2.5	74.6	9.7	0.0	0.2	2.4	3.2	13.3	77.0	9.7
Corn	0.0	11.8	1.9	30.5	54.2	0.9	0.4	0.0	0.3	14.4	30.5	55.1
Palm	0.9	38.8	5.3	42.7	11.6	0.3	0.1	0.0	0.0	45.4	42.7	11.9

[1]Cn:m*c*: n is the number of carbon atoms; m is the number of double bonds; *c* means *Cis*.

All vegetable oils used were purchased from local traders, only soybean oil was purchased from Merck KGaA (soybean oil dietary source of long-chain triglycerides and other lipids); they are all edible oils for food use and are used for the CDO reaction without any previous treatment. The batch and the other components described on the label of the various oils used are given in the experimental part.

2.4.2 Catalytic deoxygenation reaction in a batch reactor.

The catalytic deoxygenation reaction was performed with a batch reactor. A batch reactor is a sealed vessel used to carry out discontinuous chemical reactions in which all the reagents are charged into the reactor[258].

This kind of reactor is mainly used to perform catalyst screening and reaction conditions screening because, compared with a continuous reactor, it has the advantage of being simpler, cheaper, and faster[178]. In this work, the rector used to perform the catalytic deoxygenation

reaction is a Parr batch reactor consisting of a 4590 Micro Bench Top Reactors, Magnetic drives, and a 4848 Reactor Controller (Figure 17).

Figure 17. Batch reactor.

In a typical test, the reactor was loaded with 2g of oil, 20g of solvent and the catalyst in the chosen catalyst-to-oil wt% ratio. The reactor was then charged to the desired H_2 pressure, the temperature was set to the chosen value, and stirring was applied (kept constant for each reaction). Once the set temperature has been reached, the reaction was carried out for the chosen time. At the end of the reaction, the reactor was cooled down to room temperature, and the product was collected and filtered to remove the catalyst. Finally, the solvent was removed, and the obtained product was weighed to assess the yield of the organic liquid product obtained (OLP) (Equation 7).

$$OLP\ Yield = \frac{g\ OLP}{g\ Oil} x100 \qquad \textit{Equation 7}$$

2.5 Reaction mixture (OLP) characterization analysis and data analysis.

To assess the conversion and the distribution of the products in the mixture, the OLP was analyzed using the following instrument:

- *Attenuated Total Reflection Fourier Transform Infrared (ATR FT-IR)*
- *Gas chromatography with flame ionization detection (GC-FID)*
- *Gas Chromatography Mass Spectrometry (GC-MS)*

2.5.1 OLP composition analysis: Attenuated Total Reflection Fourier Transform Infrared (ATR FT-IR).

The ATR FT-IR is a rapid and useful analytical method to qualitatively assess the conversion degree of the CDO reaction[259]. To better understand the utility of the FT-IR, a comparison of the IR spectrum of rapeseed oil and the OLP obtained from a reaction with 100% conversion and 100% hydrocarbon content is shown (Figure 18).

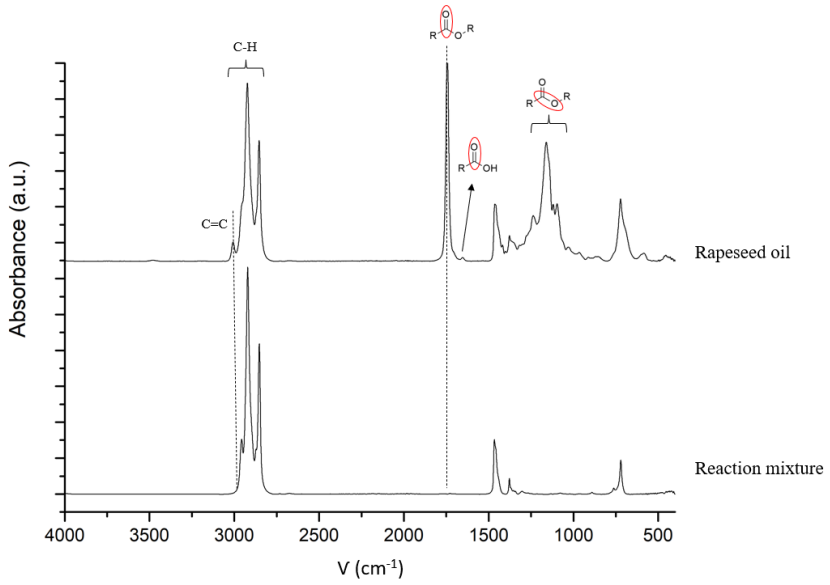

Figure 18. Comparison of IR spectra between rapeseed oil and a full conversion reaction mixture.

The most evident difference between the two spectra can be seen in the band centered at 1745 cm^{-1}; the area between 1745-1700 cm^{-1} corresponds to the C=O bond vibration of the triglyceride esters (around 1745 cm^{-1}) and of the free fatty acids (around 1710 cm^{-1}), so, as in the case shown in Figure 18, if the reaction mixture does not show any signals in this area, we can affirm that the triglycerides in the oil have been fully converted.

In addition, the area between 1350-900 cm^{-1} also corresponds to the vibration of the C-O bonds and is also indicative of the conversion degree. The other signals are related to the vibrational modes of the C-H bonds. After the reaction, a slight difference in the region 2750-3150 cm^{-1} can be seen as a consequence of the hydrogenation of the double bond of the triglycerides. All the analytical details are reported in the experimental part.

2.5.2 OLP composition analysis: Gas chromatography with flame ionization detection (GC-FID).

Biofuel composition obtained from the different catalytic tests was identified by GC-FID analysis. Before analysis, OLP was processed via transesterification in the same way performed for vegetable oils characterization[257]. The transesterification reaction was used to convert unreacted oil into FAME that can be analyzed via GC-FID. After transesterification, the OLP was analyzed with a GC-FID equipped with a nonpolar HP-5 19091J-413 capillary column (30m x 0.32mm x 0.25µm, stationary phase = (5%-Phenyl)-methylpolysiloxane) able to effectively separating the hydrocarbons in the OLP (the GC used is different with respect to the GC used for oil characterization). Chromatographic peaks corresponding to *n*-alkanes were identified by comparison with a linear saturated alkane C_7-C_{40} standard solution. An example of the comparison is shown in Figure 19.

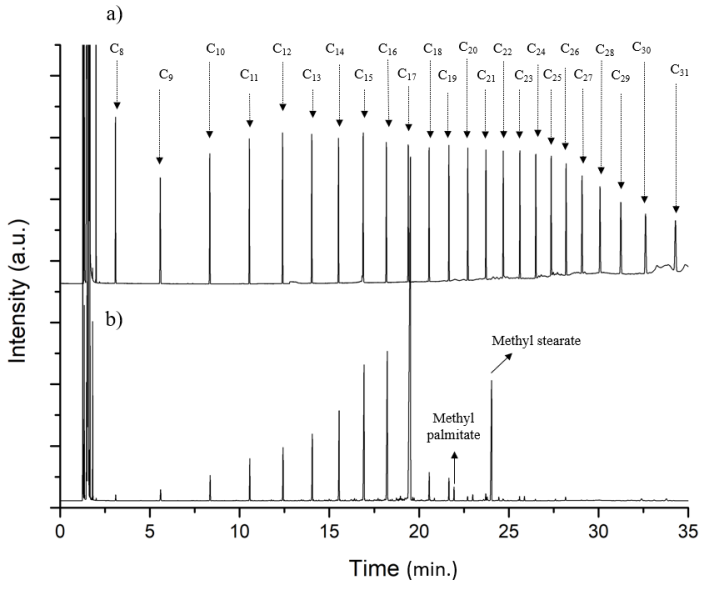

Figure 19. Chromatogram comparison between n-Alkane C_7-C_{40} standard solution (a) and a typical reaction mixture (b).

Methyl palmitate and methyl stearate reported in Figure 19 were identified by GC-MS (as we will describe below). The composition of the OLP under investigation was expressed as GC Area %. Conversion (Equation 8), Green Diesel yield (Equation 9), Green Diesel yield, and HDO/DCO-DCO_2 selectivity (Equation 10), were calculated as follows:

$$Conversion\ (X) = 1 - [\left(\frac{Area\%\ FAME * g\ OLP}{gOil}\right)] * 100 \qquad \textit{Equation 8}$$

$$Green\ Diesel\ Yield = \left(\frac{Area\%\ C_{15} - C_{18} * g\ OLP}{gOil}\right) * 100 \qquad \textit{Equation 9}$$

$$\mathrm{HDO/DCO} - DCO_2\ = \left(\frac{Area\%\ nC_{16} + nC_{18}}{Area\%\ nC_{15} + nC_{17}}\right) * 100 \qquad \textit{Equation 10}$$

When an incomplete conversion was obtained, the transesterified sample was also analyzed with the same gas chromatograph used for the characterization of vegetable oils to identify eventual FAME isomers.

2.5.3 OLP composition analysis: Gas Chromatography Mass Spectrometry (GC-MS).

Any unidentified chromatographic peaks were identified via GC-MS analysis. The GC is equipped with a nonpolar column (similar to that used with GC-FID) so as to separate the hydrocarbons in the reaction mixture. A dilute sample of the transesterified OLP was injected into the GC, and the retention time of the hydrocarbons was compared with a linear saturated alkane C_7-C_{40} standard solution. Unknown peaks were identified by comparing the corresponding mass spectra with a library (NIST 2014); moreover, the identification of

unknown peaks was also implemented by calculating the Kovats retention index (RI) of each unknown peak and comparing it with the RI reported in the reference library. The retention index is a number, relative to the chromatographic peak under consideration, obtained by interpolation between the retention time of the unknown peak (tr_i) and the retention times of two standards, one of which must elute at a lower retention time than that of the unknown peak (tr_z) while the other must elute at a higher retention time (tr_{z+1})[260]. In the specific case of the Kovats retention index used in gas chromatography, the standards in question are represented by *n*-alkane. The Kovats retention index is calculated from Equation 11.

$$RI = 100 \times [\frac{tr_i - tr_z}{tr_z - tr_{z+1}} + z] \qquad \textit{Equation 11}$$

Where: (tr_i) = retention time of the unknown compound, (tr_z) = retention time of the linear alkane eluting before the unknown peak, (tr_{z+1}) = retention time of the linear alkane eluting after the unknown peak, z = number of carbon atoms of the linear alkane eluting before the unknown peak. For the same column used, the Kovats retention index is a value independent of the operating conditions used in the chromatographic run and the physical characteristics of the column.

Figure 20 shows an example of how unknown compounds were identified using the reference library and retention index.

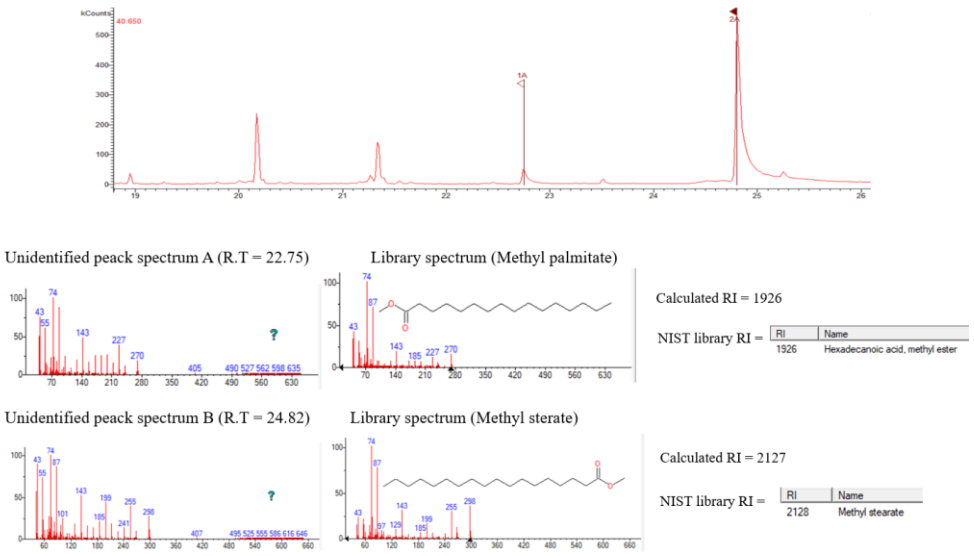

Figure 20. GC-MS analysis for two unidentified peaks.

Figure 20 shows that the mass spectra of the unknown peaks are very similar to the spectra provided by the library, indicating the identity of the two peaks as methyl palmitate and methyl stearate. In addition, the calculated retention indices match those provided by the reference library. From the combination of these two evidence, we are confident that the two peaks in question refer to methyl stearate and methyl palmitate (it also makes sense considering that the starting substrate is an oil, which after complete hydrogenation consists principally of methyl stearate and to a lesser extent of methyl palmitate).

2.6 Catalytic tests performed with FAC-supported catalysts.

The first catalysts examined were FAC-supported catalysts. A catalytic screening was first addressed, and then the most efficient catalyst was used for further studies to evaluate the solvent effect, catalyst recyclability, and the effect of different feedstock (different oils). Finally, catalytic tests performed on the NiMo (5/15)/FAC-Zeo catalyst are reported; this catalyst is reported individually because it was synthesized and reduced differently than the others.

2.6.1 FAC-supported catalysts screening.

During my master's thesis, a screening of reaction conditions was performed using other FACs-supported catalysts, and from these studies, it has been observed that the reaction conditions needed to observe appreciable *n*-C_{15}-C_{18} hydrocarbon concentrations are the following:

- Temperature = 320°C
- Pressure of H_2 = 40bar
- Reaction time = 6h
- Catalyst/oil % = 10%$_{w/w}$
- Oil = 2g
- Solvent (Hexane) = 20g

Therefore, the catalyst screening was performed using this reaction condition and the feedstock used was sunflower oil.

FT-IR analyses of the mixtures obtained after catalysts screening are shown in Figure 21.

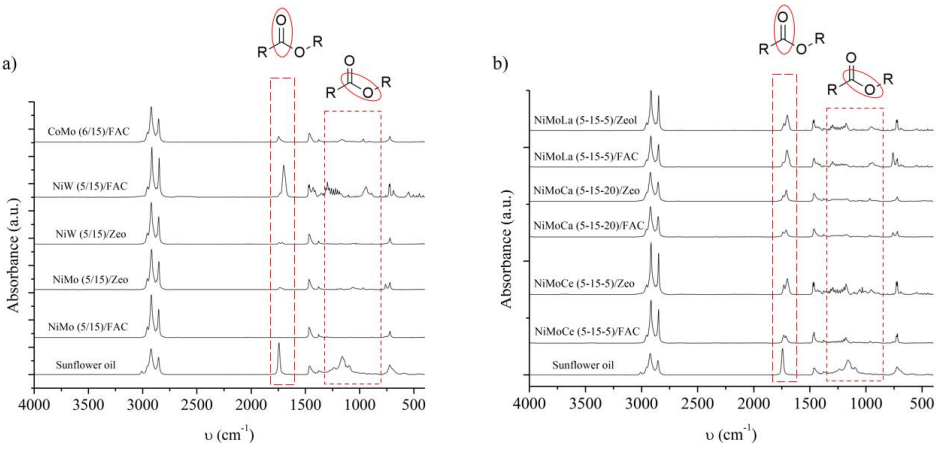

Figure 21. FT-IR spectra of the OLP obtained from catalysts screening: a) bimetallic catalysts; b)trimetallic catalysts.

FT-IR analyses of the mixtures obtained using the bimetallic catalysts (Figure 21a) show that only for NiMo (5/15)/FAC, no signal related to carbonyl ester and C-O vibration are present; with NiMo (5/15)/FAC, the mixture presents only C-H vibrational modes (2750-3050cm^{-1}, 1460cm^{-1}, 1377cm^{-1}, 720cm^{-1}) suggesting complete triglyceride's conversion into hydrocarbons.

In the case of NiMo (5/15)/Zeo and NiW (5/15)/Zeo, two peaks are observed between 1750-1710 cm^{-1}, indicating the presence of both triglycerides and free fatty acids. On the other hand, with NiW/FAC, an intense peak, centered at 1710 cm^{-1}, is observed, suggesting that the catalyst easily converts triglycerides into fatty acids but is not active enough to convert the latter into hydrocarbons. In addition, an effect of support type is evident; with NiMo (5/15)/FAC, complete conversion is achieved, while with NiMo (5/15)/Zeo significant concentration of triglycerides and fatty acids was observed.

Respect NiW/FAC, CoMo (6/15)/FAC shows an opposite effect, with the carbonyl peak being centered at 1750cm^{-1}, suggesting that the catalyst breaks the triglyceride with more

difficulty. Looking at the IR spectra for the reactions performed with the trimetallic catalysts (Figure 21b), in each case, the two peaks relating to triglyceride esters and fatty acids are present, resulting in poor conversion.

The IR spectra are also helpful to evaluate the presence of water (deriving from HDO reaction) or glycerol (which could be present if not hydrogenated to propane) by observing the OH characteristic band in the region spectra between 3700-3000cm^{-1}. In any case no band is observed in this region suggesting two possible interpretations:

- The water content derived from the HDO reaction is negligible, indicating either a negligible water content relative to the total mass of the liquid product or that the catalysts have greater selectivity in favor of DCO-DCO_2.
- The reaction pathway for triglyceride cleavage is the β-elimination because no glycerol is formed. In addition, the signal observed at 1710cm^{-1} (free fatty acids) in many reactions confirmed this hypothesis.

However, IR spectra provide only a generic interpretation of the catalytic activity of the catalysts; in contrast, GC-FID analysis provides a more detailed analysis of the composition of reaction mixtures (Table 9).

Table 9. FAC-supported catalysts' screening.

Entry[1]	Catalyst	Alkenes	*n*-C_7-C_{14}	*n*-C_{15}-C_{18}[2]	C >18	FAME	Other	Conversion (%)	OLP Yield (wt%)	Green Diesel yield (wt%)
1	-	0	0	**0**	0	81.9	18.1	15	85.1	0
2	FAC	2.4	1.0	**1.6**	0.2	79.3	15.4	15	95.3	1.8
3	NiMo (5/15)/FAC	0	4.4	**91.7**	3.9	0	0	100	72.2	66.2
4	NiMo (5/15)/Zeo	12.5	2.6	**39.1**	0.9	12.9	32	87.7	96.1	37
5	CoMo (6/15)/FAC	20.6	5	**67.1**	0	3.4	3.9	97.3	75.5	50.6
6	NiW (5/15)/FAC	11.3	0.6	**11**	0	72.2	4.9	32.5	87.4	9.6
7	NiW (5/15)/Zeo	1.9	3.5	**90**	1.5	2.3	0.8	97.3	82.6	74.3
8	NiMoCe (5/15/5)/FAC	22.7	1.4	**22.9**	0.2	52.8	0	52.3	90.3	20.7
9	NiMoCe (5/15/5)/Zeo	12.6	0.5	**8.1**	0	78.8	0	35.4	82	6.6
10	NiMoCa (5/15/20)/FAC	15	2.8	**28.6**	0.8	52.4	0.4	54.7	86.4	24.7
11	NiMoCa (5/15/20)/Zeo	7.5	1.5	**5.5**	0	85.5	0	26	86.4	4.8
12	NiMoLa (5/15/5)/FAC	4.3	0.3	**2.7**	0	82.2	10.5	17.6	88.9	2.4
13	NiMoLa (5/15/5)/Zeo	17.4	1.3	**10.8**	0.2	57.4	12.9	31.7	97.2	10.2

[1]All the reactions were performed at 320°C, 40barH_2, 20g of Hexane, 2g of Sunflower oil, 0.200g of Catalyst and 6h of reaction time.
[2]This column has been highlighted to focus the attention on hydrocarbons in the diesel range (the hydrocarbons of our interest).

To evaluate the effect of the FAC support on the CDO reaction, two different blank tests were addressed (entries 1 and 2 Table 9); in one blank the CDO reaction was evaluated in the absence of catalyst and support (entry 1), while in the other blank (entry 2) the reaction was performed using only the HCl-treated FAC support.

From the results obtained it can be stated that FAC support shows negligible activity in the CDO reaction because results in entry 1 and entry 2 are very similar (reaction performed in entry 2 shows only a small amount of hydrocarbons, 5.2%).

Data reported in Table 9 shown that bimetallic catalysts are more efficient than trimetallic ones (except in the case of NiW/FAC, entry 6); the addition of the third metal negatively affects the reaction conversion, in fact, trimetallic catalysts report high FAME content (even over 50%) in any case.

Based on the catalytic screening, the best catalytic activity is shown by NiMo (5/15)/FAC (entry 3), displaying 100% conversion and 91.7% hydrocarbon in the diesel range (*n*-C_{15}-C_{18}). Therefore NiMo (5/15)/FAC catalyst produces a fully hydrocarbon biofuel (72.2wt%) with high diesel selectivity. A significant effect of the support can be seen here; for the same nominal amount of metal, the NiMo/Zeolite catalyst (entry 4) shows a lower activity than its counterpart supported on FACs (100% conversion vs. 87%).

To follow, the catalysts with the highest activity are CoMo (6/15)/FAC and NiW (5/15)/Zeo (entries 5 and 7). CoMo (6/15)/FAC shows 97.3 % conversion and a mostly hydrocarbon biofuel in 75.5 wt% yields. In this case, the catalyst shows a lower hydrogenation activity than NiMo (5/15)/FAC resulting in high unsaturated hydrocarbon content (20.6%) and, thus, lower *n*-C_{15}-C_{18} hydrocarbon contents (67.1%). For CoMo-based catalysts, a higher selectivity towards unsaturated hydrocarbons is often observed [138, 139]. The NiW (5/15)/Zeo system shows the same conversion as CoMo (6/15)/FAC, but the biofuel contains

a higher concentration of alkanes in the diesel range (90%), indicating a higher degree of hydrogenation than CoMo (6/15)/FAC.

For all the catalysts tested, a low cracking activity is observed; in any case, less than 5% content of *n*-C_7-C_{14} hydrocarbon is produced. Note that catalysts with better performance (NiMo (5/15)/FAC, CoMo (6/15)/FAC, and NiW (5/15)/Zeolite) lead to lower OLP yield, and this is due to the nature of the catalytic deoxygenation reaction; as the conversion increases, the formation of volatile hydrocarbons (propane from glycerol, light hydrocarbons from cracking, and CO and CO_2 from DCO-DCO_2) also increases[147].

At incomplete conversion and after transesterification, several reaction mixtures report high FAME concentrations (so high amount of triglycerides or free fatty acid), mainly methyl stearate, small percentages of methyl palmitate, and, in a few cases, also methyl elaidate (this reflects the composition of vegetable oils, which, except in the case of palm oil, consisting mainly of fatty acids with 18 carbon atoms). These compounds were identified after GC-MS analysis (Figure 22).

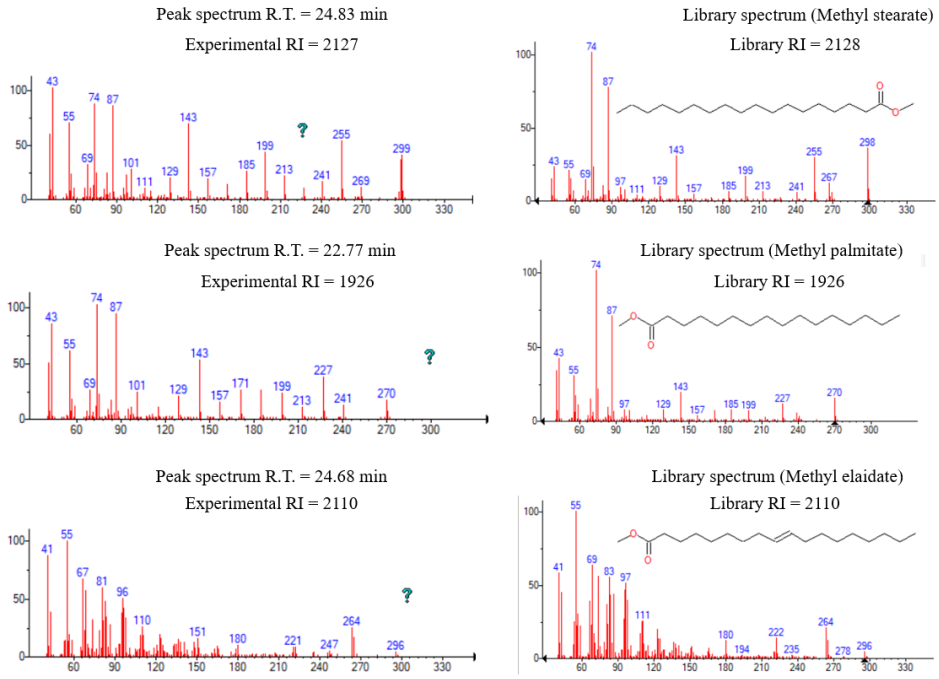

Figure 22. GC-MS analysis: identification of methyl stearate, methyl palmitate and methyl elaidate.

As mentioned earlier, unsaturated vegetable oils fatty acids have a *cis*-type configuration; however, the presence of methyl elaidate is feasible because a *cis-trans* isomerization reaction will occur [167, 261].

The observed FAMEs are mainly derived from free fatty acids and triglycerides. However, some other oxygenated compounds, not visible after derivatization via transesterification, can also be formed from the catalytic deoxygenation reaction. In fact, by analyzing the reaction mixture via GC-MS prior to the transesterification step, other compounds such as 1-octadecanol (also visible in the transesterified mixture), propyl stearate, and propyl palmitate can be observed (Figure 23).

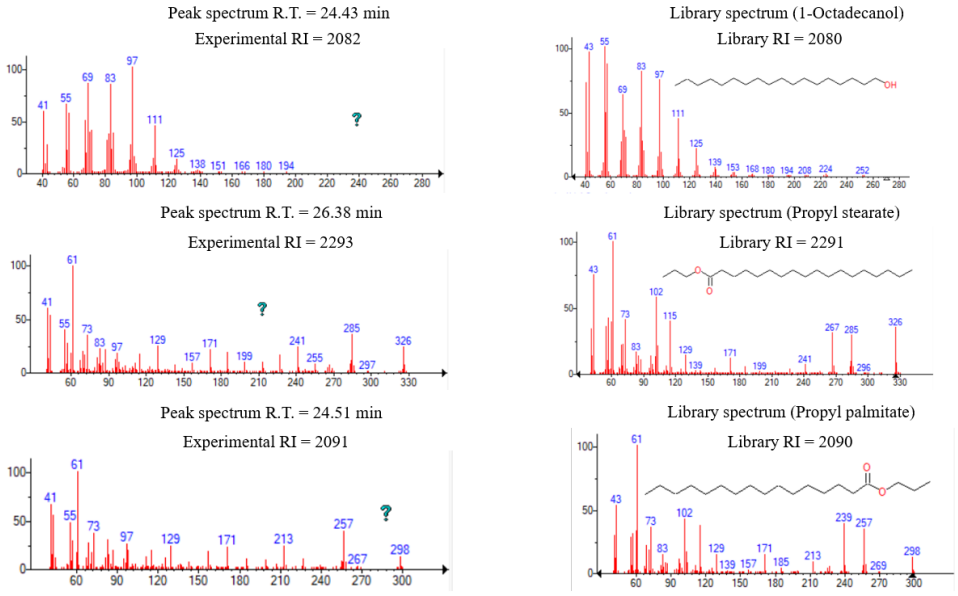

Figure 23. GC-MS analysis: Identification of 1-octadecanol, propyl stearate and propyl palmitate.

1-octadecanol can be formed as a reaction intermediate after hydrogenation of the enol of octadecanal (not observed in any reaction mixture). As a reaction intermediate, 1-octadecanol has been frequently observed[85, 108, 111, 113, 140, 262, 263]. In contrast, octadecanal is rarely observed due to their high decomposition rate to produce C_{17} hydrocarbons or high conversion rate to produce 1-octadecanol[107, 117, 118]. The presence of propyl stearate (and similarly propyl palmitate) is further evidence that the triglyceride cleavage proceeds through successive β-elimination and hydrogenation reactions; in this case, the reaction stops after the second hydrogenation, thus forming propyl stearate[85, 111].

To be able to describe the HDO/DCO-DCO_2 reaction selectivity, we need to go into more detail about *n*-C_{15}-C_{18} hydrocarbons distribution (Table 10).

Table 10. n-C_{15}-C_{18} hydrocarbon distribution according to the catalyst used.

Entry	Catalyst	*n*-C_{15}	*n*-C_{16}	*n*-C_{17}	*n*-C_{18}	Reaction selectivity[1]
1	NiMo (5/15)/FAC	3.6	5.9	32.5	49.7	1.5
2	NiMo (5/15)/Zeo	1.8	2.3	13.8	20.6	1.5
3	CoMo (6/15)/FAC	2.3	6.	8.0	50.3	6.3
4	NiW (5/15)/FAC	1.1	0.5	6.6	2.8	0.4
5	NiW (5/15)/Zeo	5.7	2.9	60.9	20.5	0.4
6	NiMoCe (5/15/5)/FAC	1.4	1.5	10.8	9.2	0.9
7	NiMoCe (5/15/5)/Zeo	0.9	0.8	3.9	2.5	0.7
8	NiMoCa (5/15/20)/FAC	2.6	2.8	15.2	8.0	0.6
9	NiMoCa (5/15/20)/Zeo	1.1	0.5	2.4	1.5	0.6
10	NiMoLa (5/15/5)/FAC	0.5	0.1	1.6	0.5	0.3
11	NiMoLa (5/15/5)/Zeo	1.1	0.2	5.4	3.8	0.6

[1]Calculated as (*n*-C_{18}+*n*-C_{16}/*n*-C_{17}+*n*-C_{15}) (Equation 8).

Looking at the reaction selectivity, NiMo catalysts and CoMo/FAC catalysts prefer the HDO reaction, while NiW catalysts and trimetallic catalysts favor the DCO-DCO_2 reaction (recall that reaction selectivity can be is expressed by Equation 8). NiMo catalysts slightly prefer HDO reaction, and this agrees with what has been observed for other NiMo systems[111]. Both NiMo (5/15)/FAC and NiMo (5/15)/Zeolite have the same selectivity value (1.5), so there is no support effect on reaction selectivity, and this is also true for the other catalysts studied.

It is interesting to note that CoMo (6/15)/FAC shows a high selectivity towards the formation of *n*-C_{18} and *n*-C_{16} hydrocarbons (HDO route); this is in agreement with several authors[112, 137, 148].

In conclusion, according to the catalytic screening, the activity of the synthesized catalysts follows the trend NiMo (5/15)/FAC > NiW (5/15)/Zeo > CoMo (6/15)/FAC > NiW (5/15)/FAC~trimetallic catalysts. Given the higher activity, NiMo (5/15)/FAC catalyst was used for further studies.

2.6.2 Solvent effect.

The catalytic screening reported in the previous paragraph was performed using hexane as the solvent. To evaluate a possible solvent effect, the NiMo (5/15)/FAC catalyst was tested either without solvent (using 20g of oil) or with dodecane as solvent; the reaction conditions used are 320°C, 40bar H_2, 10wt% catalyst (0.2g catalyst/2g oil) and 6h of reaction time. The results obtained from these studies are shown in Figure 24.

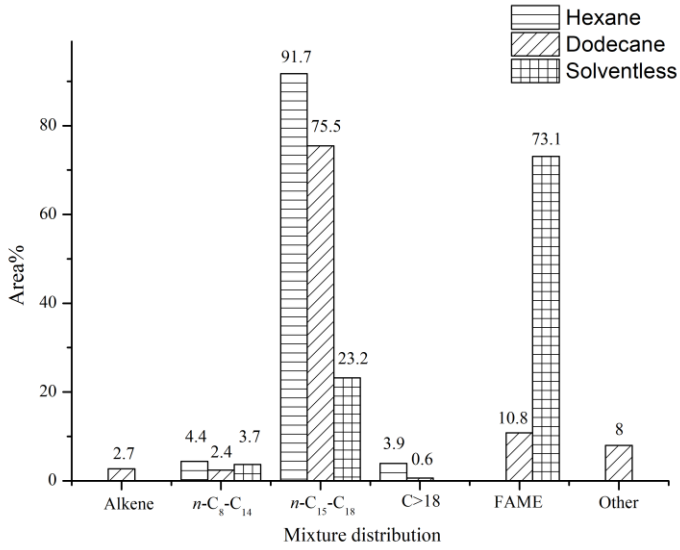

Figure 24. Solvent effect on NiMo (5/15)/FAC activity.

Unfortunately, the reaction performed without solvent did not yield good results; the catalyst is not very active, and the biofuel produced is rich in FAME (73.1%) and thus unconverted oil. This could be due to low amount of H_2 in the reaction environment or from low solubility of H_2 in pure oil.

The use of dodecane or hexane greatly improves the catalytic activity of the catalyst; however, the two solvents affect catalytic activity differently. By performing the reaction in dodecane, the catalyst is not able to fully convert the oil, leading to 10.8% of FAME and 75.5% of hydrocarbons in the diesel range (compared to 91.7% working in hexane). The higher catalyst's activity in hexane can be explained by the fact that the solvent, at the reaction conditions used, is under supercritical conditions; in this state, hexane has the hydrogen-shuttling capacity that makes it a hydrogen donor and solubilizes hydrogen more readily, facilitating the reaction [264, 265]. Working with hexane also results in easy work-up; indeed, hexane can be easily evaporated, leaving only the reaction product; on the other hand, dodecane does not separate from the rest of the product via evaporation. Focusing on reaction selectivity, there is no solvent effect; in hexane, catalyst HDO/DCO-DCO_2 selectivity is 1.5, while in dodecane is 1.4 (not shown).

2.6.3 NiMo (5/15)/FAC recycling tests.

The efficiency of a catalyst is also expressed as a function of its activity for successive reaction cycles. To evaluate this, NiMo (5/15)/FAC catalyst was recycled setting the reaction condition at 320°C, 40bar H_2, 10wt% catalyst ad 6h reaction time. In the first reaction cycle, 20g of Hexane, 2g of sunflower oil and 0.2g of catalyst were used, while for subsequent reaction cycles, the amounts of oil were adjusted according to the amount of catalyst recovered (to maintain the 10wt% catalyst to oil ratio) and the amounts of solvent were adjusted to maintain the oil to hexane ratio at 1:10.

After each reaction cycle, the catalyst was recovered and reused in the subsequent reaction without further treatment. The results obtained after three reactions are shown in Figure 25.

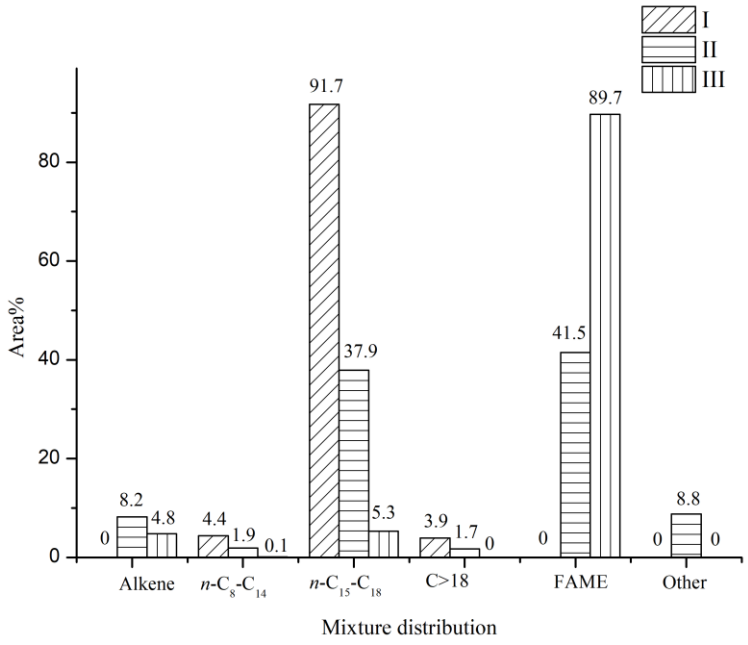

Figure 25. Recycling test of NiMo (5/15)/FAC.

Unfortunately, the catalyst quickly loses its activity; in the second reaction cycle, it loses about 50% of its activity, leading to a drop in *n*-C_{15}-C_{18} content from 91.7% to 37.9% and, consequently, in high FAME content (41.5%). At the third reaction cycle, the catalyst completely loses its activity resulting in a biofuel consisting mainly of FAME (89.7%), of which 85.1% is methyl stearate.

This loss of activity is consequently reflected on the conversion degree, OLP yield, and green diesel yield (Table 11).

Table 11. Recycling tests.

Cycle[1]	Conversion (%)	OLP Yield (wt%)	Green Diesel Yield (wt%)	Selectivity
I	100	72.2	66.2	1.5
II	61.1	92.7	28.5	0.7
III	19.7	89.5	4	0.5

[1]Reaction conditions: 320°C, 40bar H_2, 10wt% catalyst, ratio oil/Hexane = 1:10.

Table 11 shows a significant decrease in conversion from 100% (I) to 19.7% (III), and this is also reflected in the diesel yield, which drops from 66.2% to 4%. In addition, inversion in reaction selectivity is also noted; in the first reaction (I), there is a greater prevalence for HDO reaction, while in the following reactions, DCO-DCO_2 reaction is preferred.

Generally, the loss of activity for CDO catalysts can be attributed to three main causes: active metal leaching, active metal sintering, and coke formation on the catalyst (which blocks catalyst pores)[175, 262, 266-270]. From the ICP-MS analysis of the post-test catalyst, no appreciable Ni leaching is observed (about 4.4wt% for both fresh and post-test catalyst); on the other hand, Mo leaching occurred (11.7wt% fresh catalyst vs. 7.7% post-test catalyst).

This evidence suggests that catalyst deactivation is partly attributable to Mo leaching. In addition, the final weight of the recovered catalyst after the second reaction cycle was higher than the amount before the reaction; this means coke formation over the catalyst, suggesting that catalyst deactivation may also be due to this phenomenon. To evaluate the effect of coke on conversion, the catalyst was calcined at 400°C for 3h (to remove the coke) and tested again after reduction. The reaction was performed under the same reaction conditions adjusting the proportions according to the amount of catalyst obtained after reduction. The results obtained showed 100% conversion and a biofuel consisting of 100% hydrocarbons including 88.6% in the diesel range (n-C_{15}-C_{18}). From what has been observed, the main cause of catalyst deactivation is attributable to coke formation.

Mo leaching and coke formation may also explain the observed reaction selectivity inversion; since is reported that Ni favor DCO-DCO_2 while Mo to favor HDO, a lower amount of Mo explains a lower selectivity toward HDO. Furthermore, the presence of coke prevents H_2 adsorption onto the catalyst, thus hindering the HDO reaction.

2.6.4 NiMo (5/15)/FAC feedstock screening.

The feedstock used for the DCO reaction can affect the whole process of Green Diesel synthesis. Generally, more readily available and less expensive feedstock is used, and this depends mainly on the geographical area. For this reason, we decided to evaluate the catalyst activity using different oil as feedstocks to assess its robustness.

Oil screening was performed by setting the reaction conditions at 320°C, 40bar H_2, 6h reaction time, 0.200g NiMo (5/15)/FAC, 2g oil, and 20g of hexane.

The IR spectra recorded from the reaction mixtures obtained from NiMo (5/15)/FAC with different oils are reported in Figure 26.

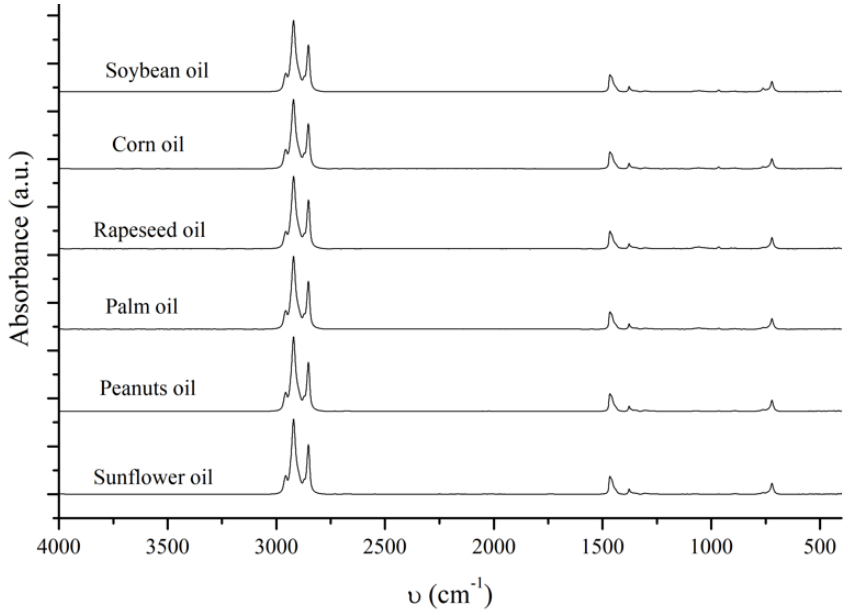

Figure 26. FT-IR oil screening.

The IR spectra are all very similar to each other and show the signals of the vibrational modes of C-H bonds exclusively, suggesting a mostly complete conversion for each oil used.

GC-FID analysis confirms what was observed via FT-IR (Table 12).

Table 12. Compound mixture distribution with different oils.

Oil	Alkenes	*n*-C_8-C_{14}	*n*-C_{15}-C_{18}	C>18	FAME	Other	Conversion (%)	OLP Yield (wt%)	Green Diesel yield (wt%)	Selectivity
Sunflower	0	4.4	91.7	3.9	0	0	100	72.2	66.1	1.5
Peanuts	0.4	4.4	87.4	7.7	0	0	100	88.0	77.0	3.5
Palm	2.9	6.3	89.5	1.4	0	0	100	82.2	73.6	3.2
Rapeseed	7.5	5.2	85.2	2.1	0	0	100	84.7	72.0	3.9
Corn	5.6	5.0	87.5	1.8	0	0	100	80.6	69.8	3.4
Soybean	5.2	8.5	83.4	2.8	0	0	100	79.1	65.3	3.8

Reaction conditions: 320°C, 40bar H_2, 10wt% catalyst, 20g Hexane, 2g oil, 6h of reaction time.

Table 12 shows that a complete conversion is achieved in all cases. Sunflower oil is the one with the highest presence of hydrocarbons in the diesel range (91.7%); on the other hand, it is the one with the lowest OLP yield (72.2 wt%), and thus lower Green Diesel yield (66.1wt%). Lower OLP yield means lower atom economy and higher cracking degree (in this case, formation of C<6 volatile hydrocarbons), which can be explained by observing the reaction selectivity. Compared to the other oils, sunflower oil is the only one where the catalyst leads to higher selectivity toward DCO/DCO_2; this reaction pathway is favored with a higher cracking degree and leads to lower atom economy and, consequently, lower yield. For all the oil used, *n*-C_{15}-C_{18} hydrocarbon content higher than 80% is observed, but several differences can be reported. The highest biofuel yield is obtained with peanut oil (88.0%) but is also the reaction with the highest content of C>18 hydrocarbons. The higher concentration of long-chain hydrocarbons is due to the feedstock used; peanut oil has high content of long-chain fatty acids (5.8%, see Table 8). When palm oil is used, no remarkable differences can be seen in terms of Green Diesel yield and OLP yield; however, palm oil is rich in palmitic acid, and, after the reaction, the biofuel obtained results in high *n*-C_{16} hydrocarbon contents (29.8%). A high hexadecane amount is beneficial for Green Diesel production because it

increases the cetane number (the maximum value of cetane number is 100 and is attributed to pure hexadecane). The use of rapeseed, soybean and corn oil results in a higher unsaturated hydrocarbon concentration; the reason is not fully understood and will be the subject of further study. Observing reaction selectivity, the catalyst promotes the hydrodeoxygenation reaction in each case. In the case of rapeseed oil, the highest reaction selectivity in favor of HDO (3.9) was obtained, while the lowest value occurred with sunflower oil. As explained before, this is related to the higher cracking activity observed for this feedstock.

2.6.5 NiMo (5/15)/FAC-Zeo catalytic test.

This section reports the results obtained using the NiMo (5/15)/FAC-Zeo catalyst. As described before, this catalyst was synthesized slightly differently than the other FACs and Zeolite-supported catalysts; moreover, it was tested by reducing it in batch at 320°C, 60bar H_2 and 8h (differently from what has been done for the other catalysts).

The catalytic activity was tested at the same reaction condition used for the other FACs and Zeolite-supported catalysts, i.e., 320°C, 40bar H_2, 6h of reaction time, 20g hexane, 2g oil and 0.200g catalyst and the results obtained are shown in Figure 27.

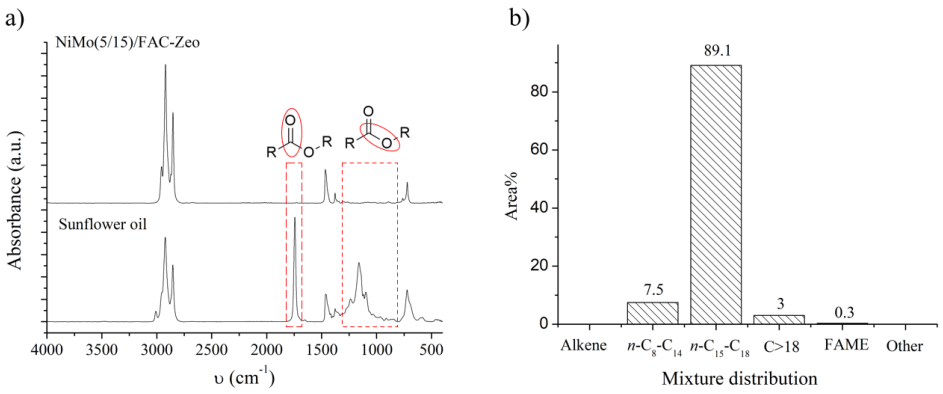

Figure 27. NiMo (5/15)/FAC-Zeo catalytic activity. a) FT-IR spectra. b) hydrocarbon distribution from GC-FID analysis.

From the IR spectrum (Figure 27a), no peaks related to the carbonyl groups of the esters and fatty acids are observed, indicating complete conversion; this was also confirmed by GC-FID analysis (Figure 27b). The mixture compounds distribution shows that the biofuel obtained is composed mainly of hydrocarbons, of which 89.1% are in the diesel range. Only a small amount of methyl stearate (0.3%) was observed.

By carrying out the reaction with NiMo (5/15)/FAC-Zeo, a conversion of 99.8% resulted, and 67.7wt% OLP yield and 59.9wt% Green Diesel yield was obtained (Table 13). Regarding reaction selectivity, the catalyst appears to be particularly selective toward DCO-DCO_2.

Table 13. NiMo (5/15)/FAC-Zeo catalytic activity.

Conversion (%)	OLP yield (wt%)	Green Diesel yield (wt%)	Selectivity
99.8	67.7	59.9	0.2

From the discussion above, it can be claimed that the NiMo (5/15)/FAC-Zeo catalyst appears to be very effective, with activity comparable to that of the NiMo (5/15)/FAC catalyst; in fact, by analyzing the results obtained with this two catalyst (Figure 27 and Table 13 vs Table 9 entry 1) it can be seen that there isn't a remarkable difference in the hydrocarbon distribution (91.7% *n*-C_{15}-C_{18} hydrocarbons for NiMo (5/15)/FAC vs 89.1 % for NiMo(5/15)/FAC-Zeo). In contrast, differences can be seen in terms of Green Diesel yield and reaction selectivity (66.2wt% Green Diesel yield and HDO selectivity for NiMo (5/15)/FAC vs. 59.9wt% Green diesel yield and DCO-DCO_2 selectivity for NiMo(5/15)/FAC-Zeo). However, in this case, the catalysts were reduced in two different ways; therefore, to make a more effective comparison, NiMo (5/15)/FAC was tested again (under the same reaction conditions done for NiMo (5/15)/FAC-Zeo) after batch reduction at 320°C, 60bar H_2 and 8h reduction time. The comparison between the two catalyst is show in Figure 28.

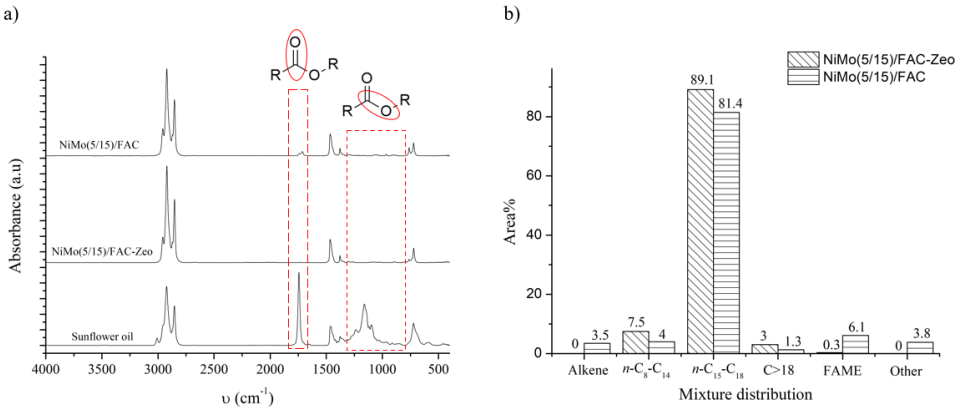

Figure 28. Comparison between NiMo (5/15)/FAC and NiMo (5/15)/FAC-Zeo (batch reduced). a) FT-IR spectra. b) hydrocarbon distribution from GC-FID.

From the analysis of the IR spectra (Figure 28 a), while for NiMo (5/15)/FAC-Zeo vibrational modes of C=O are not present, for NiMo (5/15)/FAC a low intensity peak is detected in the area between 1750-1710 cm^{-1} indicating that for NiMo (5/15)/FAC complete conversion is not achieved. This is confirmed after GC-FID analysis (Figure 28b). Indeed, for NiMo (5/15)/FAC, a small amount of FAME is observed (6.1%). Therefore, the *n*-C_{15}-C_{18} hydrocarbon distribution is slightly different; with NiMo (5/15)/FAC-Zeo, the biofuel is composed of 89.1% Green Diesel hydrocarbons, while for NiMo (5/15)/FAC is composed of 81.4% in Green Diesel hydrocarbons.

By analyzing Table 14, it is possible to affirm that the NiMo (5/15)/FAC-Zeo catalyst appears to be slightly more efficient; with NiMo (5/15)/FAC-Zeo, there is almost complete conversion (99.8% vs. 94.8%). Looking at the yields obtained, with NiMo (5/15)/FAC higher OLP yield, and Green Diesel yield are obtained; however, the biofuel obtained contains appreciable amounts of FAME and oxygenated compounds (classified as other in Figure 28b) making it less suitable as a biofuel. The two catalysts show different reaction selectivity. NiMo (5/15)/FAC-Zeo leads to a higher prevalence of *n*-C_{15} + C_{17} hydrocarbons (DCO-

DCO_2) while NiMo (5/15)/FAC prefers HDO reaction; these results suggest that, for NiMo (5/15)/FAC, the reaction selectivity is not particularly affected by the reduction process (Table 10 and Table 14). Thus, the difference in selectivity between the two catalysts may be attributable to the different method of synthesis (since the two catalysts have the same metals and the same nominal metal amount).

Table 14. Comparison between NiMo (5/15)/FAC and NiMo (5/15)/FAC-Zeo (batch reduced).

Entry	Catalyst	Conversion (%)	OLP yield (wt%)	Green Diesel yield (wt%)	Selectivity
1	NiMo (5/15)/FAC-Zeo	99.8	67.7	59.9	0.2
2	NiMo (5/15)/FAC	94.8	85.3	69.5	2.0

2.6.6 NiMo (5/15)/FAC characterization.

This section reports the results obtained from the characterization of NiMo (5/15)/FAC. This catalyst was characterized because it proved to be the most active.

2.6.6.1 ICP elemental analysis.

To evaluate the real amount of metals impregnated on the support, elemental analysis of FACs and NiMo (5/15)/FAC catalyst was investigated using ICP-MS. In addition, to assess the potential leaching of the metals after the reaction, the elemental composition of the catalyst after the first reaction cycle was also analyzed (in this case, only Ni and Mo amounts were evaluated as they are the metals that could undergo leaching).

The results obtained from the ICP-MS analysis are reported in Table 15.

Table 15. ICP-MS elemental analysis.

Catalyst	Si (wt%)	Al (wt%)	Ni (wt%)	Mo (wt%)	Nominal (Ni/Mo)[1]	Experimental (Ni/Mo)[1]
FACs	35±2	16.0±0.4			-	-
NiMo (5/15)/FAC	20±1	13.0±0.3	4.4±0.1	11.7±0.3	0.67	0.67
NiMo(5/15)/FAC post test[2]	-	-	4.2±0.1	7.5±0.3	-	-

[1]Molar ratio

[2]For this analysis only Ni and Mo content were evaluated.

Since FACs are composed principally of aluminosilicates, it is not surprising that our FACs are composed of 35wt% Si and 16wt% Al. The addition of Ni and Mo during catalyst synthesis is confirmed by ICP analysis that shows 4.4 wt% of Ni and 11.7 wt% of Mo. The

measured values are compatible with the nominal weight and Ni/Mo molar ratio chosen for the synthesis, which is not surprising since synthesis does not involve steps where there is a risk of losing metal from the substrate (e.g., washing and filtration steps). The ICP analysis of the catalyst shows a reduction of wt% of Si and Al, which is logical since now Ni and Mo contribute to the total weight of the material.

2.6.6.2 FT-IR.

FT-IR analysis provides information regarding the surface characteristics of the catalyst. A comparison between the spectra obtained from FACs support and NiMo (5/15)/FAC after calcination was performed to evaluate the surface modifications after metals' impregnation on the support (Figure 29). The IR spectra of NiMo (5/15)/FAC in a reduced state are not recorded because reduced metals are IR inactive.

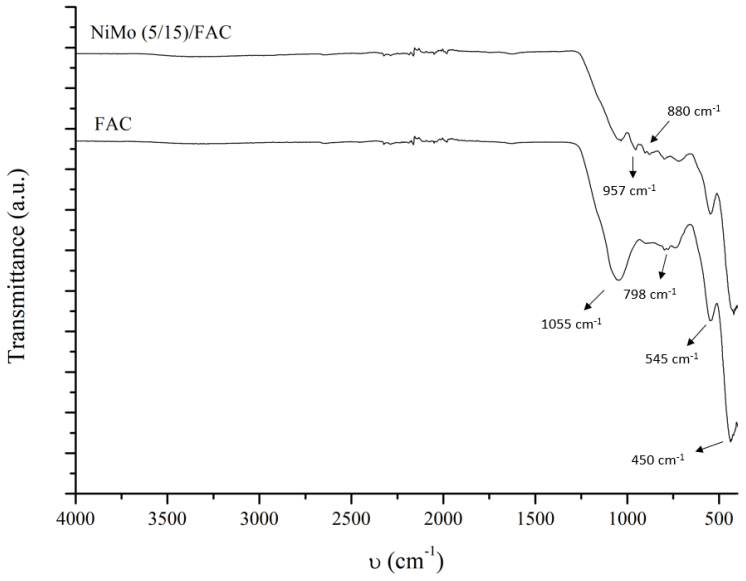

Figure 29. FT-IR spectra of FACs and NiMo (5/15)/FAC (calcined) (spectra recorded in ATR mode and with solids in powder form).

The band centered at 1055 cm^{-1} is attributed to the asymmetric stretching of Si-O-Si, while those at 798 cm^{-1} and 450 cm^{-1} are related to the symmetric stretching and bending of Si-O-Si, respectively; in addition, a weak peak at 545 cm^{-1} attributed to asymmetric Si-O-Al stretching is also observed[271-273]. After the addition of Ni and Mo, there is a reduction in intensity of the signals related to Si and Al; this is probably because NiO and MoO_3 do not enter the pores of the FACs but are deposited on the surface, thus covering the Si and al species, decreasing the intensity of the signals. However, the presence of new peaks is observed after the addition of the metals. The peak at 957 cm^{-1} and the peak at 880 cm^{-1} are attributed to the asymmetric and symmetric stretching of the Mo=O bond, respectively, confirming the presence of MoO_3 [274]. No peaks are observed related to the NiO species, but this could be due to the low concentration of this compared to the Si- and Al-based species; thus, the NiO signals are covered by the Si and Al signals.

2.6.6.3 XRD analysis.

To assess the type of phases present in both the catalyst and support, XRD analysis of FACs and NiMo (5/15)/FAC (in reduced state) was carried out. The XRD diffractograms recorded are reported in Figure 30.

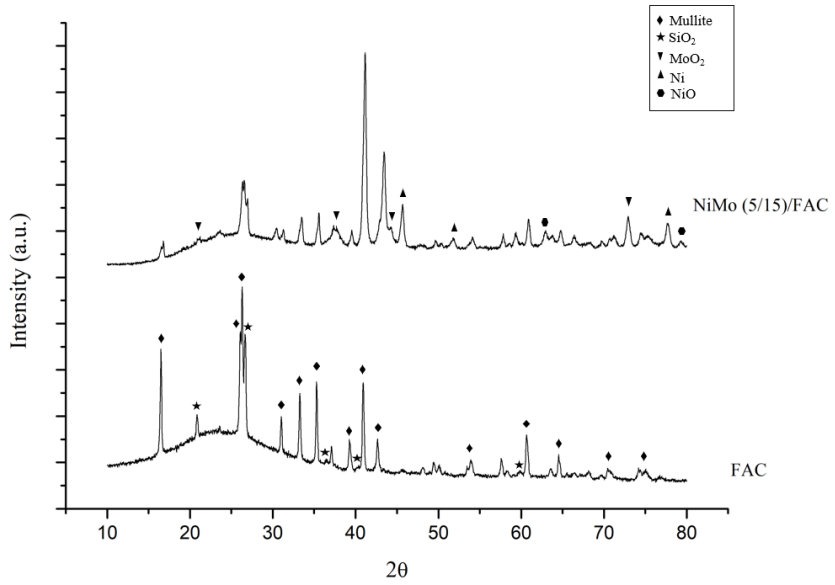

Figure 30. XRD diffractograms of FAC support and NiMo (5/15)/FAC

From the XRD of the support (FACs), the characteristic reflections of mullite are observed (2θ = 16.4°, 26°, 26.2°, 30.5°, 33.5°, 35.5°, 40.9°, and 60.8°). Mullite is an aluminosilicate frequently observed in FAC[201, 272, 275, 276]. In addition to mullite, another characteristic phase of FACs is quartz, present in crystalline and amorphous forms. Crystalline quartz is attributed to reflections 2θ of 20.9°, 26.6°, 36.5°, 50.1°, and 59.93° while amorphous quartz is found in the broad hump between 10° and 40° (centered at about 2θ = 25°)[277, 278]. After synthesis, the reduced NiMo (5/15)/FAC catalyst still exhibits the reflections given by the

support but in a less intense way, indicating that, after the addition of the metals, there is a loss of crystallinity of the material. However, besides the support phases, new reflections attributable to the addition of Ni and Mo are observed. Given the reduction conditions, we expect MoO_3 to be reduced to MoO_2 which should give reflections at 21.2°, 26.8°, and 44.3°; in our case, the signals at 21.2° and 44.3° are visible, while the reflection at 26.8° is not observable. This is probably due to the mullite reflection covering this signal [279, 280]. On the other hand, the peaks at 45°, 51°, and 76° are attributed to metallic Ni, thus confirming that Ni has been reduced under the reduction conditions used [281, 282]. In addition, there are also reflections attributable to NiO (2θ = 37.2°, 43.3°, 62.8°, and 75.5°) indicating either partial re-oxidation of the catalyst or uncomplete reduction of the catalyst[281].

2.6.6.4 BET-BJH analysis.

N_2 physisorption analysis provides information about the textural properties of materials, such as porosity and surface area.

In accordance with the IUPAC (International Union of Pure and Applied Chemistry) classification, the FACs support and the catalyst seems to show a type II isotherm due to unrestricted monolayer-multilayer adsorption typical of non-porous and macroporous materials, but, in the case of NiMo(5/15)/FAC, the presence of hysteresis loop seems to suggest a type IV isotherm, characteristic of mesoporous material (Figure 31)[251]. An increase in the amount of adsorbent is observed upon impregnation of FACs with Ni and Mo, suggesting a change in the adsorption properties of the material. An H3-type hysteresis is observed in each case, indicating capillary condensation inside the pores. In the case of the support, the loop is narrow, while, for the catalyst, the loop is spread over large ranges similar to that observed by Deka et al.[283].

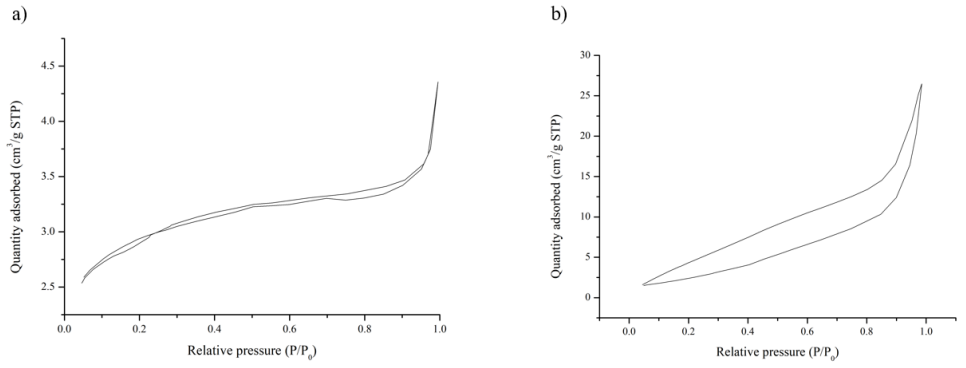

Figure 31. Adsorption isotherm of FAC (a) and NiMo (5/15)/FAC (b).

Table 16shows the textural properties of materials. As it can be seen, there is no significant change in surface area after impregnation, however, there is a notable increase in pore volume (0.004 cm^3/g vs. 0.04 cm^3/g) and average pore diameter (1.6nm vs. 23.3nm); this can be explained by the formation of new pores by NiO and MoO_3 [284, 285]. As graphical evidence of the data shown in Table 16, Figure 32 shows the BJH desorption graphs for the FAC support and the NiMo (5/15)/FAC R catalyst.

Table 16. Textural properties of FACs and NiMo (5/15)/FAC.

Sample	BET surface area (m^2/g)	BJH pore volume (cm^3/g)	Avarage pore diameter ($4V/S_{BET}$)(nm)
FACs	10.10±0.01	0.004±0.001	1.59±0.02
NiMo (5/15) /FAC R.	8.40±0.01	0.047±0.01	23.33±0.003

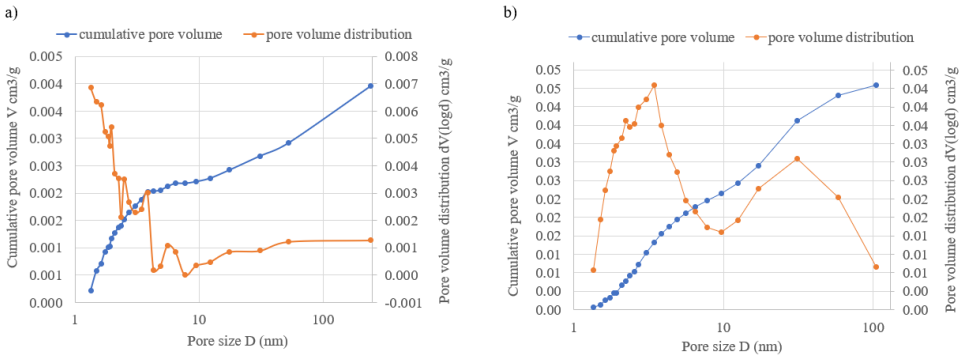

Figure 32. BJH desorption pore size distribution; a) FAC. b) NiMo(5/15)/FAC R.

2.6.7 Conclusions.

In conclusion, from what has been said so far, we can affirm the following:

- From the catalytic screening performed on different FACs-supported catalysts, the most efficient catalyst is NiMo (5/15)/FAC, providing a hydrocarbon biofuel (100% conversion) with a Green Diesel yield of 66.2 wt% and consisting of 91.7% of *n*-C_{15}-C_{18} hydrocarbons.
- Bimetallic catalysts are found to be more efficient than trimetallic catalysts.
- Regarding the HDO-DCO-DCO_2 reaction selectivity, NiMo (5/15)/FAC catalyst prefers the HDO reaction, thus ensuring greater atom economy of the reaction. However, among the studied catalyst, the one with the highest HDO selectivity is CoMo (6/15)/FAC but the biofuel obtained is rich in alkenes.
- NiMo (5/15)/FAC catalytic activity is solvent dependent. With hexane, 100% conversion is achieved; this is attributable to the hydrogen-shuttling capacity of supercritical hexane.
- NiMo (5/15)/FAC recycling test shows that the catalyst loses activity after three reaction cycles, reaching 9% conversion at the third cycle. This deactivation is mainly attributed to the presence of coke on the surface of the catalyst.
- Oil screening shows that NiMo (5/15)/FAC catalyst reaches 100% conversion for all the oil tested. In addition, different oils modulate the HDO/DCO-DCO_2 reaction selectivity of NiMo (5/15)/FAC; with Sunflower oil, HDO selectivity is lower than with other oils.
- Having fixed the reaction conditions and catalyst reduction mode (batch reduction), NiMo (5/15)/FAC-Zeo is more efficient than NiMo (5/15)/FAC. With NiMo (5/15)/FAC-Zeo, almost complete conversion is reached, and 59.9wt% Green

Diesel yield is obtained. NiMo (5/15)/FAC displays a higher yield, but the biofuel contains some unconverted oil. The two catalysts show different reaction selectivity; NiMo (5/15)/FAC-Zeo prefers DCO-DCO_2 reaction while NiMo (5/15)/FAC retains his HDO selectivity (probably the different selectivity is due to the diverse catalyst synthesis process).

- NiMo (5/15)/FAC characterization provided several findings. The ICP-MS analysis confirms the effective incorporation of the metals on the FACs support in accordance with the nominal quantities chosen. The FT-IR spectrum indicates the presence of MoO_3 on the support. However, no NiO-related signals are observed; since ICP-MS confirms the presence of Ni, the lack of NiO signals is due to the low concentrations of NiO on the support. XRD diffractograms confirm the presence of mullite and quartz as support phases; signals related to MoO_2 and metallic Ni are observed, suggesting the effective reduction of the catalyst. Finally, BET-BJH analysis reveals the microporous characteristic of the support; however, after metals impregnation, the material exhibits mesoporous characteristics, suggesting the formation of new pores after metal impregnation in the support.

In conclusion, we can state that cenospheres can be used as a supporting material for the synthesis of CDO catalysts. As mentioned before, FACs are polluting by-products, so their use in the synthesis of catalysts represents a green strategy for their recycling. In this work, several FACs-supported catalysts were synthesized, and two showed suitable catalytic activities, NiMo (5/15)/FAC and NiMo (5/15)/FAC-Zeo. Further studies can be performed to increase NiMo (5/15)/FAC stability and to evaluate NiMo (5/15)/FAC-Zeo activity for multiple reaction cycles or at different reaction conditions; however, the studies performed have shown how an appropriate formulation allows the synthesis of efficient catalysts for the catalytic deoxygenation reaction.

2.7 LDH-based catalysts.

This section reports the results obtained from catalytic tests performed with layered double hydroxides derived catalysts. In the first part, reaction condition screening data obtained with NiMoAl (0.6) catalyst are presented, while in the second part, the data obtained from a catalytic screening of several LDHs catalysts are reported. Finally, the characterization of the most promising catalyst is reported.

2.7.1 NiMoAl (0.6) performance investigation.

Preliminary catalytic tests have shown high catalytic activity of NiMoAl (0.6) R. Therefore, we decided to address an in-depth study of this catalyst first. Reaction conditions such as temperature, pressure, catalyst percentage, reaction time, and reduction time were then analyzed. In addition, the catalytic activity of the catalyst for multiple catalytic cycles was also studied to evaluate its stability. Finally, the activity of the catalyst in the calcined state was also reported.

2.7.1.1 NiMoAl (0.6) reaction condition screening.

We first evaluated the catalytic activity of NiMoAl (0.6) R. depending on temperature, pressure, and catalyst weight percentage.

The fixed reaction conditions were 2g of rapeseed oil, 20g of Hexane, and 6h reaction time while temperature, H_2 pressure, and catalyst/oil wt% ratio have been varied: T = 320°C, 240°C, P = 20, 40bar, catalyst/oil wt% ratio = 10wt%, 4wt%. Before the reaction, the catalyst was reduced in batch at 320°C, 60bar H_2, and 8h of reduction time.

Figure 33 shown the IR spectra of the obtained mixtures.

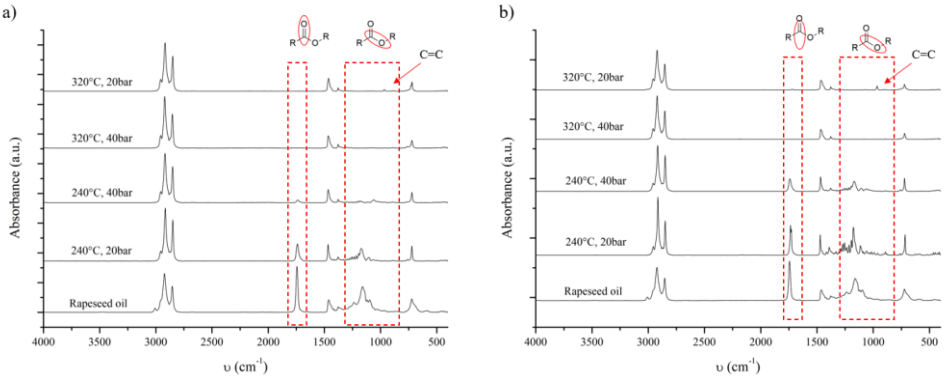

Figure 33. FT-IR spectra at different temperature and pressure: a) FT-IR at 10wt% catalyst, b) FT-IR at 4wt% catalyst.

Using 10wt% of catalyst (Figure 33 a), maximum conversion (absence of signals relating to the vibrational modes of the C=O and C-O bonds) is observed for reactions performed at temperatures above 240°C, indicating that temperature plays a crucial role in oil conversion. At 320°C and 10wt% of catalyst, the IR spectra do not seem to show any differences as the pressure varies, except for a low-intensity peak at about 966 cm^{-1} observed in the case of the reaction performed at 20bar; this signal is related to the bending of substituted C=C bonds (*trans*), suggesting the presence of unsaturated hydrocarbons due to the lower H_2 pressure. Interestingly, by increasing the pressure at 240°C from 20 to 40bar, there is a significant reduction in the peak related to the carbonyl group, indicating that a pressure increase promotes triglycerides conversion. On the other hand, working with 4wt% of catalyst (Figure 33 b), complete conversion is achieved only at 320°C and 40bar H_2, confirming that higher temperatures are needed to fully convert oil. In addition, 40bar H_2 are needed at 320°C to achieve complete conversion; in fact, a decrease in pressure results in a low-intensity peak related to the carbonyl group, indicating incomplete conversion; moreover, the signal related

to the C=C bonds (966 cm^{-1}) is also more evident in comparison to the same reaction performed with 10wt% of catalyst, confirming that a higher H_2 pressure favors the conversion and saturation of the double bonds of the alkenes formed during the reaction.

GC-FID analysis (table 17) shows more clearly what observed via FT-IR.

Table 17. NiMoAl (0.6) R. reaction conditions screening.

Entry[1]	Temperature (°C)	Pressure (bar)	Catalyst (%)	Alkenes	*n*-C_7-C_{14}	*n*-C_{15}-C_{18}	C >18	Branched C_{15}-C_{18}	FAME	Other	Conversion (%)	OLP Yield (wt%)	Green Diesel yield (wt%)	Selectivity
1	320	40	10	0	1.7	94.1	2.0	2.2	0	0	100	69.1	65.7	1.8
2	320	20	10	8.7	7	70.5	6.9	4.5	0	2.4	100	75.7	53.4	2.4
3	320	40	4	0	3.1	92	2.8	2.1	0	0	100	72.9	67.1	2.7
4	320	20	4	18	6.6	66.5	2.8	1.8	0	4.2	100	74.7	49.7	2.3
5	280	30	7	1.9	3.1	86.4	4.0	0.7	4	0	97	88.3	76.3	1.3
6	240	40	10	0	0.1	88.2	2.4	0.1	7.2	1.8	94	85.6	75.6	0.7
7	240	20	10	0	0.2	37.6	0.6	0	57.1	4.3	45	95.7	36	1
8	240	40	4	0.1	0	30.3	0.8	0	64.3	4.5	37	97.4	29.5	0.8
9	240	20	4	0.1	0	14.5	1	0	77.2	7.1	25	97.1	14.1	0.8

[1]Fixed reaction conditions: 6h of reaction time, 20g of hexane and 2g of rapeseed oil.

In all cases, to achieve 100% conversion (no FAME content, i.e., no residual oil), the reaction must be carried out at temperatures above 280°C, confirming what we see in the IR analysis. The positive effect of the temperature on the catalytic deoxygenation reaction has been reported by many authors [140, 142, 147, 159].

As can be seen from entries 6 and 7, at 10wt% of catalyst and 240°C, a pressure increase (from 20 to 40bar) promotes conversion, starting from 45% (entry 7) to 94% (entry 6), and this is in agreement with many authors[129, 170, 172, 174]. This pressure effect is less evident working with 4wt% and 240°C (entries 8 and 9), but higher pressures favor diesel range hydrocarbon content for both catalyst amounts studied due to the lower alkenes contents. The positive pressure effect can be explained by higher H_2 solubilized at higher pressure value. In addition, lower pressure slightly enhances cracking reaction favoring *n*-C_8-C_{14} hydrocarbons content (entry 2,4)[169].

Both at 4wt% and 10wt% of catalyst, the best reaction conditions are 320°C and 40 bar, resulting in both cases in a 100% hydrocarbon biofuel of which 94% (entry 1) and 92% (entry 3) in the diesel range, and 65wt% and 67wt% Green Diesel yield, respectively. As expected, as conversion increases, OLP yield decreases because more gaseous products are formed, like propane (deriving from the hydrodeoxygenation of the glycerol of the triglyceride), CO, and CO_2 (deriving from the DCO and DCO_2 reactions).

Reaction at intermediate reaction conditions (entry 5) was also performed. In this case, incomplete conversion (97%) and less diesel range hydrocarbon percentage (86.4%) are obtained; on the other hand, higher OLP and Green Diesel yield are reported, and this is probably due to the reaction condition used (low reaction temperature inhibiting cracking reactions and thus higher OLP yield).

Entries 5 and 6 show that for these reaction conditions, greater Green Diesel yield is obtained, but the biofuel also contains FAME and other oxygenated compounds that make the biofuel a viscous liquid less suitable as a biofuel, so the best conditions chosen are those given in the entry 3 (greater Green Diesel yield and lower catalyst amount).

Temperature and pressure also influence the HDO/DCO-DCO_2 reaction selectivity; higher temperatures seem to promote the hydrodeoxygenation reaction, i.e., greater content of *n*-C_{16}+C_{18} hydrocarbons. Given the exothermic nature of the HDO reaction, the reverse would be expected, but the results agree with what was observed by Santillan-Jimenez et al. for LDHs system[286]. In addition, as stated for FACs-supported catalysts, the hydrogen-shuttling capacity of supercritical hexane improved hydrogen solubility, promoting HDO selectivity.

The same effect is observed with pressure; as expected, an increase in pressure favors HDO as this reaction pathway requires more hydrogen consumption[127]. On the other hand, catalyst % does not affect the reaction selectivity.

Set the reaction conditions at 320°C, 40bar H_2, and 4wt% of catalyst, the catalyst activity was also investigated at different reaction times. IR analysis of the reactions at 6, 4, and 2h (Figure 34) shows no differences. In all cases, signals related to C=O and C-O bonds are absent, suggesting complete conversion even at a reaction time of 2h.

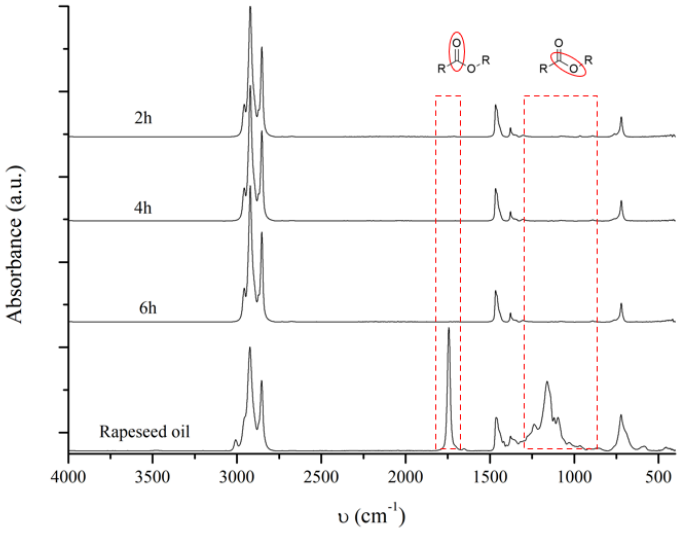

Figure 34. IR spectra at different reaction time.

GC-FID analysis also shows no differences between reactions performed at different reaction times; always 100% conversion and *n*-C_{15}-C_{18} hydrocarbon content higher than 90% are obtained (Table 18 and Table 19). Slight differences were observed for the reaction performed for 2h, in which very small amounts of methyl stearate (0.4%) and other compounds (1.1%) are observed (Table 18). Given the negligible percentages of these compounds, it can be affirmed that NiMoAl (0.6) R. is able to fully convert rapeseed oil even after only 2h of reaction time, producing a hydrocarbon biofuel consisting of 91% hydrocarbon in the diesel range and with a Green Diesel yield of 73.6wt% (Table 19). Table 19 reports that, as the reaction time decreases, an increase in the OLP yield is observed (72.9wt% after 6h of reaction time vs. 81.2wt% after 2h of reaction time); this should not be surprising since a shorter reaction time also means less time for cracking reactions to take place[155]. In addition, a slight decrease in selectivity is noted as reaction time decrease, starting from HDO/DCO-DCO_2 value of 2.7 at 6h to 2.3 after 2h of reaction time [155].

Table 18. Effect of reaction time on mixture composition.

Entry	Reaction time	Alkenes	*n*-C_8-C_{14}	*n*-C_{15}-C_{18}	C>18	Branched	FAME	Other
1	6	0	3.1	92.0	2.8	2.1	0	0
2	4	0.1	2.3	93.1	3.2	1.3	0	0
3	2	0.8	2.3	91.0	2.9	1.5	0.4	1

Fixed reaction conditions: 320°C, 40bar of H_2, 4wt% of catalyst, 2g of rapeseed oil and 20g of hexane.

Table 19. Effect of reaction time.

Entry	Reaction time	Conversion	OLP yield (wt%)	Green Diesel yield (wt%)	Selectivity
1	6	100	72.9	67.1	2.7
2	4	100	76.9	71.6	2.1
3	2	100	81.2	73.6	2.2

Fixed reaction conditions: 320°C, 40bar of H_2, 4wt% of catalyst, 2g of rapeseed oil and 20g of hexane.

2.7.1.2 Catalyst Reduction time effect and activity of catalyst in calcined state..

After exploring the effect of reaction parameters, we also wondered what influence the catalyst reduction activation time could have on the reaction mixture. Therefore, the catalyst was reduced for 2h or 4h at 320°C and 60bar of H_2. After activation, the catalyst was tested in the CDO reaction at 320°C, 40bar of H_2, 4wt% of catalyst (2g of rapeseed oil and 0.08g of catalyst), and for 6h.

From the IR spectra of the reaction mixture obtained at different catalyst reduction times (Figure 35), it can be observed that no differences are present, which means that the catalyst is able to fully convert oil even after 2h of activation by reduction.

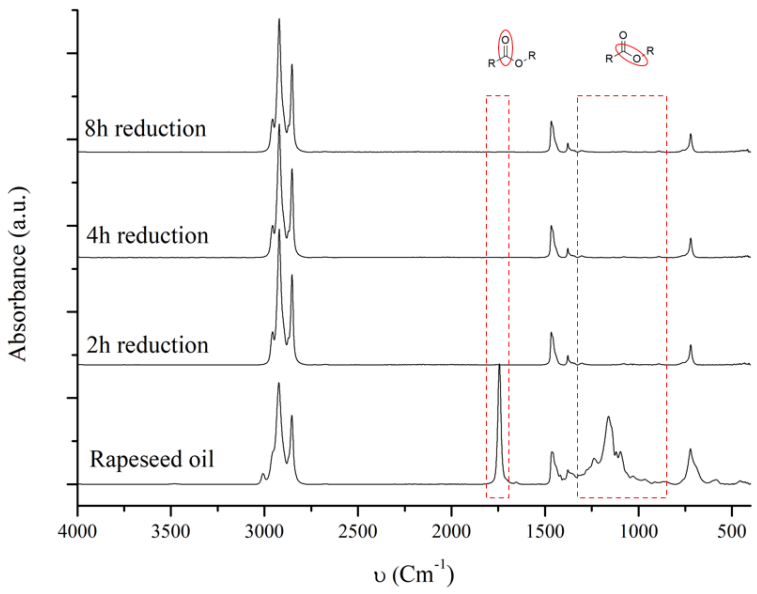

Figure 35. IR spectra at different reduction time.

The GC analysis (Table 20) confirms the results obtained from the IR analysis; in any case, there is no effect due to the reduction time, and the hydrocarbon distribution is essentially the same, with diesel range hydrocarbon content greater than 90%.

The differences are more pronounced focusing on the reaction selectivity and OLP yield (Table 21). As the reduction time decreases, a decrease in HDO selectivity and an increase in OLP yield is observed; from entry 1 to entry 3, the OLP yield increases from 72.9 wt% to 81.1 wt% and since the hydrocarbon distribution is the same, also Green Diesel yield increases (from 67.1wt% to 75.5wt%). These two evidences can be explained by the minor reduction degree of Mo and Ni; since Mo-based catalysts are reported to promote HDO reaction, probably less amount of reduced Mo could decrease HDO selectivity (with the reduction condition used in this work, the most probable state of reduced Mo is MoO_2); on the other hand, less amount of metallic Ni could lead to a lower cracking degree [146]. By analyzing Table 21 and Table 19, it seems to be no differences, and this suggests that catalyst reduction time and CDO reaction time (at fixed reduction time) have complementary effects; in particular, by observing Table 18 entry 3 and Table 20 entry 3, it can be speculated that at the conditions of Table 18 entry 3, higher catalyst amounts are in a reduced state allowing complete conversion even after only 2 hours, while at the conditions of Table 20 entry 3, probably some of the hydrogen in the reaction is used to further reduce the catalyst (reach a reduction degree similar to the catalyst of Table 18 entry 3) and obtain a similar biofuel after 6 hours of reaction time.

Table 20. Effect of catalyst's reduction time on mixture composition.

Entry	Reduction time	Alkenes	*n*-C_8-C_{14}	*n*-C_{15}-C_{18}	C>18	Branched	FAME	Other
1	8	0	3.1	92.0	2.8	2.1	0	0
2	4	0	2.4	93.2	2.8	1.6	0	0
3	2	0	2.6	92.1	4.1	1.2	0	0

Fixed reaction conditions: 320°C, 40bar of H_2, 4wt% of catalyst, 2g of rapeseed oil, 20g of hexane and 6h of reaction time.

Table 21. Effect of catalyst's reduction time.

Entry	Reduction time	Conversion	OLP yield (wt%)	Green Diesel yield (wt%)	Selectivity
1	8	100	72.9	67.1	2.7
2	4	100	76.0	70.8	2.1
3	2	100	81.1	75.5	1.6

Fixed reaction conditions: 320°C, 40bar of H_2, 4wt% of catalyst, 2g of rapeseed oil, 20g of hexane and 6h of reaction time.

The catalytic activity of NiMoAl (0.6) was also evaluated without the previous reduction step, i.e., the catalyst was not reduced before the reaction but was used directly in the oxidized form (NiMoAl (0.6) C.) to evaluate if catalyst's reduction took place directly in reaction atmosphere and, thus, if the catalyst is also able to catalyze the reaction in this state.

The activity of NiMoAl (0.6) C. is evaluated by fixing the reaction conditions at 320°C, 40bar H_2, 2g rapeseed oil, and 20g hexane while the catalyst percentages (10wt% and 4wt%) and reaction time (6h, 4h, and 2h) are varied.

The IR spectra of the reaction mixture obtained using NiMoAl (0.6) C. are reported in Figure 36.

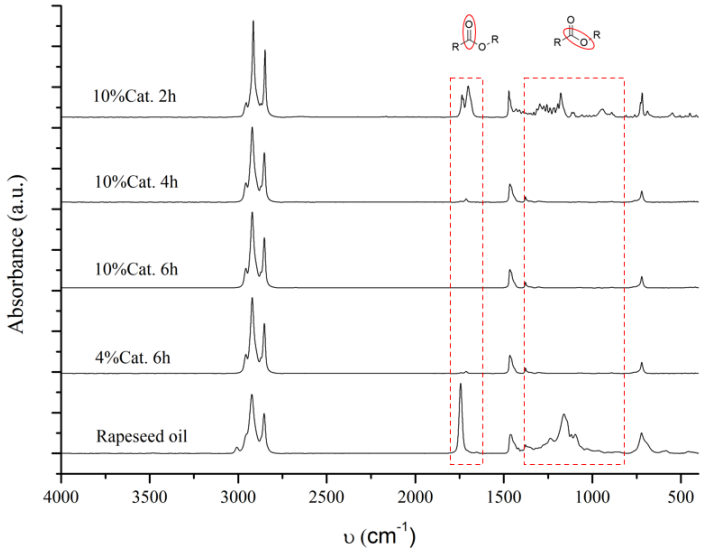

Figure 36. IR spectra of the mixtures obtained with NiMoAl (0.6) C..

IR analysis shows a low-intensity signal corresponding to the carbonyl group for the reaction performed for 6h and 4wt% catalyst, which is absent using a 10wt% catalyst. Therefore, without the reduction activation step, more catalyst must be used to achieve complete conversion. If we evaluate the effect of the reaction time, we can see that at 4h, but especially at 2h, the triglyceride signals are clearly visible. In addition, after 2h reaction time, two peaks related to the carbonyl group are present, one related to the ester carbonyl of triglycerides and one characteristic of the carbonyl of free fatty acids. This suggests that under these conditions, more than this time is needed to convert all triglycerides but also that more is needed for the conversion of free fatty acids to hydrocarbons.

The results obtained after GC-FID analysis are shown in Table 22 and Table 23.

Table 22. . Compound mixture distribution with NiMoAl (0.6) C. (oxidized state).

Entry	Catalyst wt%	Reaction time	Alkenes	*n*-C_8-C_{14}	*n*-C_{15}-C_{18}	C>18	Branched	FAME	Other
1	4	6	0.8	4.1	86.3	3.6	1.9	2.4	1
2	10	6	0.4	3.1	87	3.2	4.2	0.2	0.5
3	10	4	1.3	4.5	83.6	3.8	2.8	3.2	0.8
4	10	2	1	2.8	56.2	2.5	1.6	32.6	3.2

Fixed reaction conditions: 320°C, 40bar of H_2, 2g of rapeseed oil and 20g of hexane.

Table 23. Catalytic activity of NiMoAl (0.6) C. (oxidized state).

Entry	Catalyst (wt%)	Reaction time (h)	Conversion (%)	OLP yield (wt%)	Green Diesel yield (wt%)	Selectivity
1	4	6	98	70.4	60.8	0.4
2	10	6	100	69.6	60.6	0.4
3	10	4	98	76.4	63.9	0.3
4	10	2	72	84.7	47.6	0.3

Fixed reaction conditions: 320°C, 40bar of H_2, 2g of rapeseed oil and 20g of hexane.

Table 22 shows that with 4wt% of catalyst, even after 6h reaction time (entry 1), the reaction mixture contains a low percentage of methyl stearate (2.4%); in contrast, using 10wt% of catalyst (entry 2), the biofuel consists of 100% hydrocarbons; so, under these conditions, 100% conversion can be achieved (Table 23 entry 2). At complete conversion, comparing Table 22 entry 2 with the analogous one done after catalyst reduction (**Error! Reference s ource not found.** entry 1), it can be seen that, without the previous reduction step, there is a slight decrease in the percentage of hydrocarbons in the diesel range (87.3% vs. 94.1%) and

in the green diesel yield (60.6% vs. 65.5%); however, considering the considerable gain of time and costs in the reaction performed with catalyst in calcined form, this is a very good result. If we perform the reaction for shorter times (Table 22 entry 3,4), the presence of methyl esters at 4h and 2h is observed (3.2% and 32.6%, respectively). From 2 to 4h there is a considerable increase in conversion, from 72% to 98% (Table 23 entry 3,4). Observing the reaction selectivity, with the catalyst in oxidized state, there is a reversed selectivity compared with the reaction in which the catalyst was previously reduced (Table 23 vs **Error! Reference source not found.**). In this case, there is a greater preference for DCO-DCO_2. This could be explained by the fact that, without the previous reduction step, part of the hydrogen present in the system is used by the catalyst to reduce itself during the reaction and, therefore, is less available to carry out the HDO reaction, which is the reaction pathway which requires a greater consumption of H_2.

2.7.1.3 NiMoAl (0.6) R. recycling tests.

Finally, catalyst activity was investigated for multiple reaction cycles. As in the case of NiMo (5/15)/FAC, after each reaction, the catalyst was recovered and dried overnight in a vacuum oven. Once dry, it was reused for the subsequent reaction without further treatment.

The reaction conditions are set at 320°C, 40bar H_2, 6h reaction time, and 10wt% catalyst (10wt% of catalyst was chosen to ensure enough cycle reaction after each catalyst recovery). Similarly to what was done with NiMo (5/15)/FAC, in the first reaction cycle, 20g of hexane, 2g of rapeseed oil, and 0.2g of catalyst were used. For the subsequent reaction cycles, the amount of starting oil was adjusted according to the amount of catalyst recovered (to maintain the 10wt% catalyst to oil ratio), and the amounts of solvent were adjusted to maintain the ratio of oil to hexane at 1:10.

The results obtained from the IR spectra are sown in Figure 37.

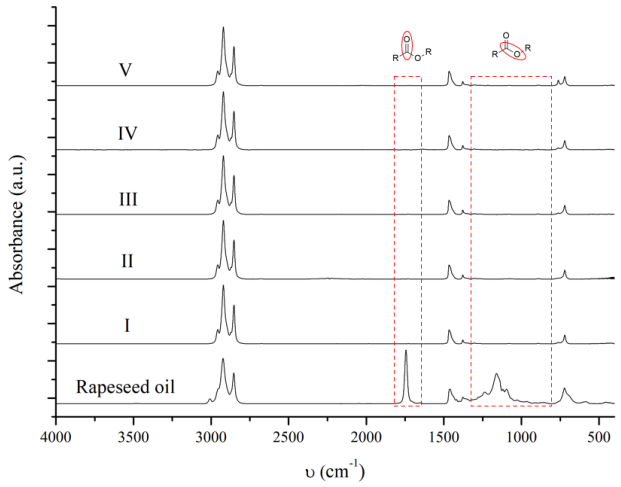

Figure 37. IR spectra of the mixture obtained from successive reaction cycle.

Comparison of the IR spectra indicates that, at least up to the fifth reaction cycle, the catalyst is able to fully convert the oil to hydrocarbons without any appreciable change in the biofuels produced. At each cycle, the typical triglyceride ester signals are not observed, and the spectra show signals related only to C-H and C-C bonds.

GC analysis confirms what was observed from IR analysis (Table 24 and Table 25).

Table 24. Recycling test.

Entry	Cycle	Conversion (%)	OLP yield (wt%)	Green Diesel yield (wt%)	Selectivity
1	I	100	69.1	65.7	1.8
2	II	100	78.5	73.6	2
3	III	100	54.5	50.7	1.8
4	IV	100	85.9	78.4	2.3
5	V	100	58.9	55.3	1.7

Fixed reaction conditions: 320°C, 40bar of H_2, 10wt% of catalyst and 6h of reaction time.

Table 25. Compound mixture distribution obtained from recycling test.

Entry	Cycle	Alkenes	*n*-C_8-C_{14}	*n*-C_{15}-C_{18}	C>18	Branched	FAME	Other
1	I	0	1.6	95.1	1.1	2.3	0	0
2	II	0	1.3	93.8	2	2.9	0	0
3	III	0	1.6	93	2.1	3.6	0	0
4	IV	0	1.5	91.2	2	5.3	0	0
5	V	0	1.6	93.8	2.1	2.4	0	0

Fixed reaction conditions: 320°C, 40bar of H_2, 10wt% of catalyst and 6h of reaction time.

Even at the fifth reaction cycle, the catalyst remains active, leading to 100% conversion (Table 24) and an almost unchanged hydrocarbon distribution for each reaction cycle; for all the reaction cycles, diesel range hydrocarbon content greater than 90% is achieved, and low cracking activity is reported (Table 25). Reaction selectivity also remains unchanged, with a prevalence of HDO reaction (Table 24). Inconsistent yields are obtained in the various catalytic cycles; the reason needs to be better understood, therefore, will be the subject of further study.

2.7.2 LDHs catalysts screening.

Given the high efficiency of NiMoAl (0.6) catalyst, we considered synthesizing other LDHs-based catalysts by varying the type of metals and the amount; therefore, the catalysts were tested to evaluate the influence of the type and amount of metal used. For this purpose, catalysts activity was evaluated both after reduction (320°C, 60bar H_2 and 4h reduction time) and in the oxidized state (in situ reduction). With the oxidized catalysts, the reaction conditions chosen were the same as used for reduced catalyst, but the catalyst amount employed was set at 10wt% (to achieve better efficiency, more catalyst is required for the oxidized catalysts).

2.7.2.1 LDHs catalysts screening (Pre-reduction activation).

Given the results obtained with NiMoAl (0.6) R., the reaction conditions used for LDHs catalysts' screening (in the reduced state) were set at 320°C, 40bar H_2, 6h reaction time, 2g of rapeseed oil, 4wt% (0.08g) of LDHs catalysts (in the case of NiMoAl (0.6) R., 4wt% of catalyst proved to be enough to reach 100% conversion).

Figure 38 shows the IR spectra of the reaction mixtures obtained with the different LDHs-based catalysts.

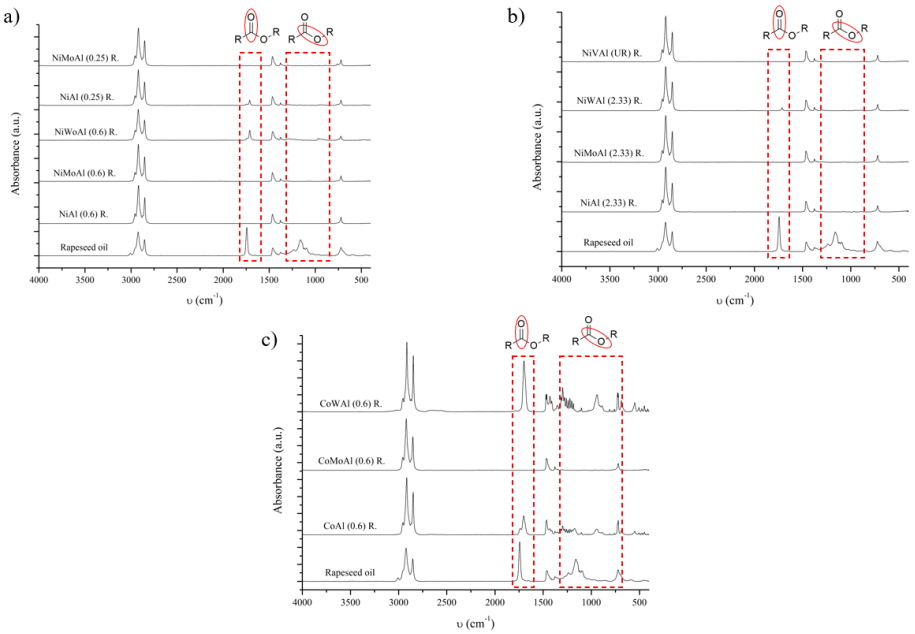

Figure 38. FT-IR of LDHs catalyst screening (reduced state): a) NiAl (0.6) + NiAl (0.25) systems. b) NiAl (2.33) + NiVAl (UR) systems. c) CoAl (0.6) systems.

Considering the LDHs system with Ni/Al = 0.6 (Figure 38 a), the NiAl (0.6) R. precursor is able to fully convert the oil (only the vibrational signals of the CH bond are present); furthermore, the addition of Mo (NiMoAl (0.6) R.) does not seem to affect the catalytic activity in any way, leading again to the production of an exclusively hydrocarbon biofuel. In contrast, the W addition negatively affects the catalytic activity, which is visible from the peak centered 1710 cm^{-1}, indicative of free fatty acids.

Varying the Ni/Al ratios of the catalyst influences the activity of the catalyst. By comparing NiAl (0.25) R., NiAl (0.6) R. (Figure 38 a) and NiAl (2.33) (Figure 38 b) catalysts, it can be seen that a lower amount of Ni results in a lower conversion; in fact, the IR spectrum of the reaction performed with NiAl (0.25) shows the C=O bond signals. However, by increasing the amount of Ni (both NiAl (0.6) and NiAl (2.33)), the reaction mixtures do not show the vibrational signals of the carbonyl groups, indicating complete conversion in both cases. On

the other hand, adding Mo to the NiAl (0.25) system shows an increase in catalytic activity as the biofuel produced consists exclusively of hydrocarbons (Figure 38 a).

Looking instead at the NiAl (2.33) system (Figure 38 b), adding Mo does not seem to be resulting in any significant differences; however, as in the case of NiAl (0.6), the IR spectrum of the mixture resulting from the NiWAl (2.33) catalyst shows a peak centered at 1710 cm^{-1} indicating a lower conversion after W addition.

A similar result is observed in the case of the CoAl (0.6) catalytic system (Figure 38 c). CoMoAl (0.6) catalyst gives complete conversion, while the addition of W (CoWAl (0.6) R.) induces a significant loss of catalyst activity.

Complete conversion is also achieved in the case of the NiVAl (UR) catalyst (Figure 38 b). The nominal x-value of NiVAl (UR) is similar to that of NiAl (2.33) systems. Thus, the higher degree of conversion of NiVAl (UR) compared to NiWAl (2.33) may depend either on a metal effect (V versus W) or on the different synthesis (or both).

GC-FID analysis of the reaction mixtures provides a more specific picture of the behavior of the various catalysts tested (Table 26).

Table 26. Compound mixture distribution according to the catalyst used.

Entry	Catalyst	Alkenes	*n*-C_8-C_{14}	*n*-C_{15}-C_{18}	C>18	Branched C_{15}-C_{18}	FAME	Other
1	NiAl (0.6) R.	4.2	17.2	74.8	3.9	0	0	0
2	NiMoAl (0.6) R.	0	2.4	93.2	2.8	1.6	0	0
3	NiWAl (0.6) R.	10.5	3.3	36.5	2.6	10.7	24.8	11.6
4	NiAl (0.25) R.	1	15.7	66.4	2.2	2	10.4	2.3
5	NiMoAl (0.25) R.	0.7	5.7	86	3.9	3.2	0	0.5
6	NiVAl (UR) R.	0	13.1	82.5	2.8	1	0	0.6
7	NiAl (2.33) R.	0.9	15.1	78.8	2.5	1.5	0.2	1
8	NiMoAl (2.33) R.	0	2.9	89.7	3	4	0	0.4
9	NiWAl (2.33) R.	0	5.5	85	3.9	1.9	4.6	3
10	CoAl (0.6) R.	0	1.6	45.2	1.7	0	46.5	10.1
11	CoMoAl (0.6) R.	2	4.1	85.9	4.2	3.1	0.1	0.6
12	CoWAl (0.6) R.	17	1	8.4	1.7	1.8	52.1	18

Fixed reaction conditions: 320°C, 40bar of H_2, 4wt% of catalyst (0.08g catalyst and 2g oil), 20g Hexane and 6h of reaction time.

As shown in Table 26, the catalyst that provides a higher concentration of diesel-range hydrocarbons is NiMoAl (0.6) R., resulting in 93.2% *n*-C_{15}-C_{18} hydrocarbons (entry 2). As observed in the IR analysis, by adding W to the NiAl (0.6) catalyst, the produced mixture exhibits high amounts of FAME (24.8%). On the other hand, NiWAl (0.6) R. shows moderate isomerization activity resulting in 10.7% of C_{15}-C_{18} branched hydrocarbons (entry 3). This is an interesting feature as the presence of branched hydrocarbons decreases the cloud point of the produced biofuel[127].

From the comparison between the NiAl catalysts (entries 1, 4 and 7), a fully hydrocarbon biofuel is obtained with NiAl (0.6) R. and NiAl (2.33) R.. On the other hand, with NiAl (0.25) R catalysts, 10.4% of FAME content is obtained (in agreement with what was seen in the IR), confirming that a suitable amount of Ni is needed to catalyze the CDO reaction[155]. However, for all the NiAl bimetallic catalysts, high amounts of *n*-C_8-C_{14} hydrocarbons (about

15 %) are obtained, indicating high cracking activity [146, 169, 287]. While an increase in Ni content promotes conversion, the same effect does not occur in the case of cracking activity; there is no significant change in light hydrocarbons content.

In the case of NiAl (0.25), adding Mo significantly increases the catalytic activity (entry 5), producing a fully hydrocarbon biofuel. Furthermore, molybdenum inhibits cracking reaction (5.7% *n*-C_8-C_{14} hydrocarbons for NiMoAl (0.25) R. vs. 15.7% *n*-C_8-C_{14} for NiAl (0.25) R.). The same effect of cracking inhibition can be observed in the case of NiMoAl (2.33) R. (entry 8). Using NiMoAl (2.33) R. instead of NiAl (2.33) R. (entry 7), light hydrocarbons content decreases to 2.9% and, as a result, diesel-range hydrocarbons increase (89.7%). Again, the catalyst with W (entry 9) has lower activity than its precursor NiAl (2.33) R. and the NiMoAl (2.33) R. catalyst.

With NiVAl (UR) R. (entry 6), a 100% hydrocarbon mixture is obtained. However, the catalyst shows some cracking activity (13.1% *n*-C_8-C_{14} hydrocarbons) resulting in a decrease of hydrocarbons in the diesel range (82.5%).

Finally, concerning Co-based catalysts, while CoWAl (0.6) R. shows low catalytic activity confirming the negative effect of W, 100% hydrocarbons mixture is obtained only in the case of CoMoAl (0.6) R.

In addition to hydrocarbon distribution, catalysts show different diesel yields and reaction selectivity (Table 27).

Table 27. Conversion, yield, and selectivity according to the catalyst used (reduced state).

Entry	Catalyst	Conversion	OLP Yield (wt%)	Green Diesel yield (wt%)	Selectivity
1	NiAl (0.6) R.	100	58.2	43.5	0.2
2	NiMoAl (0.6) R.	100	76.0	70.8	2.1
3	NiWAl (0.6) R.	79	84.7	40	2.2
4	NiAl (0.25) R.	93.2	65.4	44.7	0.2
5	NiMoAl (0.25) R.	100	83.3	71.6	1
6	NiVAl (UR) R.	100	65.4	53.5	0.2
7	NiAl (2.33) R.	99.9	55.8	44.9	0.2
8	NiMoAl (2.33) R.	100	77.4	69.4	2.6
9	NiWAl (2.33) R.	97.6	81.8	73.2	2.7
10	CoAl (0.6) R.	61.8	82.1	37.1	0.6
11	CoMoAl (0.6) R.	100	80.1	71.2	3.3
12	CoWAl (0.6) R.	54.9	85.3	8.7	0.9

Fixed reaction conditions: 320°C, 40bar of H_2, 4wt% of catalyst (0.08g catalyst and 2g oil), 20g Hexane and 6h of reaction time.

100% conversion is achieved for catalysts in entries 1, 2, 5, 6, 7, 8, and 11. At complete conversion, the catalysts leading to better Green Diesel yield are NiMoAl (0.6) (70.8wt%, entry 2), NiMoAl (2.33) (72.5wt%, entry 8), NiMoAl (0.25) (71.6wt%, entry 5), CoMoAl (0.6) (71.2wt%, entry 11); it should be noted that these catalysts contain molybdenum, confirming the positive effect of molybdenum in the CDO reaction [83, 111]. The catalysts used in entries 1, 4, 6, and 7 are the ones leading to lower OLP yields (thus also lower Green

Diesel yield), and this should not be surprising as these catalysts have the highest degree of cracking (Table 26 entry 1, 4, 6 and 7).

Regarding reaction selectivity, all the bimetallic catalysts favor DCO-DCO_2 (HDO/DCO-DCO_2 ratio = 0.2). This agrees with what has been reported in the literature for reduced Ni-based catalysts[116, 149]. Among trimetallic catalysts, only NiVAl (UR) shows a pronounced selectivity toward DCO-DCO_2. On the other hand, CoWAl (0.6) and NiMoAl (0.25) give both reaction products. All other trimetallic catalysts prefer HDO as expected, especially in the case of NiMoAl systems, since Mo is reported to enhance HDO selectivity (we have also seen this in the case of the FACs-supported catalyst)[111, 288]. As in the case of the FACs-supported catalysts, the Co-LDHs-based catalyst has the highest HDO reaction selectivity, thus confirming that cobalt-based catalysts exhibit this reaction selectivity [149].

2.7.2.2 LDHs catalysts screening (calcined state).

The same catalysts studied before were investigated without the previous reduction step. Reaction conditions set at 320°C, 40bar H_2, 6h reaction time, 2g of rapeseed oil, 0.200g of LDHs catalyst (recall that in the case of NiMoAl (0.6) C. catalyst it has been observed that it is required to work at 10wt% of catalyst to achieve 100% conversion) and 20g of Hexane. The IR spectra obtained from this catalytic screening are reported in Figure 39.

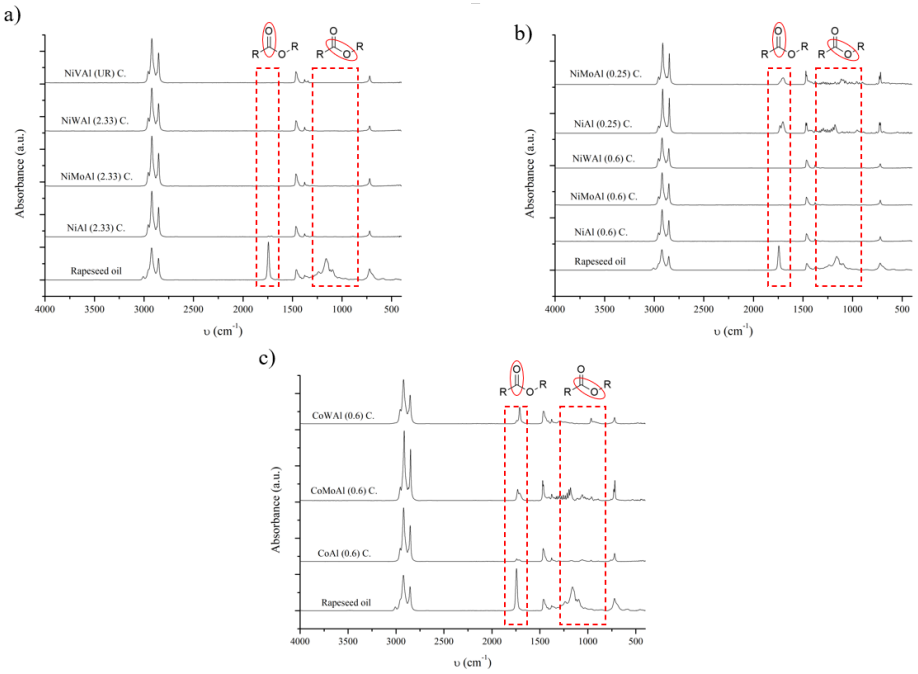

Figure 39. FT-IR of the oxidized LDHs catalyst screening: a) NiAl (0.6) + NiAl (0.25) systems. b) NiAl (2.33) + NiVAl (UR) systems. c) CoAl (0.6) systems.

For all the NiAl catalysts with Ni/Al = 0.6, no differences are visible between the IR spectra, and no C=O vibrational signals are present, indicating complete conversion. In contrast to what was observed for the same catalysts tested after reduction, in these cases, the negative effect of W is not visible, suggesting that for NiWAl (0.6) system, it is preferable to use more

catalyst or to avoid the reduction step (maybe for this catalyst the reduction step could cause sintering that partially deactivate the catalyst).

In the case of NiAl (0.25) C. (Figure 39 b), incomplete conversion is obtained, which agrees with the evidence reported for the same catalyst in a reduced state (NiAl (0.25) R.); however, after Mo addition, different data results. When reduced, the NiMoAl (0.25) R. catalyst show complete conversion (Figure 38 a and Table 27), but without the reduction step, the same catalyst (NiMoAl (0.25) C.) is not able to fully convert oil, showing a peak related to the free fatty acid (Figure 39 b). However, in comparison with NiAl (0.25) C. (in which two peaks in the 1750-1710 cm^{-1} region are visible indicating the occurrence of triglycerides as well as free fatty acids), Mo addition improves conversion (for NiMoAl (0.25) C., the IR spectrum shows only the peak related to free fatty acids). This information suggests that Mo addition slightly increases the catalytic activity by promoting triglyceride cleavage.

In the case of NiAl systems with x = 2.33 (Figure 39 a), there are no differences between NiAl (2.33) C., NiMoAl (2.33) C. and NiWAl (2.33) C., producing in all cases a fully hydrocarbon biofuel. As in the case of NiWAl (0.6) C, W addition does not produce adverse effects on conversion, as has been observed for the same catalysts after reduction. Also, for NiVAl (UR) catalyst, complete conversion is achieved.

In all cases, the Co-based catalysts display incomplete conversion (Figure 39 c), furthermore, Mo addition seems to reduce the catalytic activity of the Co-based catalyst (in contrast to what is observed for the same catalyst in reduced state).

The hydrocarbon distribution obtained after GC-FID analysis allows us to go into more detail (Table 28)

Table 28. Compound mixture distribution according to the catalyst used (oxidized state).

Entry	Catalyst	Alkenes	*n*-C_8-C_{14}	*n*-C_{15}-C_{18}	C>18	Branched C_{15}-C_{18}	FAME	Other
1	NiAl (0.6) C.	0	5.9	86.8	4.8	1.4	0	1.1
2	NiMoAl (0.6) C.	0.5	3.1	88.1	2.9	4.2	0	1.2
3	NiWAl (0.6) C.	3.1	5.1	67.5	3.4	20.9	0	0
4	NiAl (0.25) C.	7.6	2.6	48.4	3.5	1.3	29.4	7.2
5	NiMoAl (0.25) C.	6.9	5.2	59.4	2.4	6.7	12	7.4
6	NiVAl (UR) C.	0	5	89.2	4	1.8	0	0
7	NiAl (2.33) C.	0.9	6.9	82.1	3.5	3.4	1.8	1.4
8	NiMoAl (2.33) C.	0.9	5.1	83	4.6	5.7	0	0.7
9	NiWAl (2.33) C.	0	4.6	79.2	1.8	14.4	0	0
10	CoAl (0.6) C.	4.2	4.2	75.5	4.5	1.8	6.8	3
11	CoMoAl (0.6) C.	18.5	6.6	40.5	2.8	0	19.5	12.1
12	CoWAl (0.6) C.	24.6	1.8	17.4	1.5	8.2	32.8	13.7

Fixed reaction conditions: 320°C, 40bar of H_2, 4wt% of catalyst (0.2g catalyst and 2g oil), 20g Hexane and 6h of reaction time.

By analyzing the hydrocarbon distribution, the NiAl (0.6) catalytic systems show a quite similar hydrocarbon distribution (entries 1, 2, 3). NiAl (0.6) C. and NiMoAl (0.6) C. are very similar (entries 1 and 2), and the biofuels obtained contain, respectively, 86.8% and 88.1% *n*-C_{15}-C_{18} hydrocarbon. However, in comparison to their reduced counterparts, some differences are present. With both NiAl (0.6) C. and NiAl (0.6) R. the reaction mixture contains only hydrocarbons; however, in the case of NiAl (0.6) R. the mixture has discrete amounts of light hydrocarbons (Table 26 entry 1), while in the case of NiAl (0.6) C. (Table 28 entry 1), the cracking activity is reduced and, as a result, the biofuel contains a higher percentage of hydrocarbons in the diesel range (86.8%).

Between NiMoAl (0.6) R. (Table 26 entry 2) and NiMoAl (0.6) C. (Table 28 entry 2), the differences are quite small; the former leads to a slightly higher percentage of *n*-C_{15}-C_{18}

hydrocarbons (93.2%), but aside from that, NiMoAl (0.6) C. still has high catalytic activity without the reduction step (and this saves time and cost).

Even with NiWAl (0.6) C. (Table 28 entry 3) complete conversion is achieved, but the hydrocarbon distribution is different than the other NiAl (0.6) catalytic systems; with NiWAl (0.6) C. catalyst, the OLP produced has less *n*-C_{15}-C_{18} content but at the same time is rich in branched C_{15}-C_{18} hydrocarbons that improve the cold properties of the biofuel (indeed, the mixture was placed in the refrigerator at 4°C and remained in the liquid state). The isomerization-promoting effect of W was also observed in the case of the NiWAl (0.6) R. catalyst (Table 26 entry 3); however, for this catalyst, a conversion of 79% was reached versus 100% obtained with NiWAl (0.6) C.

As observed from the IR spectra, NiAl (0.25) C. and NiMoAl (0.25) C. are not able to fully convert oil; indeed, for NiAl (0.25) C., 29.4% of FAME is attained, while for NiMoAl (0.25) C the FAME content is 12.1% (entry 4,5). Also, for this system, Mo addition promotes conversion but, in comparison to NiMoAl (0.25) R. (Table 26 entry 6) it is not sufficient to fully convert oil. So, the reduction step is required for NiMoAl (0.25) catalyst to produce a FAME-free biofuel.

Like NiAl (0.6) C., also for NiAl (2.33) C. (entry 7), the cracking activity is reduced compared to the reduced state counterpart (Table 25 entry 7), but the biofuel contains small amounts of FAME (1.8%). Adding Mo, the catalyst NiMoAl (2.33) C (entry 8) produces fully hydrocarbon biofuel with 83% *n*-C_{15}-C_{18} hydrocarbons.

NiVAl (UR) C. shows high catalytic activity and leads to 89.2% Green Diesel hydrocarbons, but in comparison to NiVAl (UR) R., this catalyst has low cracking activity (5.0 % vs. 13.1% hydrocarbon *n*-C_8-C_{14}).

The W isomerization-promoting effect is also visible in NiWAl (2.33) catalyst (entry 9); with this catalyst, 14.4% branched C_{15}-C_{18} hydrocarbons are obtained. Similar to what has been

seen for NiWAl (0.6) C. and NiWAl (0.6) R. catalysts, the reduction step negatively affects the catalytic properties of the NiWAl (2.33) catalysts. NiWAl (2.33) R is unable to fully convert the oil, while with NiWAl (2.33) C., the biofuel obtained is free of FAME.

Finally, all the Co-based catalysts are unable to fully convert oil (entry 10, 11, 12); CoMoAl (0.6) C. and CoWAl (0.6) C. generate biofuels with high FAME content (19.5% for CoMoAl (0.6) C. and 32.8% for CoWAl (0.6) C.). In this case, adding a third metal negatively affects the catalyst activity; indeed, CoAl (0.6) is the one with the better hydrocarbon distribution (75.5% green diesel hydrocarbons). Compared with their counterpart in the reduced state (Table 26 entry 10, 11, 12), for the Co-based catalysts, only CoMoAl (0.6) R. completely converts oil into a hydrocarbon biofuel, suggesting that the reduction step is necessary for this catalyst.

Table 29 shows the performance of the catalysts studied in terms of conversion, green diesel yield, and selectivity.

Table 29. Conversion, yield, and selectivity according to the catalyst used (oxide state).

Entry	Catalyst	Conversion (%)	OLP yield (wt%)	Green Diesel yield (wt%)	Selectivity
1	NiAl (0.6)	100	76.0	67.0	0.1
2	NiMoAl (0.6)	100	69.6	64.2	0.4
3	NiWAl (0.6)	100	57.2	50.6	1.4
4	NiVAl (UR)	100	75.9	69.1	0.1
5	NiAl (0.25)	76	81.7	40.6	0.3
6	NiMoAl (0.25)	90	84.3	55.7	1.1
7	NiAl (2.33)	98.8	75	64.4	0.2
8	NiMoAl (2.33)	100	80.6	71.5	0.6
9	NiWAl (2.33)	100	77.4	72.4	1.6
10	CoAl (0.6)	94	84.8	65.4	0.8
11	CoMoAl (0.6)	84	83.4	33.7	2.1
12	CoWAl (0.6)	74	81.1	20.8	1.2

Fixed reaction conditions: 320°C, 40bar of H_2, 4wt% of catalyst (0.2g catalyst and 2g oil), 20g Hexane and 6h of reaction time.

Looking at the table, all the NiAl (0.6) catalysts reach 100% conversion, but differences in diesel yield and reaction selectivity are present. Between NiAl (0.6) C. and NiMoAl (0.6) C., the former is the one with the better green diesel yield (67.0wt%), suggesting that in these cases is preferable the bimetallic catalyst. Recalling the performances of their reduced counterparts (Table 27 entry 1, 2), NiAl (0.6) C. has better performance due to its greater green diesel yield (67.0 wt% respect 47.5 wt% for NiAl (0.6) R.); on the other hand, NiMoAl (0.6) R produces more green Diesel biofuel than NiMoAl (0.6) C. (70.8wt% vs. 64.2wt%), therefore, NiMoAl (0.6) R is preferable. Not surprisingly, NiWAl (0.6) leads to the lowest diesel yield among NiAl (0.6) catalysts because it has high isomerization activity, and it is reported that this reaction proceeds through cracking processes[95].

Focusing on entries 4 and 5, with NiAl (0.25) C. and NiMoAl (0.25) C., incomplete conversion is achieved. However, after Mo addition, the catalysts improve their catalytic

activity and the conversion increases from 76% with NiAl (0.25) C. to 90% with NiMoAl (0.25) C; as a result, also Green Diesel yield increases from 40.6wt% to 55.7wt%. From this, it can be stated that in order to achieve 100% conversion and good green diesel yield, the NiMoAl (0.25) catalyst must first be reduced.

NiVAl (UR) C. (entry 6) leads to 69.1wt% Green Diesel yield and is higher than NiVAl (UR) R, reflecting its lower cracking activity.

In the cases of NiAl (2.33) system, 100% conversion is achieved with NiMoAl (2.33) C. and NiWAl (2.33) C (entries 8, 9). The former leads to 71.5 wt% Green Diesel yield, being one of the catalysts leading to better Green Diesel yields; in contrast, NiMoAl (2.33) R. and also NiMoAl (0.6) R, NiMoAl (2.33) C. displayed similar green diesel yields without the need to perform a reduction, and this saves time and cost.

Regarding NiWAl (2.33) C., is the catalyst with the best green diesel yield (72.4wt%) among the catalysts tested without reduction. This is a very good result considering that this catalyst also produces a moderate amount of C_{15}-C_{18} branched hydrocarbons (14.4%).

Finally, the Co-based catalysts displayed the lower green diesel yield and the lower conversion degree (entries 10, 11, 12); by comparing them to their reduced counterparts, a better result is obtained with CoMoAl (0.6) R. (Table 27 entry 11).

Without the reduction step, the reaction selectivity of some catalysts changes sensitively; NiMoAl (0.6) C. and NiMoAl (2.33) C. prefer DCO-DCO_2 (0.4 and 0.6 respectively, entry 2, 8) while in the reduced state the same catalysts displayed HDO reaction selectivity (2.2 and 2.6 respectively Table 27 entry 2, 8). The change in selectivity may be because some of the hydrogen in the reaction environment is used to reduce the catalyst and is less available for the HDO reaction. On the other hand, NiMoAl (0.25) C. does not change its reaction selectivity compared to NiMoAl (0.25) R.; probably, less Ni content does not significantly affect hydrogen availability for the HDO reaction. For the other Ni-based catalysts, the

reaction selectivity remains unchanged, but in the case of the NiWAl catalyst the HDO/DCO-DCO_2 ratio slightly decreases compared to their reduced counterpart; the same effect is observed for CoMoAl (0.6) C catalyst.

Finally, the bimetallic catalysts and NiVAL (UR) retain their DCO-DCO_2 selectivity.

2.7.3 NiMoAl (0.6) catalyst characterization.

Given the high catalytic activity and considering that among the synthesized catalysts, it is the one that has been studied more in-depth, the NiMoAl (0.6) catalyst was characterized by ICP-MS, FT-IR, XRD and BET-BJH

2.7.3.1 ICP-MS.

To be sure that the synthesized LDH is exactly with the chosen Ni/Al ratio (in the case of NiMoAl (0.6) a Ni/Al ratio of 0.63), the elemental composition of NiMoAl (0.6) was analyzed via ICP-MS (Table 30).

Table 30 Catalyst elemental composition by ICP-MS analysis.

Sample	Al (wt%)	Ni (wt%)	Mo (wt%)	Ni/Al molar ratio (experimental)	Ni/Al molar ratio (theorical)	Ni/Mo molar ratio (experimental)	Ni/Mo molar ratio (theorical)
	15.4±0.03	21.1±0.2	21.3±0.01	0.63	0.63	1.63	0.57

The Ni/Al molar ratio obtained from the ICP-MS analysis matches perfectly with the nominal Ni/Al molar ratio chosen for the synthesis of the catalyst. The ICP-MS analysis also confirms the effective Mo intercalation in the LDH precursor after the ion exchange; however, the experimental Ni/Mo molar ratio is different than the theoretical ones. This suggests that not all the heptamolybdate intercalated within the LDH.

2.7.3.2 FT-IR.

FT-IR analysis was carried out on the NiAl (0.6) LDH precursor and NiMoAl (0.6) LDH to get qualitative information on the degree of intercalation of the heptamolidate after the ion exchange reaction. In addition, FT-IR analysis also gives us insight into the structure of the material by analyzing the vibrational signals of the bonds present within the structure. The FT-IR of the NiMoAl (0.6) C. and NiMoAl (0.6) R. are not reported because they do not provide additional information.

The FT-IR of the NiAl (0.6) LDH precursor and NiMoAl (0.6) LDH are presented in Figure 40.

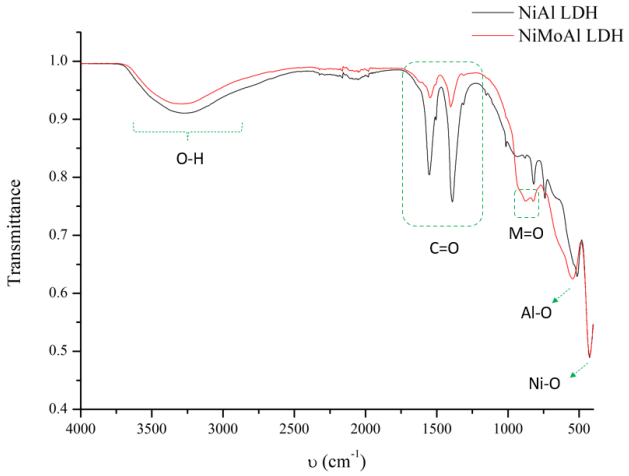

Figure 40. FT-IR comparison between NiAl (0.6) LDH (black line) and NiMoAl (0.6) LDH (red line)

The IR measurements of the NiAl LDH precursor (red line) are in accordance with Arias et al for this material [245]. Between 3600 and 3200cm^{-1}, the characteristic absorption band of structural OH and water inside the LDH layers can be observed; this band is centered at lower wave numbers than free hydroxides (>3600) due to the hydrogen bonds that occur in the

structure of the material[289]. The peaks centered at 1552 and 1389 cm^{-1} are attributed to the vibrational modes of the terephthalate carboxylates (symmetric and antisymmetric stretching, respectively)[290]. Finally, the signal at 430cm^{-1} is assigned to the Ni-O bond vibration, while the band around 520cm^{-1} is associated with Al-O stretching [245]. Comparing the spectra of uncalcined LDH before and after ion exchange, we can observe a significant decrease in terephthalate stretching signals confirming the incorporation of heptamolybdate into the structure (black line). However, the signals related to terephthalate do not disappear completely, indicating that not all heptamolybdate has intercalated into the LDH. This agrees with what it has been observed with ICP-MS analysis. The inclusion of heptamolybdate is also supported by the appearance of a band centered at around 900cm^{-1}, which is attributed to the Mo=O vibration[247].

2.7.3.3 XRD analysis.

Figure 41 shows the diffractograms obtained from the XRD analysis of the NiAl LDH precursor, NiMoAl LDH, and the NiMoAl C. catalysts.

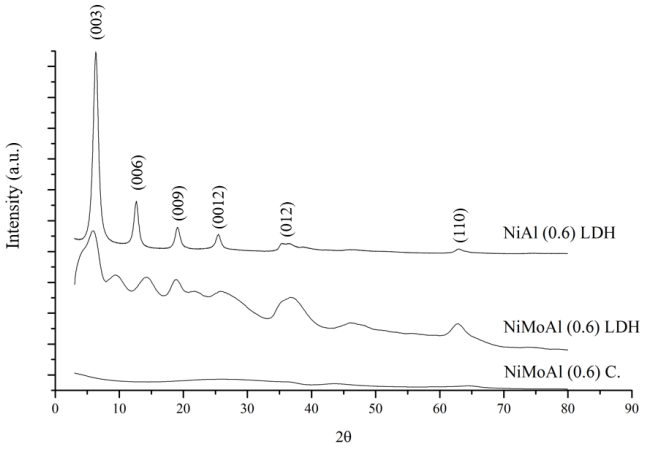

Figure 41. XRD diffractogram of NiAl (0.6) LDH, NiMoAl (0.6) LDH and NiMoAl (0.6) C.

The XRD analysis of the NiAl (0.6) LDH precursor shows the characteristic diffraction pattern of LDHs, i.e., weak and broadened reflections at angles $2\theta > 30°$ and more intense and sharp reflections at lower angles ($2\theta < 30°$)[234]. The peak (003) indicates the type of ion present in the layers as it corresponds to the distance of the interlayer space plus the thickness of a layer. The measured distance is 14 Å which agrees with the size of the terephthalate (9 Å) plus the thickness of a layer (4.8 Å), confirming the formation of an LDH with terephthalate as the intercalating ion[245]. After the ion exchange, the material (NiMoAl (0.6) LDH) significantly loses its crystallinity but retains some of the characteristic reflections of the NiAl LDH precursor like the (003), (009), (0012) positions and the reflections at angles greater than 35°. In addition to the reflection of the precursor LDH, the diffractogram of uncalcined NiMoAl (0.6) LDH shows three new peaks at 9.4°, 14.8° and 22.0° attributable to the intercalation of the heptamolybdate ion[247]. The characteristic reflections of these materials also include a peak at 7.3°, which is not present in the diffractogram. However, it is reported that this reflection is often very low in intensity and often undetectable. In contrast, the reflections at 14.8° and 22.0° are evident and therefore attributable to LDH intercalated with heptamolybdate. Finally, the reflection at 9.4° is attributed to the presence of two different crystalline phases of molybdenum, i.e., as molybdate as well as heptamolybdate[291, 292]. After calcination, the resulting material is completely amorphous.

2.7.3.4 BET-BJH analysis

The isotherm of the NiAl (0.6) LDH precursor, NiMoAl (0.6) C. and NiMoAl (0.6) R. are reported in Figure 42. Analysis of the reduced sample is also reported here because the adsorptive capacity of the reduced sample governs the adsorption of hydrogen in the reaction environment.

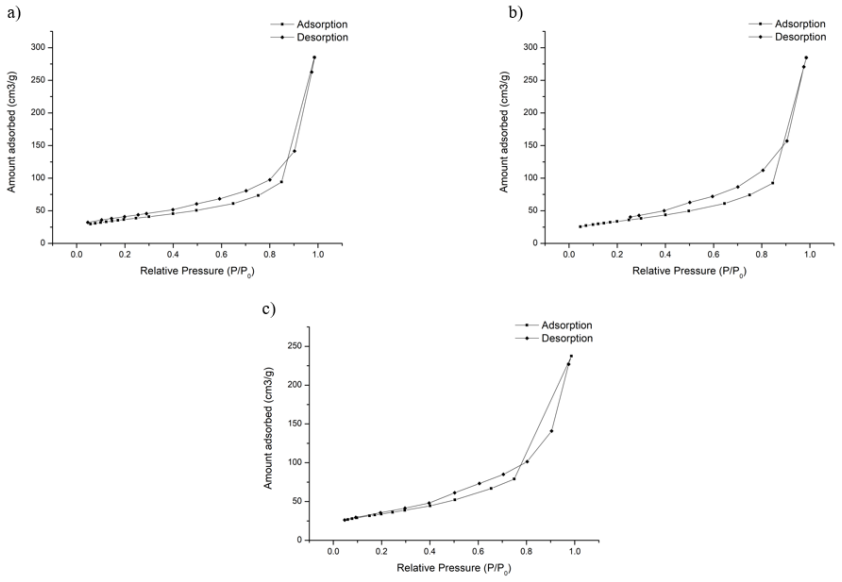

Figure 42. BET isotherm of a) NiAl uncalcined precursor, b) NiMoAl calcined and c) NiMoAl reduced.

In all cases, in the P/P_0 =1 point, the curve is not flat and, in accordance with IUPAC classification, the isotherms are likely to type II, then suggesting a material with macroporous structure but the presence of an H3-type hysteresis also indicates a mesoporous character of the materials[205, 251].

The mesoporous structure is also confirmed by the average pore diameter shown in Table 31; in all cases, a pore diameter in the range 12-14nm is calculated. Given the high metal content

of these materials, the measured surface area is large and is in agreement with what Arias et al. observed for these systems[293].

Table 31. Textural properties of the synthesized materials.

Sample	BET surface area (m^2/g)	BJH pore volume (cm^3/g)	Average pore diameter ($4V/S_{BET}$) (nm)
NiAl (0.6) LDH	130.27	0.43	13.17 (132 Å)
NiMoAl (0.6) C.	120.49	0.44	14.54 (145 Å)
NiMoAl (0.6) R.	121.66	0.37	12.17 (122 Å)

2.7.3 Conclusions.

From the study carried out on LDHs-based catalysts, many relevant information can be derived:

- The effects of the reaction conditions (temperature, pressure, and catalyst amount) are evaluated with NiMoAl (0.6) R. catalyst; a temperature rise greatly promotes conversion and, for NiMoAl (0.6) R. catalyst, 320°C are required to achieve complete conversion. The same effect is observed with pressure increase; in addition, a higher pressure promotes saturated hydrocarbon formations. At 320°C, the catalyst amount does not particularly affect the reaction. The best reaction conditions found are 320°C, 40bar H_2, and 4wt% catalyst.
- Temperature and pressure affect HDO/DCO-DCO_2. At higher temperatures and pressure, the HDO reaction is preferred.
- At 320°C, 40bar H_2 and 4wt% catalyst, complete conversion is achieved after 2h reaction time. Reaction time analysis shows that a longer reaction time results in a lower OLP yield due to a higher cracking degree.
- At the same reaction conditions and fixed reaction time of 6h, the reduction time effect is studied. As in the case of the reaction time, lower reduction times result in higher OLP yield. Reduction time and reaction time effects are complementary.
- NiMoAl (0.6) catalyst shows high catalytic activity also without the reduction step (i.e., in the oxidized state). However, to reach 100% conversion, 10wt% catalyst, 320°C, 40bar H_2, and 6h reaction time are required. At these reaction conditions, a fully hydrocarbon biofuel with 60.6 wt% diesel yield is obtained. Compared to its counterpart in the reduced state, NiMoAl (0.6) C. shows opposite selectivity by favoring DCO-DCO_2.

- NiMoAl (0.6) R. stability test displays that the catalyst retains its catalytic activity (100% conversion) at least until the fifth reaction cycle, maintaining unchanged *n*-C_{15}-C_{18} hydrocarbons content (higher than 90%).
- Given the high catalytic activity of NiMoAl (0.6) R., other reduced LDH-based catalysts are tested. In all cases, catalysts containing Mo show high catalytic activity (100% conversion) and Green Diesel yield by about 70wt%.
- On the other hand, adding W to the NiAl and CoAl systems worsens the catalytic properties of the catalyst. However, NiWAl (0.6) R. shows moderate isomerization activity producing 10.7% branched hydrocarbons C_{15}-C_{18}.
- Higher cracking activity is noted for NiVAl (UR) R. and NiAl-based catalysts (about 15% *n*-C_8-C_{15} hydrocarbons). In addition, for NiAl-based-catalyst, higher Ni amounts promote conversion.
- In the cases of Co-based catalysts, only CoMoAl (0.6) R. shows 100% conversion.
- Except in the case of NiMoAl (0.25), Mo-based catalysts have high HDO selectivity, especially for CoMoAl (0.6) R., while for NiVAl (UR) R. and bimetallic catalysts, particularly NiAl catalysts, DCO-DCO_2 are preferred.
- The same catalysts were tested at the same reaction conditions but without the reduction activation and with 10wt% catalyst. The most efficient catalysts are NiMoAl (2.33) C. and NiWAl (2.33) C. providing 100% conversion and 71.5wt% and 72.4wt% Green Diesel yield, respectively. This evidence suggests that at these conditions, more Ni amount is needed to improve catalyst activity. In addition, NiWAl (2.33) C. shows isomerization activity producing 14.4% of branched C_{15}-C_{18} hydrocarbons; for this reason, given the similar Green Diesel yield between NiWAl (2.33) C. and NiMoAl (2.33) C., the former is preferable.

- In the oxidized state, adding W to the catalyst brings no adverse effects as seen in the case of reduced-state catalyst; in fact, catalysts with excellent catalytic performance and good isomerization activity are obtained (for both NiWAl (0.6) C. and NiWAl (2.33) C. 100% conversion is reached, and the biofuels produced does not solidify at temperatures of 4°C).
- NiVAl (UR) and NiAl bimetallic catalysts cracking activity are remarkably reduced without the previous reduction step.
- In oxidized state, Mo addition does not always improve catalyst performance; in the case of NiAl (0.25), Mo addition promotes conversion (however, NiMoAl (0.25) catalyst does not achieve complete conversion) while in the case of CoAl (0.25), catalytic performance worsens significantly (same effect by adding W).
- Concerning reaction selectivity, in each case, differences occur with respect to reduced catalysts; catalysts that, after reduction, show HDO selectivity, in the oxidized state displayed either pronounced DCO-DCO_2 selectivity or lower HDO selectivity. This suggests that catalyst reduction promotes HDO reaction selectivity.
- The ICP-MS of the NiMoAl (0.6) catalyst confirms the effective synthesis of an LDH with the Ni/Al molar ratio chosen; in addition, the analysis shows the effective incorporation of Mo, but the experimental Ni/Mo molar ratio is higher than the theoretical one (less Mo than expected). This is also confirmed by FT-IR that, after Mo intercalation, shows a decrease of the signal related to the terephthalic anion in favor of $Mo_7O_{24}^{6-}$ but residue terephthalate is still present. Signals related to Mo=O are present, confirming the Mo intercalation. The XRD analysis confirms the effective formation of the NiAl LDH phase showing the typical XRD peaks of this system. After the ion exchange (Mo intercalation), a remarkable loss in crystallinity is observed, but the material retains the LDH structure; however, after calcination,

the catalyst is entirely amorphous. Finally, the BET -BJH shows that the catalyst has good surface area and a pore diameter in the mesoporous range. No remarkable differences in the adsorption properties of the NiAl (0.6) precursor and the NiMoAl (0.6) in calcined and reduced state can be seen.

In conclusion, LDHs-derived catalysts have proven to be very efficient catalysts in CDO reaction. In particular, NiMoAl (0.6) R., due to its high activity and stability, represents a valid alternative to the actual used Noble or sulfided metal catalysts. In addition, LDHs-based catalysts are Green catalysts and the catalytic screening performed shows that, thanks to the tunability properties of this material, several efficient catalysts with different catalytic activity (like isomerization or cracking activity) can be synthesized.

Chapter 3. Conclusions.

The research work addressed in this thesis concerns a particularly topical issue. Nowadays, alternative energy development is of great interest due to growing concerns about global warming due to high GHGs atmospheric concentration. Action must be taken quickly against greenhouse gas emissions and global warming, otherwise the consequences could be catastrophic and irreversible. Since the transport sector contributes particularly to GHGs emissions, biofuel development is crucial to achieve carbon neutrality and counter global warming. In particular, biofuels derived from vegetable oils are renewable, carbon neutral, and significantly reduce emissions of pollutant gases compared with conventional fuels.

Knowing these problems, the purpose of this thesis was to contribute to scientific research by studying the catalytic deoxygenation (CDO) reaction of vegetable oils for green diesel synthesis, an innovative biofuel chemically like mineral diesel but with all the advantages of biofuels. Since the current process to synthesize green diesel involves using expensive noble-metal catalysts or sulfided transition metal-based catalysts (producing a sulfur-polluted biofuel), we focused mainly on the development of catalysts that can provide an economical and green alternative to the catalysts currently in use.

For this purpose, we synthesized several catalysts, supported on fly ash cenosphere (FACs) or derived from layered double hydroxide (LDH), and they were tested to evaluate their catalytic activity on Green Diesel synthesis.

- FACs supported catalyst: The FACs are chosen to recycle a waste material (FACs are a by-product of coal combustion and are waste generated in high amounts every year) and use them as a support for catalyst synthesis has a significant advantage from an economic perspective but mainly from an environmental perspective.

Thus, several transition metal catalysts supported on FACs and Zeolites (synthesized from FACs) were prepared. From the catalytic screening performed, the NiMo (5/15)/FAC catalyst was found to be very active. This catalyst displays 100% conversion and produces a fully hydrocarbon biofuel (72.2wt% respect to oil) with high diesel selectivity (91.7% hydrocarbon in the diesel range). The catalyst retains its activity with all the edible oils tested; unfortunately, it is not much stable as it loses its activity after three reaction cycles.

Despite these drawbacks, we have shown that an appropriate FACs-supported catalyst formulation enables the synthesis of efficient catalysts for CDO reaction. In this regard, using a slightly different synthetic process, another NiMo-based catalyst (NiMo (5/15)/FAC-Zeo) was synthesized and showed high activity. We have carried out only preliminary studies for this catalyst, so further studies are planned to evaluate its potential. The excellent results obtained with these catalysts encouraged us to plan further studies involving these systems. First, we are interested in solving the problem of catalyst recycling stability. In addition, we want to evaluate the activity of this type of catalysts in the CDO of waste vegetable oils and test their activity in a continuous reactor.

Given the green aspect of these catalytic systems and the potential shown by this research work, we believe that further studies will allow us to find a FAC-supported catalyst formulation that can be a viable alternative to the catalysts currently in use.

- LDH-based catalyst: These synthetic materials were chosen because they could provide an economical and green alternative to the current catalysts. LDH are anionic clays often used in heterogeneous catalysis because of their good catalytic properties. Their synthesis is green (uses water as a solvent), and they are environmentally friendly; in addition, a large number of LDHs can be synthesized

by varying the metals constituting them, therefore, modulating the catalyst's activity depending on the metals used.

We first synthesized a Ni-, Mo-, and Al-based LDH (NiMoAl (0.6) R.) that proved highly active toward the CDO of rapeseed oil. The activity of this catalyst was evaluated by varying the reaction conditions. It was observed that the catalyst leads to 100% conversion even after only 2h of reaction time and at low catalyst/oil wt%. Moreover, the catalyst maintains its catalytic activity unchanged for at least five reaction cycles confirming its high activity. In addition, the catalyst proved to be active even without activation by reduction. From the data obtained, NiMoAl (0.6) R. represents a suitable catalyst being inexpensive, safe, and very active.

The excellent results prompted us to synthesize several other LDHs, and their activity was evaluated both after and without reduction activation. From the catalytic screening performed on the reduced catalysts, NiMoAl (0.6) R. catalyst was always found to be the most efficient for Green Diesel synthesis. However, changing metals or the ratio between them leads to the synthesis of catalysts with different activities. For example, NiAl-based bimetallic catalysts exert marked cracking activity (useful for bio-jet-fuel synthesis).

More interesting are the results obtained from catalytic screening without reduction activation. In this case, the most active catalyst was NiWAl (2.33), leading to a 100% conversion with a green diesel yield of 71.5 wt%. However, the most interesting feature of this catalyst is its hydroisomerization activity that leads to a biofuel with 14% of branched hydrocarbons in the C_{15}-C_{18} range. This result in a biofuel with better cold properties (it remains liquid at 4°C in the refrigerator). These results show that the catalyst can simultaneously catalyze deoxygenation and hydroisomerization reactions.

The study on LDH-based catalysts has shown how these can be viable alternatives; they are very active catalysts and, in the case of NiMoAl (0.6)R., also stable for several reaction cycles. Furthermore, we have shown that by modulating the constituent metals of these materials, it is possible to synthesize catalysts with different catalytic activities, such as cracking and hydroisomerization. A positive aspect of these catalysts is the high catalytic activity without reduction activation, saving time and cost. Given the excellent results shown by these catalysts, further studies are planned.

In conclusion, the work addressed in this thesis reports several innovations in the field of biofuels. We have shown how a waste material, FACs, can be effectively used as support for the synthesis of catalysts for DCO reaction. For sure, further studies are needed to optimize the synthesis of this catalyst but the results obtained clearly demonstrate its potential. The use of these catalysts would not only provide an economical alternative but, more importantly, would help to greatly increase the environmental sustainability of the green diesel synthesis process.

In addition to FACs-supported catalysts, we have also reported the catalytic efficiencies of LDH-based catalysts. From the data obtained, these catalysts are a viable alternative to the current catalyst; they are very active, stable, and active even in an oxidized state, saving cost and time. Of these catalysts, a catalyst that can simultaneously catalyze the reaction of deoxygenation and hydroisomerization has also been synthesized; simultaneously promoting these two reactions has a significant advantage in that, in a single step, it leads to the production of biofuel with good cold properties (recall that currently, the green diesel synthesis process involves these reactions in two separate processes implying higher cost and energy consumption). Therefore, the use of LDH-based catalytic systems has numerous advantages on the sustainability of the process; they are green synthesized materials, are

environmentally friendly and non-toxic, and are very active and stable. The research on green diesel carried out in our laboratories does not stop at what is exposed in this thesis, but there are numerous goals that we still have in mind:

- Solvent-less reaction: Removing reaction solvent use has many benefits, such as greater process sustainability, lower costs, and less waste.
- Continuous reaction: For the intensive production of green diesel, the use of continuous reactors is indispensable. Therefore, one objective is to evaluate the activity of catalysts presented in a continuous reactor.
- Hydrogen free reaction: Removing the use of hydrogen has safety and cost advantages. This can be done by using chemical species that can release H_2 into the reaction environment.
- Other synthetic approaches: The most common green diesel synthesis method involves hydrotreatment in continuous reactors; however, other processes are possible. One possibility we want to explore in our laboratory is to carry out the process sonochemically. The extreme conditions experienced during sonochemical cavitation could favor the catalytic deoxygenation reaction. Performing the process via sonochemistry means using less hazardous chemicals and solvents, and minimizing the energy consumption for chemical transformations.

4. Experimental section.

This section provides an extensive description of the experimental procedures carried out in the thesis work. The experimental procedures regarding catalyst synthesis and analytical details on their characterization are first reported. Next, follow the experimental details of the catalytic deoxygenation reaction and the workup of the synthesized biofuel. Finally, the analytical techniques used to characterize the reaction product are reported.

4.1 Catalyst synthesis.

4.1.1 Acid treatment of row FACs.

Before being used as a support, the cenospheres underwent an acid treatment to remove any impurities. The acid treatment performed is proposed by Sutarno ed Arryanto[224]. 10g of FACs are added in a 200ml flask containing a 5M HCl (37%, Carlo Erba) aqueous solution, and the suspension is treated for 1h under reflux conditions and vigorously stirred. After this, the resulting suspension is filtered, and the resulting solid is dried in an oven overnight at 110°C. Finally, the HCl-treated FACs are stored before being used for catalyst synthesis.

4.1.2 Example of FACs-supported bimetallic catalyst synthesis (NiMo (5/15)/FACs synthesis).

The chemicals used to synthesize bimetallic FAC-supported catalysts are: $Ni(NO_3)_2 \cdot 6H_2O$ (98%, Alfa Aesar), $Co(NO_3)_2 \cdot 6H_2O$ (98.0-102.0%, Alfa Aesar), $(NH_4)_6Mo_7O_{24} \cdot 4H_2O$ (99%, Alfa Aesar), $(NH_4)_6W_{12}O_{39} \cdot xH_2O$ (Alfa Aesar).

To illustrate the experimental procedure for synthesizing bimetallic catalysts supported on FACs, the synthesis of NiMo (5/15)/FAC catalyst is reported.

In a 50ml flask containing 10ml of H_2O milli-Q, 0.529g of $Ni(NO_3)_2 \cdot 6H_2O$ (1.8mmol) and 0.501g of $(NH_4)_6Mo_7O_{24} \cdot 4H_2O$ (0.4mmol) are dissolved under stirring. Once the salts are completely solubilized, 2.174g of HCl-treated FACs are added. The amounts are calculated to obtain a catalyst with a nominal content of 5wt% of NiO and 15wt% of MoO_3. After FACs addition, the suspension is left under stirring for 3h at room temperature. After this, the water is evaporated with rotavapor (50°C, 40torr), and the resulting solid is dried in an oven at 110°C overnight. Once completely dried, the solid is recovered from the flask and transferred to a crucible for the next calcination step. Before calcination occurs, the NiMo (5/15)/FAC catalyst is crushed to uniform the powder and then calcined at 400°C (5 °C/min) for 4h. The calcination temperature was chosen according to the decomposition temperature of the metal salts to form the corresponding metallic oxides. Finally, the solid is recovered in a bottle waiting for the reduction process. The same procedure was done for the other bimetallic catalysts. Table 32 reports the chemical amounts and the calcination conditions used for the synthesized FAC-supported bimetallic catalysts.

Table 32. FAC-supported bimetallic catalysts.

Entry	Catalyst	FACs (g)	$Ni(NO_3)_2 \cdot 6H_2O$ (g)	$Co(NO_3)_2 \cdot 6H_2O$ (g)	$(NH_4)_6Mo_7O_{24} \cdot 4H_2O$ (g)	$(NH_4)_6W_{12}O_{39} \cdot xH_2O$ (g)	H_2O	Calcination conditions
1	NiMo (5/15)/FAC	2.174	0.529	-	0.501	-	10	400°C (5°C/min) 4h
2	CoMo (6/15)/FAC	2	-	0.590	0.466		10	600°C (5°C/min) 2h
3	NiW (5/15)/FAC	2	0.416	-	-	0.408	10	600°C (5°C/min) 4h

4.1.3 Example of FACs-supported trimetallic catalyst synthesis (NiMoCe (5/15/5)/FAC synthesis).

The chemicals used in the synthesis of FAC-supported trimetallic catalysts are the following: $Ni(NO_3)_2 \cdot 6H_2O$ (98%, Alfa Aesar), $(NH_4)_6Mo_7O_{24} \cdot 4H_2O$ (99%, Alfa Aesar), $Ce(NO_3)_3 \cdot 6H_2O$ (99.5%, Alfa Aesar), $Ca(CH_3CO_2)_2 \cdot H_2O$ (≥99.0%, Sigma-Aldrich), $(NH_4)_6W_{12}O_{39} \cdot xH_2O$ (Alfa Aesar), $La(CH_3CO_2)_3 \cdot xH_2O$ (99.9%, Sigma Aldrich).

As an example, the synthetic procedure of NiMoCe (5/15/5)/FAC is reported.

0.523g of $Ni(NO_3)_2$ (1.8mmol), 0.492g of $(NH_4)_6Mo_7O_{24} \cdot 4H_2O$ (0.4mmol) and 0.338g di $Ce(NO_3)_3 \cdot 6H_2O$ (0.7mmol) are dissolved in 15ml of H_2O milli-Q. After complete dissolution, 2g of treated HCl FAC are added, and the resulting suspension is stirred at R.T. for 3h. The amounts of chemicals are calculated to obtain a catalyst with a nominal content of NiO, MoO_3, and CeO_2 of 5, 15 and 5wt% respectively. When the impregnation is concluded, water is evaporated with rotavapor (50°C, 40torr), and the obtained solid is dried in an oven at 110°C over-night. Once dried, the solid is pounded in a crucible and calcined at 400°C (5 °C/min) for 4h. The calcination temperature was chosen according to the decomposition temperature of the metal salts to form the corresponding metallic oxides. Finally, the solid was recovered in a bottle waiting to be reduced. All the other trimetallic

catalyst are synthesized in the same way. Table 33 reports all the FAC-derived trimetallic catalysts.

Table 33. FAC-supported trimetallic catalysts.

Entry	Catalyst	FACs (g)	$Ni(NO_3)_2 \cdot 6H_2O$ (g)	$(NH_4)_6Mo_7O_{24} \cdot 4H_2O$ (g)	$Ce(NO_3)_3 \cdot 6H_2O$ (g)	$Ca(CH_3CO_2)_2 \cdot H_2O$ (g)	$La(CH_3CO_2)_3 \cdot xH_2O$ (g)	Calcination condition
1	NiMoCe (5/15/5)/FAC	2	0.529	0.501	0.334	-	-	400°C (5°C/min) 4h
2	NiMoCa (5/15/20)/FAC	2.5	0.809	0.766	-	2.616	-	800°C (20°C/min) 4h
3	NiMoLa (5/15/5)/FAC	2	0.566	0.736	-	-	0.328	800°C (10°C/min) 4h

4.1.4 FACs zeolitization process.

FACs-derived zeolites were synthesized through the alkali fusion method described by Sutarno and Arryanto[224]. 10g of FACs are pounded in a crucible with 12g of NaOH (97%, Lancaster) (weight ratio FAC:NaOH 1:1.2) and melted in a muffle furnace at 550°C (5°C/min) for 1h. After the melting step, the resulting solid is ground again to uniform the powder. The solid is divided equally (5g each) into two Teflon beakers each containing 50ml of H_2O, and the slurry is stirred overnight at room temperature. At this point, the slurry is transferred into four Teflon beckers (25ml portions), and the beckers are then placed in four stainless steel reactors. The mixtures are then hydrothermally treated at 110°C for 72h. Finally, the slurry is vacuum filtered and washed with H_2O milli-Q to neutrality, and the resulting solid is dried in an oven at 110°C overnight. The obtained zeolites are recovered in a bottle.

4.1.5 Example of Zeolite-supported bimetallic catalysts synthesis (NiW (5/15/)/Zeo synthesis).

The chemicals used to synthesize Zeolite-supported bimetallic catalysts are the following: $Ni(NO_3)_2 \cdot 6H_2O$ (98%, Alfa Aesar), $(NH_4)_6Mo_7O_{24} \cdot 4H_2O$ (99%, Alfa Aesar), $(NH_4)_6W_{12}O_{39} \cdot xH_2O$ (Alfa Aesar).

Zeolite-supported bimetallic catalysts are synthesized using the same impregnation method used for FACs-supported catalysts (wet impregnation method).

Below is reported the synthetic procedure for NiW (5/15)/Zeo catalyst.

In a 100ml flask containing 30ml of H_2O milli-Q, 0.973g of $Ni(NO_3)_2 \cdot 6H_2O$ (3.3mmol) and 0.815g of $(NH_4)_6W_{12}O_{39} \cdot xH_2O$ (2.7mmol) are dissolved under stirring. Once the salts are completely solubilized, 4g of Zeolites are added. The amounts of chemicals are calculated to obtain NiW (5/15)/Zeo catalyst with a nominal content of 5wt% NiO and 15wt% WO_3. After Zeolite addition, the suspension is stirred for 3h at room temperature. After this, the water is evaporated with rotavapor (50°C, 40torr), and the resulting solid is dried in an oven at 110°C overnight. Once completely dried, the solid is recovered and calcined at 600°C (5 °C/min) for 4h. Finally, the solid is recovered in a bottle before the reduction step. The same procedure was done for the other bimetallic catalysts. Table 34 reports the Zeolite-supported bimetallic catalysts synthesized.

Table 34. Zeolite-supported bimetallic catalysts.

Entry	Catalyst	Zeolite (g)	$Ni(NO_3)_2 \cdot 6H_2O$ (g)	$(NH_4)_6Mo_7O_{24} \cdot 4H_2O$ (g)	$(NH_4)_6W_{12}O_{39} \cdot xH_2O$ (g)	Calcination condition
1	NiMo (5/15)/Zeolite	2.174	0.529	0.501	-	400°C (5°C/min) 4h
2	NiW (5/15)/Zeolite	4	0.973	-	0.815	600°C (5°C/min) 4h

4.1.6 Example of Zeolite-supported trimetallic catalysts synthesis (NiMoCa (5/15/20)/Zeo synthesis).

The chemicals used in the synthesis of Zeolite-supported trimetallic catalysts are the following: $Ni(NO_3)_2 \cdot 6H_2O$ (98%, Alfa Aesar), $(NH_4)_6Mo_7O_{24} \cdot 4H_2O$ (99%, Alfa Aesar), $Ce(NO_3)_3 \cdot 6H_2O$ (99.5%, Alfa Aesar), $Ca(CH_3CO_2)_2 \cdot H_2O$ (≥99.0%, Sigma-Aldrich), $(NH_4)_6W_{12}O_{39} \cdot xH_2O$ (Alfa Aesar), $La(CH_3CO_2)_3 \cdot xH_2O$ (99.9%, Sigma Aldrich).

As an example, the synthesis of NiMoCa (5/15/20)/Zeo is given.

In a 100ml flask containing 15ml of H_2O milli-Q, 0.580g of $Ni(NO_3)_2 \cdot 6H_2O$ (2mmol), 0.538g di $(NH_4)_6Mo_7O_{24} \cdot 4H_2O$ (0.4mmol) and 1.832g di $Ca(CH_3CO_2)_2 \cdot H_2O$ (10.4mmol) are dissolved under stirring. Once the salts are completely solubilized, 1.75g of Zeolites are added, and the suspension is stirred for 3h at room temperature. The amounts of chemicals are calculated to obtain NiMoCa (5/15/20)/Zeo catalyst with a nominal content of 5wt% NiO, 15wt% MoO_3, and 20wt% of CaO respectively. At the end of the impregnation, the water is evaporated with rotavapor (50°C, 40torr), and the resulting solid is dried in an oven at 110°C overnight. Once completely dried, the solid is recovered and calcined at 800°C (20 °C/min) for 4h. Finally, the solid is recovered in a bottle before the reduction step. The same procedure was done for the other trimetallic catalysts. Table 35 report the Zeolite-supported trimetallic catalysts synthesized.

Table 35. Zeolite-supported trimetallic catalysts.

Entry	Catalyst	FACs (g)	$Ni(NO_3)_2 \cdot 6H_2O$ (g)	$(NH_4)_6Mo_7O_{24} \cdot 4H_2O$ (g)	$Ce(NO_3)_3 \cdot 6H_2O$ (g)	$Ca(CH_3CO_2)_2 \cdot H_2O$ (g)	$La(CH_3CO_2)_3 \cdot xH_2O$ (g)	Calcination condition
1	NiMoCe (5/15/5)/Zeo	2	0.523	0.490	0.334	-	-	400°C (5°C/min) 4h
2	NiMoCa (5/15/20)/Zeo	1.75	0.580	0.538	-	1.832	-	800°C (20°C/min) 4h
3	NiMoLa (5/15/5)/Zeo	2	0.565	0.736	-	-	0.328	800°C (10°C/min) 4h

4.1.7 Reduction in a fixed bed reactor.

FACs- and Zeolites-supported catalysts are reduced in a fixed bed reactor. The reactor consists of a steel tube inside which the catalyst is placed. At the top end, the reactor is connected to the gas inlet, whose flow is regulated by mass flow meters, while the base of the reactor is connected to a line that carries the outlet gases under a fume cupboard. During the reduction, the reactor is placed in a tubular furnace, and a controller regulates the temperature of the furnace.

As an example, the reduction of NiMo (5/15)/FAC is reported, but the same procedure can be extended to all other reduction reactions.

To reduce NiMo (5/15)/FAC, the reactor is filled as shown in Figure 43

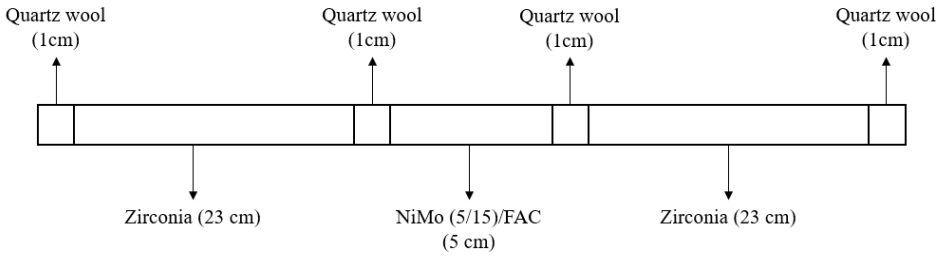

Figure 43. Reaction filling of the reactor for the fixed bed reduction.

To a better reduction, the catalyst should be placed at the center of the reactor where the temperature is most uniform; for this reason, the reactor must be filled with fillers. Zirconia is an inert and thermally stable material that is used to fill the reactor gaps, while quartz wool is used as a separator between the zirconia and the catalyst and to prevent the zirconia and the catalyst from leaving the reactor during reactor loading. Based on the available data, the reactor is filled in accordance with the calculations made below.

reactor length (l) = 55cm

reactor inner diameter (d) = 1.5cm

amount of catalyst = 2.242g

Catalyst volume (measured by the volume occupied by the catalyst inside a graduated cylinder) = 3.2ml

zirconia density (ṕ) = 2.270 g/cm^3

$$section\ (s) = \pi\ \frac{d^2}{4} = 0.636cm^2$$

$$Fixed\ bed\ height\ (h) = \frac{V}{s} = 5cm$$

$$V_{Zirconia} = S\ x\ h_{Zirconia} = 14.63cm^3$$

$$g_{Zirconia} = V_{Zirconia}\ x\ \acute{\rho}_{Zirconia} = 33.2g$$

At this point, we proceed with the filling of the reactor. We then insert 1cm of quartz wool, 33.2g of zirconia (about 23cm), 1cm of quartz wool, the catalyst, 1cm of quartz wool, another 33.2g of zirconia, and finally, 1cm of quartz wool. After loading is completed, the reactor is placed inside the furnace; the inlet of the reactor is connected to the inlet gas line, and the end of the reactor is connected to the outlet gas line. At this point, the inlet gas flow is adjusted by sending 20Nml/min of H_2 and 180Nml/min of N_2 (H_2/N_2 ratio on 10:90%), and the reactor is heated to 700°C (5 °C/min) and maintained for 3h at 700°C. At the end of the reduction, the reactor is cooled to room temperature while flowing 200 Nml/min of N_2 to avoid possible oxidation. When the reactor reaches room temperature, it is disassembled, and the catalyst is recovered inside a flask and held under an argon atmosphere to avoid possible oxidation.

This same procedure was carried out for all other FACs- and Zeolites-supported catalysts; the same H_2 and N_2 fluxes were always used, but the reduction temperatures varied. Table 36 shows the reduction conditions used for all FACs- and Zeolites-supported catalysts.

Table 36.FACs- and Zeolite-supported catalysts reduction conditions.

Entry	Catalyst[1]	T (°C)	Ramp (°C/min)	Stasis (h)
1	NiMo (5/15)/FAC	700	5	3
2	CoMo (6/15)/FAC	800	10	3
3	NiW (5/15)/FAC	800	10	3
4	NiMoCe (5/15/5)/FAC	820	5	3
5	NiMoCa (5/15/20)/FAC	700	5	3
6	NiMoLa (5/15/5)/FAC	800	10	3
7	NiMo (5/15)/Zeo	700	5	3
8	NiW (5/15)/Zeo	750	5	3
9	NiMoCe (5/15/5)/Zeo	720	5	3
10	NiMoCa (5/15/20)/Zeo	780	5	3
11	NiMoLa (5/15/5)/Zeo	850	10	3

[1]The catalyst are all reduced with 20Nml/min of H_2 and 180Nml/min of N_2

An ABB gas analyzer was used to evaluate the reduction temperature of the catalysts. The procedure is very similar to that of the reduction seen above. The reactor is filled in the same way with the catalyst for which we want to know the reduction temperature; however, in this case, a thermocouple is added inside the catalyst bed to measure the temperature inside the bed. Once filled, the reactor is placed inside the tubular furnace, and the upper part of the reactor is connected to the incoming gases. The lower part of the reactor is connected to the gas outlet which, in this case, sends the gases to the analyzer. The reactor is then heated to 900°C (10 °C/min), and hydrogen consumption is measured during the heating processes. At the temperature where a decrease in hydrogen flux is observed, the catalyst is reducing; therefore, the catalyst will have to be reduced at that temperature.

4.1.8 NiMo (5/15)/FAC-Zeo synthesis.

The NiMo (5/15)/FAC-Zeo catalyst is synthesized with a method slightly different than the other FACs- and Zeolite-supported catalysts. In the first step is synthesized the NiMo (5/15)/FAC in the same way described above. In a 50ml flask containing 10ml of H_2O milli-Q, 0.529g of $Ni(NO_3)_2 \cdot 6H_2O$ (1.8mmol) and 0.501g of $(NH_4)_6Mo_7O_{24} \cdot 4H_2O$ (0.4mmol) are dissolved under stirring. Once the salts are completely solubilized, 2.174g of HCl-treated FACs are added. The amounts are calculated to obtain a catalyst with a nominal content of 5wt% of NiO and 15wt% of MoO_3. After FACs addition, the suspension is left under stirring for 3h at room temperature. After this, the water is evaporated with a rotavapor (50°C, 40torr), and the resulting solid is dried in an oven at 110°C overnight. Now the catalyst is not calcined but undergoes the same zeolitization process done for the row FAC. Therefore 2.5g grams of NiMo(5/15)/FAC were pounded into a crucible with 2.4g of NaOH. The quantities are calculated according to the weight ratio FAC:NaOH 1:1.2; since in 2.5g grams of NiMo(5/15)/FAC there is a nominal amount of FAC of 80% (thus 2g), then 2.4g of NaOH will be needed. Then the solid mixture is melted in the muffle furnace at 550°C (5°C/min) for 1h. The fused solid is ground again to uniform the powder and is put into a Teflon becker containing 20ml of H_2O milli-Q, and the slurry is left overnight under stirring. After the aging step, the slurry is transferred into another Teflon becker that is placed in a stainless-steel autoclave to perform the hydrothermal reactions. The mixture is then hydrothermally treated for 72h in an oven at 110°C. At the end of the hydrothermal treatment, the slurry is vacuum filtered and washed with H_2O milli-Q to neutrality. The resulting catalyst, called NiMo (5/15)/FAC-Zeo, is dried in an oven at 110°C overnight. Finally, the catalyst is calcined in a muffle furnace at 400°C (5°C/min) for 4h and stored in a flask awaiting reduction. In this case, the catalyst is reduced in a batch reactor before being used in the reaction (the batch reduction experimental details are presented later).

4.1.9 Example of NiAl LDHs synthesis (NiAl 0.6 LDH synthesis).

Chemicals used for LDHs synthesis are: $Al(NO_3)_3 \cdot 9H_2O$ (≥98%, Sigma Aldrich), $Ni(NO_3)_2 \cdot 6H_2O$ (98%, Alfa Aesar), $C_8H_6O_4$ (95.0%, Fluorochem), NaOH (97%, Lancaster).

Three NiAl LDHs precursors are prepared according to the co-precipitation method proposed by Arias et al [245]. The synthesis of NiAl (0.6) LDH is shown as an example, but the same procedure can be used to synthesize NiAl (0.25) LDH and NiAl (2.33) LDH (only the amounts of the reagents used change).

In a 1L 4-neck flask, 400ml of H_2O milli Q are added; one neck is connected to a reflux cooler (at the end of which is placed a calcium chloride tube that prevents infiltration of atmospheric moisture), and in the second neck is inserted a tube that bubbles Ar inside the water. The other necks are temporarily plugged with caps. After fixing the system, water is boiled for 1h under continuous stirring and Ar bubbling. This step is designed to decarbonate the water to limit the presence of carbonate ions, promoting the intercalation of terephthalate ions. After the boiling step, the system is cooled to 50°C, and two dropping funnels are connected to two of flask necks. The two dropping funnel are loaded with two solutions; the first solutions is prepared by dissolving 31 mmol of $Al(NO_3)_3 \cdot 9H_2O$ and 20 mmol of $Ni(NO_3)_2$ in 100ml of H_2O milli-Q, while the second is prepared by dissolving 17mmol of Terephthalic Acid and 100mmol of NaOH in 100ml of H_2O-milli-Q (at the top of one of the two dropping funnel Ar is flushed to maintain an inert atmosphere). Finally, a pH meter is inserted into another neck, and the last neck remains connected to the reflux coolant. After that, the co-precipitation is performed by slowly adding the two solution and adjusting the flow to maintain the pH in the range 6.3-6.8. When the addition of the two solutions is finished, the dropping funnels are removed, and the necks are capped again; the pH-meter is then removed, the tube for Ar bubbling is added again, and the system is left for 4h under stirring at 50°C. At the end of 4h, the mixture is cooled to room temperature and the system

is aged for 16h under stirring and Ar bubbling. The solid is vacuum filtered, washed with abundant H_2O milli-Q and then dried overnight at 110°C. Finally, the solid is recovered in a bottle before being used in the next ion exchange step. When used as a catalyst, NiAl (0.6) LDH was first calcined in a muffle furnace at 450°C (10°C/min) for 3h and finally reduced in batch before being used for the catalytic deoxygenation reaction. After the calcination, the catalyst is named NiAl (0.6) C., while after reduction, the catalyst is named NiAl (0.6) R. Table 37 reports the chemical amount used for the synthesis of the three NiAl LDH systems.

Table 37. Chemicals amount used for NiAl LDH precursors synthesis.

Entry	LDH precursor	$Al(NO_3)_3 \cdot 9H_2O$	$Ni(NO_3)_2 \cdot 6H_2O$	NaOH	$C_8H_6O_4$	X value	Ni/Al ratio
1	NiAl (0.6) LDH	11.74	5.79	4.04	2.86	0.61	0.63
2	NiAl (0.25) LDH	15.37	2.95	4.04	3.74	0.80	0.25
3	NiAl (2.33) LDH	5.74	10.49	4.04	1.40	0.30	2.33

4.1.10 CoAl LDH (0.6) synthesis.

Chemicals used for CoAl (0.6) LDH synthesis are: $Al(NO_3)_3 \cdot 9H_2O$ (≥98%, Sigma Aldrich), $Co(NO_3)_2 \cdot 6H_2O$ (98.0-102.0%, Alfa Aesar), $C_8H_6O_4$ (95.0%, Fluorochem), NaOH (97%, Lancaster).

The CoAl precursor is synthesized according to Coelho et al[248].

In a 1L 4-neck flask, 400ml of H_2O milli Q are added; one neck is connected to a reflux cooler (at the top of which is placed a calcium chloride tube that prevents infiltration of atmospheric moisture), and in the second neck is inserted a tube that bubbles Ar inside the water. The other necks are temporarily plugged with caps. After fixing the system, water is boiled for 1h under continuous stirring and Ar bubbling. This step is designed to decarbonate the water to limit the presence of carbonate ions, promoting the intercalation of terephthalate ions. After the boiling step, the system is cooled to 60°C, and two dropping funnels are connected to two of flask necks. The two dropping funnel are loaded with two solutions; the first solution is prepared by dissolving 31 mmol of $Al(NO_3)_3 \cdot 9H_2O$ and 20 mmol of $Co(NO_3)_2 \cdot 6H_2O$ in 100ml of H_2O milli-Q, while the second is prepared by dissolving 17mmol of Terephthalic Acid and 100mmol of NaOH in 100ml of H_2O-milli-Q (at the top of one of the two dropping funnel Ar is flushed to maintain an inert atmosphere). Finally, a pH meter is inserted into another neck, and the last neck of the flask remains connected to the reflux coolant. After that, the co-precipitation is performed by slowly adding the two solution and adjusting the flow to maintain the pH in the range 6.3-6.8. When the addition of the two solutions is finished, the dropping funnels are removed and the necks are capped again; the pH-meter is then removed, the tube for Ar bubbling is added again, and the system is left for 48h under stirring at 60°C. At the end of 48h, the solid is vacuum filtered, washed with abundant H_2O milli-Q and then dried over-night at 110°C. Finally, the solid is recovered in a bottle before being used in the next ion exchange step. When used as a catalyst, CoAl

(0.6) LDH was first calcined in a muffle furnace at 450°C (10°C/min) for 3h and finally reduced in before being used for the catalytic deoxygenation reaction. After the calcination the catalyst is named CoAl (0.6) C. while after the reduction the catalyst is named CoAl (0.6) R.

4.1.11 Example of ion exchange (NiMoAl 0.6 LDH synthesis).

Chemicals used for LDHs synthesis are: $(NH_4)_6Mo_7O_{24} \cdot 4H_2O$ (99%, Alfa Aesar), $(NH_4)_6W_{12}O_{39} \cdot xH_2O$ (Alfa Aesar). The ion exchange between terephthalate and $(NH_4)_6Mo_7O_{24} \cdot 4H_2O$ or $(NH_4)_6W_{12}O_{39} \cdot xH_2O$ is performed according to Arias et al[247].

As an example, the ion exchange between NiAl (0.6) LDH with $(NH_4)_6Mo_7O_{24} \cdot 4H_2O$ (for NiMoAl (0.6) LDH synthesis) is reported. Except for NiVAl (UR) catalyst, the synthetic procedure is the same as for all other trimetallic LDH-based catalysts.

1 g of the dried NiAl (0.6) LDH precursor is placed in a Teflon beaker with a 0.07 M solution of $(NH_4)_6Mo_7O_{24} \cdot 4H_2O$ in H_2O milli-Q (1.507g in 17ml H_2O, the amount of heptamolybdate used is 50% in excess respect the required stoichiometric amount). The Teflon beaker is then placed in a stainless-steel reactor, and ion exchange is carried out under hydrothermal conditions at 80°C and continue stirring for 24 hours. Finally, the solid is vacuum filtered, washed with H_2O milli-Q and dried at 110°C in an oven for 4 hours. NiMoAl mixed oxides (named NiMoAl (0.6) C.) are obtained by calcination in air at 450°C (10°C/min) for 3h. Finally, the catalyst is reduced in batch. The final form of the catalyst is referred to as NiMoAl (0.6)R.

Table 38 reports the chemical amount used for the synthesis of the other trimetallic LDH-based catalysts (except NiVAl (UR) that is reported later).

Table 38. Trimetallic LDH-based catalysts.

Entry	Catalyst	$(NH_4)_6Mo_7O_{24} \cdot 4H_2O$ (g)	$(NH_4)_6W_{12}O_{39} \cdot xH_2O$ (g)	Ni (or Co) / Al ratio	Ni (or Co) / Me ratio
1	NiMoAl (0.25)	1.82	-	0.25	0.21
2	NiMoAl (0.63)	1.507	-	0.63	0.57
3	NiMoAl (2.33)	0.853	-	2.33	2.2
4	NiWAl (0.63)	-	3.584	0.63	0.33
5	NiWAl (2.33)		2.027	2.33	2
6	CoMoAl (0.63)	1.507	-	0.63	0.57
7	CoWAl (0.63)	-	3.584	0.63	0.33

4.1.12 NiVAl (UR) synthesis.

Chemicals used for LDHs synthesis are: $Al(NO_3)_3 \cdot 9H_2O$ (≥98%, Sigma Aldrich), $Ni(NO_3)_2 \cdot 6H_2O$ (98%, Alfa Aesar), CH_4N_2O (99%, Sigma Aldrich), NH_4VO_3 (99%, Alfa Aesar).

The NiAl (UR) precursor is synthesized using the urea co-precipitation method proposed by Pancrecious et al[249].

In a 500 ml 2-neck flask, 100ml of H_2O milli-Q, 5mmol of $Ni(NO_3)_2 \cdot 6H_2O$, 2.5mmol of $Al(NO_3)_3 \cdot 9H_2O$ and 17.5mmol of CH_4N_2O are added. A reflux condenser is connected to one neck of the flask while the inlet for Ar is connected to the other neck (as in the case of the other LDHs, the inert atmosphere is used to prevent carbonate formation). At this point, the reaction is refluxed for 24 h, and after this, the solid is filtered and washed with H_2O and dried under vacuum at 60°C for 24 h. The NiAl (UR) catalyst is then recovered and used for the next ion exchange step.

100ml of H_2O milli Q are added into a two-neck flask. Before NiAl (UR) addition, the flask undergoes three vacuum and Ar washes to ensure an inert atmosphere. After this, one neck

is connected to Ar inlet while the other neck is used to add 0.234g of NH_4VO_3. When all NH_4VO_3 is dissolved, 0.500g of NiAl (UR) is added, and the system is left for 10min at room temperature under continuous stirring. At this point, the pH is measured, and the value must be 7.4. Finally, the ion exchange is performed, under stirring and Ar flow, for 24h at room temperature. At the end of the ion exchange, the solid is vacuum filtered, washed with H_2O milli-Q, and dried under vacuum at 60°C for 24h. Once dried, the catalyst was recovered and placed in a crucible to undergo calcination at 450°C (10°C/min) for 3h to obtain NiVAl mixed oxides (UR) (named NiVAl (UR) C.). Before carrying out the catalytic deoxygenation reaction, the catalyst is reduced in batch (in this state the catalyst is named NiVAl (UR) R.)

4.2 Catalysts characterization.

4.2.1 Inductively coupled plasma-mass spectrometry (ICP-MS).

The elemental composition of the catalysts studied is performed via inductively coupled plasma-mass spectrometry (ICP-MS). The instrument used is an iCAP TQe ICP-MS (Thermo scientific) with a triple quadrupole MS detector (Figure 44). To analyze the catalysts, the solid samples are dissolved with concentrated strong acid solution (suprapure nitric acid, 65%, Merck KGaA) and then diluted in deionized water. Briefly, 20mg of solid is added to a 200ml volumetric flask and the solid is put in contact with 70wt% of HNO_3 to facilitate the dissolution of the sample. H_2O is then added and solubilization is facilitated by sonicating the volumetric flask for 10min. Once the sample is solubilized, the volumetric flask is brought to volume. 10 µl are taken from that solution and placed in a 20ml flask. 300 µl of 70wt% HNO_3 and 200 µl of internal standard (indium) are then added to the volumetric flask and brought to volume. An aliquot of this solution is placed in a test tube and analyzed by ICP-MS.

Figure 44. iCAP TQe ICP-MS

4.2.2 Surface area and porosity analysis.

The textural properties, surface area, pore volume, pore diameter, and pore size distribution of the materials studied are determined via N_2 physisorption using a NOVA 1200e Surface Area & Pore Size Analyzer from Quantachrome Instruments (Figure 45). BET-BJH method calculations are performed with Nova Station A software. The sample under investigation (100-200 mg) is degassed under high vacuum at 200°C (10 °C/min) for at least 8h before the physisorption analysis.

Figure 45. NOVA 1200e Surface Area & Pore Size Analyzer

4.2.3 Powder X-ray diffraction.

The phase composition of catalysts has been determined with a PANalytical X'Pert PRO diffractometer with Bragg-Brentano geometry (Figure 46) that uses a Cu $K\alpha_1$ radiation (1,540598**Å)**. The diffractogram were recorded with 2θ angle ranging from 5° to 90° and analyzed by X'Pert HighScore Plus collector software. The powder is ground and sieved with standard sieves UNI 2331 and ISO R565 to obtain a powder with dimensions less than 150 μm and then pressed onto a zero-background sample holder. The phase identification was performed by matching the obtained diffractograms with international reference database (inorganic crystal structure database (ICSD)).

Figure 46. PANalytical X'Pert PRO diffractometer.

4.2.4 Fourier-transform infrared spectroscopy (FT-IR).

The FT-IR measurements were performed using a PerkinElmer Spectrum instrument working in ATR mode (Figure 47). The ATR crystal is made of diamond and the available area is a 2x2mm square. Before analysis, the sample was pounded finely to improve the acquired spectrum. After that, a small amount of the sample is placed on the crystal, and the IR spectrum is obtained by averaging 16 scans with $4cm^{-1}$ resolution.

Figure 47. FT-IR PerkinElmer Spectrum

4.3 Catalytic deoxygenation reaction.

4.3.1 Batch reactor. Catalyst reduction and catalytic deoxygenation reaction (NiMo (5/15)/FAC-Zeo reduction and successive DO reaction).

In this work, the rector used to perform the catalytic deoxygenation reactions, and catalysts reductions is a Parr batch reactor consisting of a 4590 Micro Bench Top Reactors, Magnetic drives, and a 4848 Reactor. Figure 48 shows a schematic representation of the reactor.

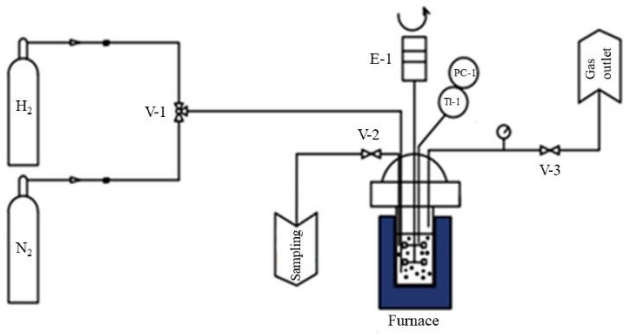

Figure 48. Schematic view of the used reactor.

The reactor consists of a fixed head containing the stirring system (E-1) and a movable cylinder (100 ml), into which is inserted the liner (glass vessel with high thermal and pressure resistance) containing oil, solvent, and catalyst. The cylinder and the reactor head are connected by a ring equipped with screws and safety hinges, which provide an excellent pressure seal. On the fixed head is placed a pressure manometer that measures the pressure inside the reactor (PC-1). Heating is done by an electric furnace, which is connected to the

controller, and a J-type thermocouple (Tl-1) senses the temperature inside the reactor. The controller regulates temperature and stirring (not shown in figure 8). Three different valves are placed on the head of the reactor, one allows gases to enter the reactor (V-1), another can be used to take samples from the reaction mixture (V-2), and finally, the third is the gas outlet valve (V-3) (the outlet can also be used for gas phase sampling). Two tanks supply incoming gases (H_2 and N_2). Finally, the reactor is connected to a cooling system necessary for the continuous cooling of the stirring system.

Before carrying out the catalytic deoxygenation reaction, NiMo(5/15)/FAC-Zeo catalyst and LDH-based catalysts are reduced in a batch reactor. As an example, the reduction procedure of NiMo(5/15)/FAC-Zeo is reported. In addition, the catalytic deoxygenation reaction performed after NiMo(5/15)/FAC-Zeo reduction is reported. This procedure can be extended for all the reductions and the reactions performed.

0.2412g of NiMo(5/15)/FAC-Zeo are placed inside a glass liner, which is placed inside the reactor cylinder. The cylinder is then mounted on the reactor head using the metal ring, and the screws are tightened to ensure a seal. Once assembled, the cooling system is opened, and the reaction environment is flushed three times with N_2 and another three times with H_2. After the washing steps, the reactor is charged with 60 Bar of H_2. The cylinder is then placed inside the furnace, and, through the control unit, the temperature is set at 320°C, and the reduction takes place for 8h. At the end of the reduction, the reactor is cooled to room temperature, and then the remaining gas is vented from the reaction environment. The rector is then disassembled, and the catalyst is recovered and immediately used to carry out the catalytic deoxygenation reaction.

0.200g of reduced NiMo (5/15)/FAC-Zeo, 2g of oil, and 20g of hexene are then added to the liner, and the liner is inserted into the cylinder. As in the case of the reduction, the reactor cylinder is connected to the reactor head, and the screws are tightened to ensure a seal. The

reaction environment is then cleaned from the air by washing three times with N_2 and three times with H_2. Cleaned the reaction environment, the rector is charged with 40bar of H_2, the furnace temperature is set to 320°C, and stirring is applied (kept constant for all the reactions performed). Next, the cylinder is placed inside the oven, and the heating is started. The reaction is started once the reactor temperature reaches 320°C and remains stable. In this case, the reaction was sent for 6h. Once cooled, the reactor is disassembled and washed with hexane and $CHCl_3$ to recover all the product before processing the reaction.

4.3.2 Reaction mixture work-up.

After the reaction, the catalyst is vacuum filtered by washing several times with hexane and $CHCl_3$ to wash the catalyst and recover all the reaction mixture. The filtered catalyst is then dried under vacuum at 60°C over night, while the reaction mixture is recovered in a previously weighted 250ml flask. The reaction mixture is then evaporated by rotavapor and dried under vacuum for 30min. At this point the flask is weighted to asses the OLP yield. After that, small amount of OLP is used for IR analysis while another portion undergoes transesterification to convert any residual oil into methyl esters that can be analyzed via GC-FID.

4.4 Organic liquid product (OLP) analysis.

4.4.1 FT-IR-ATR analysis of the OLP produced.

The FT-IR measurements were performed with a PerkinElmer Spectrum instrument working in ATR mode (the same used for catalyst characterization). Before performing the analysis, background was taken to remove the signals arising from the air. At this point a small amount of OLP is placed on the ATR crystal and the analysis is performed at 4 scans and resolution of $4cm^{-1}$. The collected spectra are analyzed and, when compared, they are normalized respect to the CH stretching, since it is assumed that they do not vary particularly before and after the reaction [259]. Normalization balances the effects caused by a different amount of OLP placed on the ATR crystal.

4.4.2 OLP transesterification.

Before GC-FID and GC-MS analysis, a portion of the OLP is transesterified according to the standard AOAC 969.33[257]. 350 mg of the OLP and 6 ml of 2N solution of NaOH in methanol are added to a 50-mL flask. The flask is connected to a reflux condenser, and the mixture is heated to 150°C under continuous stirring. The reaction is allowed to reflux for 10 minutes, and, after that, 7ml of a solution of 10wt% of BF_3 in methanol is added, and after one minute, 5ml of hexane are added. Another minute has waited, and then the reaction is cooled to room temperature. Finally, a NaCl saturated solution is added until to the neck of the flask and the separation of the organic phase (containing the methyl esters and our reaction mixture) from the aqueous phase occurs. Then 1.3ml of the organic phase is taken and placed in a Vial containing anhydrous Na_2SO_4 to remove any residual water. This sample is injected directly into the GC-FID.

This same procedure is used for the characterization of the several oils used. Table 39 presents the information reports on the label on the oils used. The soybean oil was purchased from Merck KGaA (dietary source of long-chain triglycerides and other lipids, CAS: 8001-22-7, lot number: MKBV2450V).

Table 39. Information listed on the label of oils.

Oil	Batch	kcal	fats	saturated	Unsaturated (mono)	Unsaturated (poly)	Carbohydrates	Proteins	Salt	Vitamins
Sunflower	L18313	828	92.0	10.2	29.5	52.3	0	0	0	-
Mais	L101943	826	91.8	13.3	-	-	0	0	0	-
Rapeseed	L170277808	828	92.0	7.0	57.0	28.0	0	0	0	25mg
Palm	B/H 06/20U	920	100	50	-	-	0	0	2	-
Peanuts	E6165S-REV.0348	823	91.4	16.3	-	-	0	0	0	-

Data shown on the label for 100ml of oil

All the oils used for the CDO reaction were used without any modifications.

4.4.3 GC-FID apparatus for transesterified reaction mixture analysis.

1µl of the transesterified mixture is injected (split injection) into an Agilent GC/7820A gas chromatograph equipped with a flame ionization detector (FID) and an HP-5 19091J-413 capillary column (30m x 0.32mm x 0.25µm, stationary phase = (5%-Phenyl)-methylpolysiloxane) (Figure 49). The chromatographic run lasts 35 minutes, during which the column is initially maintained at 50°C for 5 minutes, then increased to 280°C (10°C/min) and finally maintained at 280°C for 7 minutes. The eluent gas is H_2 and the flux is set to 2ml/min; the injector and FID are set at 250°C and the inlet pressure is set to 0.4bar. Chromatographic peaks corresponding to *n*-alkanes are identified by comparison with a linear saturated alkane C_7-C_{40} standard solution (C7-C40 Saturated Alkanes Standard, 1000µg/ml each component, Supelco).

Figure 49. Agilent GC/7820A gas chromatograph

4.4.4 GC-FID apparatus for vegetable oil characterization.

The vegetable oils are characterized with a Trace GC Ultra 7820 gas chromatograph (Figure 50) coupled with a flame ionization detector (FID) and with a Supelco® SP-2380 capillary column (30 m x 0.25mm x 25 µm, stationary phase = Poly(90% biscyanopropyl/10% cyanopropylphenyl siloxane)). 1 µl of the transesterified sample is manually injected in the GC (using the sandwich method), and the chromatographic run is carried out under isothermal conditions by setting the column temperature at 180°C and performing the run for 25 min. The eluent gas is H_2 (split 25ml/min), and the injector and FID temperature are both set at 250°C. Chromatogram peaks are identified by comparison with a commercially available FAME standard (F.A.M.E. MIX, C14-C22, Supelco), and the chromatograms are analyzed with the Xcalibur software.

Figure 50. Trace GC Ultra 7820 gas chromatograph.

4.4.5 Gas Chromatography Mass Spectrometry (GC-MS).

Any unidentified chromatographic peaks are identified via GC-MS analysis (GC model: Varian star 3400cx, MS model: Varian saturn 2000) after injection of the transesterified mixture (20µl of the transesterified sample is diluted in 1.3 ml of hexane, and 1µl of this sample is injected to the GC-MS apparatus) (Figure 51). The GC is equipped with an HP-5 column (30m × 0.25µm × 0.25 mm stationary phase = 5% phenyl-methyl polysiloxane). The chromatographic run has a duration of 35 minutes in which the column is initially maintained at 50°C for 5 minutes, after which the temperature is increased by 10°C/min to 280°C and maintained at this temperature for 7 minutes. The trap and injector temperatures are both set at 250°C and the eluent gas is He (split 50 ml/min). *n*-alkanes are identified by comparison with C_7-C_{40} standard (C7-C40 Saturated Alkanes Standard, 1000µml/ml each component, Supelco), also used to calculate Kovats retention index. Unknown peaks are identified by comparing the corresponding mass spectra with a library (NIST 2014) and matching the Kovats retention index (RI) calculated with the RI provided by the library.

Figure 51. GC-MS. Varian star 3400cx (GC model), Varian saturn 2000 (MS model).

Bibliography.

1. Warr, B.S. and R.U. Ayres, *Evidence of causality between the quantity and quality of energy consumption and economic growth.* ENERGY, 2010. **35**(4): p. 1688-1693.
2. Smil, V., *World History and Energy*, in *Encyclopedia of Energy*, C.J. Cleveland, Editor. 2004, Elsevier: New York. p. 549-561.
3. Wrigley, E.A., *Energy and the English Industrial Revolution.* Philosophical Transactions of the Royal Society A: Mathematical, Physical and Engineering Sciences, 2013. **371**(1986): p. 20110568.
4. Fernihough, A. and K.H. O'Rourke, *COAL AND THE EUROPEAN INDUSTRIAL REVOLUTION*. Economic Journal, 2021. **131**(635): p. 1135-1149.
5. Melsted, O. and I. Pallua, *The Historical Transition from Coal to Hydrocarbons: Previous Explanations and the Need for an Integrative Perspective.* Canadian Journal of History-Annales Canadiennes D Histoire, 2018. **53**(3): p. 395-422.
6. Price, D., *ENERGY AND HUMAN-EVOLUTION*. Population and Environment, 1995. **16**(4): p. 301-319.
7. Scheffran, J., M. Felkers, and R. Froese, *Economic Growth and the Global Energy Demand*, in *Green Energy to Sustainability*. 2020. p. 1-44.
8. Matsuo, Y., A. Yanagisawa, and Y. Yamashita, *A global energy outlook to 2035 with strategic considerations for Asia and Middle East energy supply and demand interdependencies.* Energy Strategy Reviews, 2013. **2**(1): p. 79-91.
9. Energy, B.S.R.o.W., *Statistical Review of World Energy 2022.* 2022: p. 60.
10. Countries, O.o.t.P.E., *2020 OPEC World Oil Outlook*, 2020.
11. Khalili, S., et al. *Global Transportation Demand Development with Impacts on the Energy Demand and Greenhouse Gas Emissions in a Climate-Constrained World*. Energies, 2019. **12**, DOI: 10.3390/en12203870.
12. Ghabri, Y., A. Ayadi, and K. Guesmi, *Fossil energy and clean energy stock markets under COVID-19 pandemic*. Applied Economics, 2021. **53**(43): p. 4962-4974.
13. Araújo-Silva, C.L., V.C. Sarmento, and P.J.P. Santos, *Climate change scenarios of increased CO2 and temperature affect a coral reef peracarid (Crustacea) community.* Marine Environmental Research, 2022. **173**: p. 105518.
14. Mollo, M., A. Kolesnikov, and S. Makgato, *Simultaneous reduction of NOx emission and SOx emission aided by improved efficiency of a Once-Through Benson Type Coal Boiler.* Energy, 2022. **248**: p. 123551.
15. Xu, J., et al., *Fossil-fuel and combustion-related air pollution and hypertension in the Sister Study*. Environmental Pollution, 2022: p. 120401.
16. Li, C., et al., *Environmental impact and health risk assessment of volatile organic compound emissions during different seasons in Beijing.* Journal of Environmental Sciences, 2020. **93**: p. 1-12.
17. Dominici, F., M. Greenstone, and C.R. Sunstein, *Particulate Matter Matters.* Science, 2014. **344**(6181): p. 257-259.
18. Gettelman, A. and R.B. Rood, *Climate Change and Global Warming*, in *Demystifying Climate Models*. 2016, Springer Berlin Heidelberg: Berlin, Heidelberg. p. 23-35.
19. Mitchell, J.F.B., *The "Greenhouse" effect and climate change.* Reviews of Geophysics, 1989. **27**(1): p. 115-139.

20. Rogelj, J., et al., *Estimating and tracking the remaining carbon budget for stringent climate targets.* Nature, 2019. **571**(7765): p. 335-342.
21. Fang, J., et al., *Climate change, human impacts, and carbon sequestration in China.* Proceedings of the National Academy of Sciences, 2018. **115**(16): p. 4015-4020.
22. Creutzig, F., et al., *Towards demand-side solutions for mitigating climate change.* Nature Climate Change, 2018. **8**(4): p. 260-263.
23. MacIsaac, D., *Sustainable Energy — Without the hot air.* The Physics Teacher, 2009. **47**(8): p. 556-556.
24. Chen, J.M., *Carbon neutrality: Toward a sustainable future.* The Innovation, 2021. **2**(3): p. 100127.
25. *World Energy Outlook 2021.* p. 386.
26. Ovaere, M. and S. Proost, *Cost-effective reduction of fossil energy use in the European transport sector: An assessment of the Fit for 55 Package.* Energy Policy, 2022. **168**: p. 113085.
27. Nazarko, Ł., et al. *The Impact of Energy Development of the European Union Euro Area Countries on CO2 Emissions Level*. Energies, 2022. **15**, DOI: 10.3390/en15041425.
28. *World of Change: Global Temperatures*. [Text.Article] 2020 2020/01/29/ 2022/10/15/20:27:55; Available from: https://earthobservatory.nasa.gov/world-of-change/global-temperatures.
29. The Lancet Planetary, H., *COP26 in review.* The Lancet Planetary Health, 2021. **5**(12): p. e851.
30. McNutt, M., *Climate Change Impacts.* Science, 2013. **341**(6145): p. 435-435.
31. Lameh, M., D.M. Al-Mohannadi, and P. Linke, *Graphical analysis of CO2 emissions reduction strategies.* Cleaner Engineering and Technology, 2020. **1**: p. 100023.
32. Babonneau, F., M. Benlahrech, and A. Haurie, *Transition to zero-net emissions for Qatar: A policy based on Hydrogen and CO2 capture & storage development.* Energy Policy, 2022. **170**: p. 113256.
33. Chen, L., et al., *Strategies to achieve a carbon neutral society: a review.* Environmental Chemistry Letters, 2022. **20**(4): p. 2277-2310.
34. Berndes, G., et al., *Forest biomass, carbon neutrality and climate change mitigation*, I. European Forest, Editor 2016, European Forest Institute.
35. Wolf, S., et al., *The European Green Deal — More Than Climate Neutrality.* Intereconomics, 2021. **56**(2): p. 99-107.
36. Mallouppas, G., et al. *Methodology to Assess the Technoeconomic Impacts of the EU Fit for 55 Legislation Package in Relation to Shipping*. Journal of Marine Science and Engineering, 2022. **10**, DOI: 10.3390/jmse10081006.
37. Masuda, J., L. McLaren, and B. Poland, *COP26: what is the message for public health?* Canadian Journal of Public Health, 2022. **113**(1): p. 1-5.
38. Arora, N.K. and I. Mishra, *COP26: more challenges than achievements.* Environmental Sustainability, 2021. **4**(4): p. 585-588.
39. de Marco, B.A., et al., *Evolution of green chemistry and its multidimensional impacts: A review.* Saudi Pharmaceutical Journal, 2019. **27**(1): p. 1-8.
40. Anastas, P.T. and J.C. Warner, *Green Chemistry Theory and Practice*. Oxford University Press.
41. Fatih Demirbas, M., *Biorefineries for biofuel upgrading: A critical review.* Applied Energy, 2009. **86**: p. S151-S161.

42. Maher, K.D. and D.C. Bressler, *Pyrolysis of triglyceride materials for the production of renewable fuels and chemicals.* Bioresource Technology, 2007. **98**(12): p. 2351-2368.
43. Naik, S.N., et al., *Production of first and second generation biofuels: A comprehensive review.* Renewable and Sustainable Energy Reviews, 2010. **14**(2): p. 578-597.
44. Ameen, M., et al., *Catalytic hydrodeoxygenation of triglycerides: An approach to clean diesel fuel production.* Renewable and Sustainable Energy Reviews, 2017. **80**: p. 1072-1088.
45. Biswas, S., et al., *Biofuels and their production through different catalytic routes.* Chemical and Biochemical Engineering Quarterly, 2017. **31**(1): p. 47-62.
46. Leng, E., et al., *A comprehensive review on lignin pyrolysis: Mechanism, modeling and the effects of inherent metals in biomass.* Fuel, 2022. **309**: p. 122102.
47. Karmakar, B. and G. Halder, *Progress and future of biodiesel synthesis: Advancements in oil extraction and conversion technologies.* Energy Conversion and Management, 2019. **182**: p. 307-339.
48. Di Vito Nolfi, G., K. Gallucci, and L. Rossi *Green Diesel Production by Catalytic Hydrodeoxygenation of Vegetables Oils*. International Journal of Environmental Research and Public Health, 2021. **18**, DOI: 10.3390/ijerph182413041.
49. Fatih Demirbas, M., M. Balat, and H. Balat, *Biowastes-to-biofuels.* Energy Conversion and Management, 2011. **52**(4): p. 1815-1828.
50. Champagne, P., *Feasibility of producing bio-ethanol from waste residues: A Canadian perspective: Feasibility of producing bio-ethanol from waste residues in Canada.* Resources, Conservation and Recycling, 2007. **50**(3): p. 211-230.
51. Yaakob, Z., et al., *Overview of the production of biodiesel from Waste cooking oil.* Renewable and Sustainable Energy Reviews, 2013. **18**: p. 184-193.
52. Lycourghiotis, S., et al., *Nickel catalysts supported on palygorskite for transformation of waste cooking oils into green diesel.* Applied Catalysis B: Environmental, 2019. **259**: p. 118059.
53. Pattanaik, B.P. and R.D. Misra, *Effect of reaction pathway and operating parameters on the deoxygenation of vegetable oils to produce diesel range hydrocarbon fuels: A review.* Renewable and Sustainable Energy Reviews, 2017. **73**: p. 545-557.
54. Knothe, G., R.O. Dunn, and M.O. Bagby, *Biodiesel: The Use of Vegetable Oils and Their Derivatives as Alternative Diesel Fuels*, in *Fuels and Chemicals from Biomass*. 1997, American Chemical Society. p. 172-208.
55. Demirbas, A., *Bioenergy, Global Warming, and Environmental Impacts.* Energy Sources, 2004. **26**(3): p. 225-236.
56. Gnanasekaran, L., et al., *The conversion of biomass to fuels via cutting-edge technologies: Explorations from natural utilization systems.* Fuel, 2023. **331**: p. 125668.
57. Demirbas, A., *A Realistic Fuel Alternative for Diesel Engines*, 2007, Springer London2008.
58. Saladini, F., et al., *Guidelines for emergy evaluation of first, second and third generation biofuels.* Renewable and Sustainable Energy Reviews, 2016. **66**: p. 221-227.
59. Abdullah, B., et al., *Fourth generation biofuel: A review on risks and mitigation strategies.* Renewable and Sustainable Energy Reviews, 2019. **107**: p. 37-50.
60. Singh, A., et al., *A Comprehensive Review of Feedstocks as Sustainable Substrates for Next-Generation Biofuels.* BioEnergy Research, 2022.

61. Zhao, C., T. Brück, and J.A. Lercher, *Catalytic deoxygenation of microalgae oil to green hydrocarbons.* Green Chemistry, 2013. **15**(7): p. 1720-1739.
62. Ooi, X.Y., et al., *Overview on catalytic deoxygenation for biofuel synthesis using metal oxide supported catalysts.* Renewable and Sustainable Energy Reviews, 2019. **112**: p. 834-852.
63. Godbole, V., M.K. Pal, and P. Gautam, *A critical perspective on the scope of interdisciplinary approaches used in fourth-generation biofuel production.* Algal Research, 2021. **58**: p. 102436.
64. Leong, W.-H., et al., *Third generation biofuels: A nutritional perspective in enhancing microbial lipid production.* Renewable and Sustainable Energy Reviews, 2018. **91**: p. 950-961.
65. Damartzis, T. and A. Zabaniotou, *Thermochemical conversion of biomass to second generation biofuels through integrated process design—A review.* Renewable and Sustainable Energy Reviews, 2011. **15**(1): p. 366-378.
66. Szeto, W. and D.Y.C. Leung, *Is hydrotreated vegetable oil a superior substitute for fossil diesel? A comprehensive review on physicochemical properties, engine performance and emissions.* Fuel, 2022. **327**: p. 125065.
67. Gunstone, F.D. and F.B. Padley. *Lipid technologies and applications*. 1997.
68. Hermida, L., A.Z. Abdullah, and A.R. Mohamed, *Deoxygenation of fatty acid to produce diesel-like hydrocarbons: A review of process conditions, reaction kinetics and mechanism.* Renewable and Sustainable Energy Reviews, 2015. **42**: p. 1223-1233.
69. Sánchez-Muniz, F.J., S. Bastida, and J. Benedí, *Sunflower Oil*, in *Encyclopedia of Food and Health*, B. Caballero, P.M. Finglas, and F. Toldrá, Editors. 2016, Academic Press: Oxford. p. 217-226.
70. Dijkstra, A.J., *Soybean Oil*, in *Encyclopedia of Food and Health*, B. Caballero, P.M. Finglas, and F. Toldrá, Editors. 2016, Academic Press: Oxford. p. 58-63.
71. Dijkstra, A.J., *Palm Oil*, in *Encyclopedia of Food and Health*, B. Caballero, P.M. Finglas, and F. Toldrá, Editors. 2016, Academic Press: Oxford. p. 199-204.
72. Eskin, N.A.M., *Rapeseed Oil/Canola*, in *Encyclopedia of Food and Health*, B. Caballero, P.M. Finglas, and F. Toldrá, Editors. 2016, Academic Press: Oxford. p. 581-585.
73. Khan, S., et al., *A review on deoxygenation of triglycerides for jet fuel range hydrocarbons.* Journal of Analytical and Applied Pyrolysis, 2019. **140**: p. 1-24.
74. Deshmukh, S., R. Kumar, and K. Bala, *Microalgae biodiesel: A review on oil extraction, fatty acid composition, properties and effect on engine performance and emissions.* Fuel Processing Technology, 2019. **191**: p. 232-247.
75. Gosselink, R.W., et al., *Reaction Pathways for the Deoxygenation of Vegetable Oils and Related Model Compounds.* ChemSusChem, 2013. **6**(9): p. 1576-1594.
76. Zhao, X., et al. *Review of Heterogeneous Catalysts for Catalytically Upgrading Vegetable Oils into Hydrocarbon Biofuels*. Catalysts, 2017. **7**, DOI: 10.3390/catal7030083.
77. Tan, Y.H., M.O. Abdullah, and C. Nolasco-Hipolito, *The potential of waste cooking oil-based biodiesel using heterogeneous catalyst derived from various calcined eggshells coupled with an emulsification technique: A review on the emission reduction and engine performance.* Renewable and Sustainable Energy Reviews, 2015. **47**: p. 589-603.
78. Mehrpooya, M., B. Ghorbani, and H. Abedi, *Biodiesel production integrated with glycerol steam reforming process, solid oxide fuel cell (SOFC) power plant.* Energy Conversion and Management, 2020. **206**: p. 112467.

79. Chua, S.Y., et al., *Biodiesel synthesis using natural solid catalyst derived from biomass waste — A review.* Journal of Industrial and Engineering Chemistry, 2020. **81**: p. 41-60.
80. Kubičková, I. and D. Kubička, *Utilization of Triglycerides and Related Feedstocks for Production of Clean Hydrocarbon Fuels and Petrochemicals: A Review.* Waste and Biomass Valorization, 2010. **1**(3): p. 293-308.
81. Hasan, M.M. and M.M. Rahman, *Performance and emission characteristics of biodiesel–diesel blend and environmental and economic impacts of biodiesel production: A review.* Renewable and Sustainable Energy Reviews, 2017. **74**: p. 938-948.
82. Sonthalia, A. and N. Kumar, *Hydroprocessed vegetable oil as a fuel for transportation sector: A review.* Journal of the Energy Institute, 2019. **92**(1): p. 1-17.
83. Veriansyah, B., et al., *Production of renewable diesel by hydroprocessing of soybean oil: Effect of catalysts.* Fuel, 2012. **94**: p. 578-585.
84. Rogers, K.A. and Y. Zheng, *Selective Deoxygenation of Biomass-Derived Bio-oils within Hydrogen-Modest Environments: A Review and New Insights.* ChemSusChem, 2016. **9**(14): p. 1750-1772.
85. Kubička, D., M. Bejblová, and J. Vlk, *Conversion of Vegetable Oils into Hydrocarbons over CoMo/MCM-41 Catalysts.* Topics in Catalysis, 2010. **53**(3): p. 168-178.
86. Hongloi, N., P. Prapainainar, and C. Prapainainar, *Review of green diesel production from fatty acid deoxygenation over Ni-based catalysts.* Molecular Catalysis, 2022. **523**: p. 111696.
87. Oh, M., et al., *Importance of pore size and Lewis acidity of Pt/Al2O3 for mitigating mass transfer limitation and catalyst fouling in triglyceride deoxygenation.* Chemical Engineering Journal, 2022. **439**: p. 135530.
88. Liu, Q., et al., *One-step hydrodeoxygenation of palm oil to isomerized hydrocarbon fuels over Ni supported on nano-sized SAPO-11 catalysts.* Applied Catalysis A: General, 2013. **468**: p. 68-74.
89. Snåre, M., et al., *Heterogeneous Catalytic Deoxygenation of Stearic Acid for Production of Biodiesel.* Industrial & Engineering Chemistry Research, 2006. **45**(16): p. 5708-5715.
90. Mahdi, H.I., et al., *Catalytic deoxygenation of palm oil and its residue in green diesel production: A current technological review.* Chemical Engineering Research and Design, 2021. **174**: p. 158-187.
91. Yoon, J.J., *What's the difference between biodiesel and renewable (green) diesel.* Advanced Biofuels USA, 2011. **186**.
92. Orozco, L.M., et al., *Second-generation green diesel from castor oil: Development of a new and efficient continuous-production process.* Chemical Engineering Journal, 2017. **322**: p. 149-156.
93. Shi, H., et al., *Catalytic deoxygenation of methyl laurate as a model compound to hydrocarbons on nickel phosphide catalysts: Remarkable support effect.* Fuel Processing Technology, 2014. **118**: p. 161-170.
94. Wang, C., et al., *One-Step Hydrotreatment of Vegetable Oil to Produce High Quality Diesel-Range Alkanes.* ChemSusChem, 2012. **5**(10): p. 1974-1983.
95. Douvartzides, S.L., et al. *Green Diesel: Biomass Feedstocks, Production Technologies, Catalytic Research, Fuel Properties and Performance in Compression Ignition Internal Combustion Engines*. Energies, 2019. **12**, DOI: 10.3390/en12050809.

96. Loganathan, S., *Biohydro-fined diesel (BHD) and biodiesel (BOD) production process and property.* Innovations in Fuel Economy and Sustainable Road Transport, 2011: p. 97.
97. Galadima, A. and O. Muraza, *Hydroisomerization of sustainable feedstock in biomass-to-fuel conversion: a critical review.* International Journal of Energy Research, 2015. **39**(6): p. 741-759.
98. Kikhtyanin, O.V., et al., *Hydroconversion of sunflower oil on Pd/SAPO-31 catalyst.* Fuel, 2010. **89**(10): p. 3085-3092.
99. Tuli, D. and S. Kasture, *Chapter 5 - Biodiesel and green diesel*, in *Advanced Biofuel Technologies*, D. Tuli, S. Kasture, and A. Kuila, Editors. 2022, Elsevier. p. 119-133.
100. Knothe, G., *Biodiesel and renewable diesel: A comparison.* Progress in Energy and Combustion Science, 2010. **36**(3): p. 364-373.
101. Ogunkoya, D., et al., *Investigation of the effects of renewable diesel fuels on engine performance, combustion, and emissions.* Fuel, 2015. **140**: p. 541-554.
102. Aatola, H., et al., *Hydrotreated Vegetable Oil (HVO) as a Renewable Diesel Fuel Trade-off between NO_x, Particulate Emission, and Fuel Consumption of a Heavy Duty Engine.* SAE International Journal of Engines, 2009. **1**(1): p. 1251-1262.
103. Ahmad, A.L., et al., *Microalgae as a sustainable energy source for biodiesel production: A review.* Renewable and Sustainable Energy Reviews, 2011. **15**(1): p. 584-593.
104. Dijkstra, A.J., *Kinetics and mechanism of the hydrogenation process – the state of the art.* European Journal of Lipid Science and Technology, 2012. **114**(9): p. 985-998.
105. Vonghia, E., et al., *Pathways for the deoxygenation of triglycerides to aliphatic hydrocarbons over activated alumina.* Energy & Fuels, 1995. **9**(6): p. 1090-1096.
106. Santillan-Jimenez, E. and M. Crocker, *Catalytic deoxygenation of fatty acids and their derivatives to hydrocarbon fuels via decarboxylation/decarbonylation.* Journal of Chemical Technology & Biotechnology, 2012. **87**(8): p. 1041-1050.
107. Boda, L., et al., *Catalytic hydroconversion of tricaprylin and caprylic acid as model reaction for biofuel production from triglycerides.* Applied Catalysis A: General, 2010. **374**(1): p. 158-169.
108. Peng, B., et al., *Towards Quantitative Conversion of Microalgae Oil to Diesel-Range Alkanes with Bifunctional Catalysts.* Angewandte Chemie International Edition, 2012. **51**(9): p. 2072-2075.
109. Morgan, T., et al., *Conversion of Triglycerides to Hydrocarbons Over Supported Metal Catalysts.* Topics in Catalysis, 2010. **53**(11): p. 820-829.
110. Fu, J., X. Lu, and P.E. Savage, *Catalytic hydrothermal deoxygenation of palmitic acid.* Energy & Environmental Science, 2010. **3**(3): p. 311-317.
111. Kubička, D. and L. Kaluža, *Deoxygenation of vegetable oils over sulfided Ni, Mo and NiMo catalysts.* Applied Catalysis A: General, 2010. **372**(2): p. 199-208.
112. Kubička, D., P. Šimáček, and N. Žilková, *Transformation of Vegetable Oils into Hydrocarbons over Mesoporous-Alumina-Supported CoMo Catalysts.* Topics in Catalysis, 2009. **52**(1): p. 161-168.
113. Kubička, D. and J. Horáček, *Deactivation of HDS catalysts in deoxygenation of vegetable oils.* Applied Catalysis A: General, 2011. **394**(1): p. 9-17.
114. Lu, J., et al., *Microkinetic modeling of the decarboxylation and decarbonylation of propanoic acid over Pd(111) model surfaces based on parameters obtained from first principles.* Journal of Catalysis, 2013. **305**: p. 56-66.

115. Ruinart de Brimont, M., et al., *Deoxygenation mechanisms on Ni-promoted MoS2 bulk catalysts: A combined experimental and theoretical study.* Journal of Catalysis, 2012. **286**: p. 153-164.
116. Peng, B., et al., *Manipulating Catalytic Pathways: Deoxygenation of Palmitic Acid on Multifunctional Catalysts.* Chemistry – A European Journal, 2013. **19**(15): p. 4732-4741.
117. Peng, B., et al., *Stabilizing Catalytic Pathways via Redundancy: Selective Reduction of Microalgae Oil to Alkanes.* Journal of the American Chemical Society, 2012. **134**(22): p. 9400-9405.
118. Rozmysłowicz, B., et al., *Influence of Hydrogen in Catalytic Deoxygenation of Fatty Acids and Their Derivatives over Pd/C.* Industrial & Engineering Chemistry Research, 2012. **51**(26): p. 8922-8927.
119. de Klerk, A., *Fischer–Tropsch refining: technology selection to match molecules.* Green Chemistry, 2008. **10**(12): p. 1249-1279.
120. Deldari, H., *Suitable catalysts for hydroisomerization of long-chain normal paraffins.* Applied Catalysis A: General, 2005. **293**: p. 1-10.
121. Šimáček, P., et al., *Premium quality renewable diesel fuel by hydroprocessing of sunflower oil.* Fuel, 2011. **90**(7): p. 2473-2479.
122. Rabaev, M., et al., *Improvement of hydrothermal stability of Pt/SAPO-11 catalyst in hydrodeoxygenation–isomerization–aromatization of vegetable oil.* Journal of Catalysis, 2015. **332**: p. 164-176.
123. Wang, H.-Y., et al., *Study on palm oil hydrogenation for clean fuel over Ni–Mo–W/γ-Al2O3–ZSM-5 catalyst.* Fuel Processing Technology, 2015. **139**: p. 91-99.
124. Lapuerta, M., J. Rodríguez-Fernández, and E.F. de Mora, *Correlation for the estimation of the cetane number of biodiesel fuels and implications on the iodine number.* Energy Policy, 2009. **37**(11): p. 4337-4344.
125. Ardiyanti, A.R., et al., *Catalytic hydrotreatment of fast-pyrolysis oil using non-sulfided bimetallic Ni-Cu catalysts on a δ-Al2O3 support.* Applied Catalysis B: Environmental, 2012. **117-118**: p. 105-117.
126. Verma, D., et al., *Diesel and aviation kerosene with desired aromatics from hydroprocessing of jatropha oil over hydrogenation catalysts supported on hierarchical mesoporous SAPO-11.* Applied Catalysis A: General, 2015. **490**: p. 108-116.
127. Srifa, A., et al., *Production of bio-hydrogenated diesel by catalytic hydrotreating of palm oil over NiMoS2/γ-Al2O3 catalyst.* Bioresource Technology, 2014. **158**: p. 81-90.
128. Liu, Q., et al., *Hydrodeoxygenation of palm oil to hydrocarbon fuels over Ni/SAPO-11 catalysts.* Chinese Journal of Catalysis, 2014. **35**(5): p. 748-756.
129. Sotelo-Boyás, R., Y. Liu, and T. Minowa, *Renewable Diesel Production from the Hydrotreating of Rapeseed Oil with Pt/Zeolite and NiMo/Al2O3 Catalysts.* Industrial & Engineering Chemistry Research, 2011. **50**(5): p. 2791-2799.
130. Kim, T.-H., et al., *Effects of Fatty Acid Compositions on Heavy Oligomer Formation and Catalyst Deactivation during Deoxygenation of Triglycerides.* ACS Sustainable Chemistry & Engineering, 2018. **6**(12): p. 17168-17177.
131. Li, X., et al., *Heterogeneous sulfur-free hydrodeoxygenation catalysts for selectively upgrading the renewable bio-oils to second generation biofuels.* Renewable and Sustainable Energy Reviews, 2018. **82**: p. 3762-3797.
132. Rogelio, S.-B.s., T.-Z.r. Fernando, and H.n.-L. Felipe de Jesús, *Hydroconversion of Triglycerides into Green Liquid Fuels*, in *Hydrogenation*, K. Iyad, Editor. 2012, IntechOpen: Rijeka. p. Ch. 8.

133. Kubička, D. and V. Tukač, *Chapter Three - Hydrotreating of Triglyceride-Based Feedstocks in Refineries*, in *Advances in Chemical Engineering*, D.Y. Murzin, Editor. 2013, Academic Press. p. 141-194.
134. Topsøe, H., B.S. Clausen, and F.E. Massoth, *Hydrotreating Catalysis*, in *Catalysis: Science and Technology*, J.R. Anderson and M. Boudart, Editors. 1996, Springer Berlin Heidelberg: Berlin, Heidelberg. p. 1-269.
135. Ferrari, M., et al., *CoMo/carbon hydrodeoxygenation catalysts: influence of the hydrogen sulfide partial pressure and of the sulfidation temperature.* Catalysis Today, 2001. **65**(2): p. 257-264.
136. Priecel, P., et al., *The role of Ni species in the deoxygenation of rapeseed oil over NiMo-alumina catalysts.* Applied Catalysis A: General, 2011. **397**(1): p. 127-137.
137. Horáček, J., et al., *HDO catalysts for triglycerides conversion into pyrolysis and isomerization feedstock.* Fuel, 2014. **121**: p. 57-64.
138. Zhang, H., H. Lin, and Y. Zheng, *The role of cobalt and nickel in deoxygenation of vegetable oils.* Applied Catalysis B: Environmental, 2014. **160-161**: p. 415-422.
139. Toba, M., et al., *Hydrodeoxygenation of waste vegetable oil over sulfide catalysts.* Catalysis Today, 2011. **164**(1): p. 533-537.
140. Šimáček, P., et al., *Hydroprocessed rapeseed oil as a source of hydrocarbon-based biodiesel.* Fuel, 2009. **88**(3): p. 456-460.
141. Şenol, O.İ., T.R. Viljava, and A.O.I. Krause, *Effect of sulphiding agents on the hydrodeoxygenation of aliphatic esters on sulphided catalysts.* Applied Catalysis A: General, 2007. **326**(2): p. 236-244.
142. Madsen, A.T., et al., *Hydrodeoxygenation of waste fat for diesel production: Study on model feed with Pt/alumina catalyst.* Fuel, 2011. **90**(11): p. 3433-3438.
143. Chen, L., et al., *Aqueous-phase hydrodeoxygenation of carboxylic acids to alcohols or alkanes over supported Ru catalysts.* Journal of Molecular Catalysis A: Chemical, 2011. **351**: p. 217-227.
144. He, L., et al., *Highly selective and efficient catalytic conversion of ethyl stearate into liquid hydrocarbons over a Ru/TiO2 catalyst under mild conditions.* Catalysis Science & Technology, 2012. **2**(7): p. 1328-1331.
145. Berenblyum, A.S., et al., *The influence of metal and carrier natures on the effectiveness of catalysts of the deoxygenation of fatty acids into hydrocarbons.* Russian Journal of Physical Chemistry A, 2012. **86**(8): p. 1199-1203.
146. Harnos, S., G. Onyestyák, and D. Kalló, *Hydrocarbons from sunflower oil over partly reduced catalysts.* Reaction Kinetics, Mechanisms and Catalysis, 2012. **106**(1): p. 99-111.
147. Krár, M., et al., *Fuel purpose hydrotreating of sunflower oil on CoMo/Al2O3 catalyst.* Bioresource Technology, 2010. **101**(23): p. 9287-9293.
148. Srifa, A., et al., *Catalytic behaviors of Ni/γ-Al2O3 and Co/γ-Al2O3 during the hydrodeoxygenation of palm oil.* Catalysis Science & Technology, 2015. **5**(7): p. 3693-3705.
149. Srifa, A., et al., *Roles of monometallic catalysts in hydrodeoxygenation of palm oil to green diesel.* Chemical Engineering Journal, 2015. **278**: p. 249-258.
150. Wang, H., et al., *Support effects on hydrotreating of soybean oil over NiMo carbide catalyst.* Fuel, 2013. **111**: p. 81-87.
151. Kubička, D., et al., *Effect of support-active phase interactions on the catalyst activity and selectivity in deoxygenation of triglycerides.* Applied Catalysis B: Environmental, 2014. **145**: p. 101-107.

152. Kaewpengkrow, P., D. Atong, and V. Sricharoenchaikul, *Catalytic upgrading of pyrolysis vapors from Jatropha wastes using alumina, zirconia and titania based catalysts.* Bioresource Technology, 2014. **163**: p. 262-269.
153. Taufiqurrahmi, N., A.R. Mohamed, and S. Bhatia, *Nanocrystalline zeolite beta and zeolite Y as catalysts in used palm oil cracking for the production of biofuel.* Journal of Nanoparticle Research, 2011. **13**(8): p. 3177-3189.
154. Yenumala, S.R., S.K. Maity, and D. Shee, *Hydrodeoxygenation of karanja oil over supported nickel catalysts: influence of support and nickel loading.* Catalysis Science & Technology, 2016. **6**(9): p. 3156-3165.
155. Asikin-Mijan, N., et al., *Production of green diesel via cleaner catalytic deoxygenation of Jatropha curcas oil.* Journal of Cleaner Production, 2017. **167**: p. 1048-1059.
156. Duan, J., et al., *Diesel-like hydrocarbons obtained by direct hydrodeoxygenation of sunflower oil over Pd/Al-SBA-15 catalysts.* Catalysis Communications, 2012. **17**: p. 76-80.
157. Twaiq, F.A., N.A.M. Zabidi, and S. Bhatia, *Catalytic Conversion of Palm Oil to Hydrocarbons: Performance of Various Zeolite Catalysts.* Industrial & Engineering Chemistry Research, 1999. **38**(9): p. 3230-3237.
158. Wang, H., et al., *Hydrocarbon Fuels Production from Hydrocracking of Soybean Oil Using Transition Metal Carbides and Nitrides Supported on ZSM-5.* Industrial & Engineering Chemistry Research, 2012. **51**(30): p. 10066-10073.
159. Snåre, M., et al., *Production of diesel fuel from renewable feeds: Kinetics of ethyl stearate decarboxylation.* Chemical Engineering Journal, 2007. **134**(1): p. 29-34.
160. Mäki-Arvela, P., et al., *Catalytic Deoxygenation of Tall Oil Fatty Acid over Palladium Supported on Mesoporous Carbon.* Energy & Fuels, 2011. **25**(7): p. 2815-2825.
161. Cheng, J., et al., *Optimizing catalysis conditions to decrease aromatic hydrocarbons and increase alkanes for improving jet biofuel quality.* Bioresource Technology, 2014. **158**: p. 378-382.
162. Li, T., et al., *Conversion of waste cooking oil to jet biofuel with nickel-based mesoporous zeolite Y catalyst.* Bioresource Technology, 2015. **197**: p. 289-294.
163. Pinto, F., et al., *Production of bio-hydrocarbons by hydrotreating of pomace oil.* Fuel, 2014. **116**: p. 84-93.
164. Huber, G.W., P. O'Connor, and A. Corma, *Processing biomass in conventional oil refineries: Production of high quality diesel by hydrotreating vegetable oils in heavy vacuum oil mixtures.* Applied Catalysis A: General, 2007. **329**: p. 120-129.
165. Kim, S.K., et al., *Production of renewable diesel by hydrotreatment of soybean oil: Effect of reaction parameters.* Chemical Engineering Journal, 2013. **228**: p. 114-123.
166. Patel, M. and A. Kumar, *Production of renewable diesel through the hydroprocessing of lignocellulosic biomass-derived bio-oil: A review.* Renewable and Sustainable Energy Reviews, 2016. **58**: p. 1293-1307.
167. Snåre, M., et al., *Catalytic deoxygenation of unsaturated renewable feedstocks for production of diesel fuel hydrocarbons.* Fuel, 2008. **87**(6): p. 933-945.
168. Kubičková, I., et al., *Hydrocarbons for diesel fuel via decarboxylation of vegetable oils.* Catalysis Today, 2005. **106**(1): p. 197-200.
169. Santillan-Jimenez, E., et al., *Catalytic deoxygenation of triglycerides and fatty acids to hydrocarbons over carbon-supported nickel.* Fuel, 2013. **103**: p. 1010-1017.

170. Lee, S.-P. and A. Ramli, *Methyl oleate deoxygenation for production of diesel fuel aliphatic hydrocarbons over Pd/SBA-15 catalysts.* Chemistry Central Journal, 2013. **7**(1): p. 149.
171. Immer, J.G., M.J. Kelly, and H.H. Lamb, *Catalytic reaction pathways in liquid-phase deoxygenation of C18 free fatty acids.* Applied Catalysis A: General, 2010. **375**(1): p. 134-139.
172. Nimkarde, M.R. and P.D. Vaidya, *Toward Diesel Production from Karanja Oil Hydrotreating over CoMo and NiMo Catalysts.* Energy & Fuels, 2016. **30**(4): p. 3107-3112.
173. Yang, Y., et al., *Hydrotreating of C18 fatty acids to hydrocarbons on sulphided NiW/SiO2–Al2O3.* Fuel Processing Technology, 2013. **116**: p. 165-174.
174. Anand, M. and A.K. Sinha, *Temperature-dependent reaction pathways for the anomalous hydrocracking of triglycerides in the presence of sulfided Co–Mo-catalyst.* Bioresource Technology, 2012. **126**: p. 148-155.
175. Mäki-Arvela, P., et al., *Catalytic Deoxygenation of Fatty Acids and Their Derivatives.* Energy & Fuels, 2007. **21**(1): p. 30-41.
176. Morgan, T., et al., *Catalytic deoxygenation of triglycerides to hydrocarbons over supported nickel catalysts.* Chemical Engineering Journal, 2012. **189-190**: p. 346-355.
177. Kiatkittipong, W., et al., *Diesel-like hydrocarbon production from hydroprocessing of relevant refining palm oil.* Fuel Processing Technology, 2013. **116**: p. 16-26.
178. Noriega, A.K., et al., *Hydrodeoxygenation of vegetable oil in batch reactor: Experimental considerations.* Chinese Journal of Chemical Engineering, 2020. **28**(6): p. 1670-1683.
179. Mäki-Arvela, P., et al., *Continuous decarboxylation of lauric acid over Pd/C catalyst.* Fuel, 2008. **87**(17): p. 3543-3549.
180. Xin, H., et al., *Production of high-grade diesel from palmitic acid over activated carbon-supported nickel phosphide catalysts.* Applied Catalysis B: Environmental, 2016. **187**: p. 375-385.
181. Fu, J., X. Lu, and P.E. Savage, *Hydrothermal Decarboxylation and Hydrogenation of Fatty Acids over Pt/C.* ChemSusChem, 2011. **4**(4): p. 481-486.
182. Neste Proprietary Publication: Espoo, F., *Neste Renewable Diesel Handbook*, 2016.
183. Kumar, V., R.K. Sindhu, and S. Kumar, *Comparative analysis of green diesel versus petro-diesel in compression ignition engine.* Bioscience Biotechnology Research Communications, 2018. **11**(1): p. 128-135.
184. Pflaum, H., et al., *Potential of Hydrogenated Vegetable Oil (HVO) in a Modern Diesel Engine*, 2010, SAE International.
185. Hulkkonen, T., et al., *Emission performance of paraffinic HVO diesel fuel in heavy duty vehicles*, 2011, SAE International.
186. Hengst, K., et al., *Deoxygenation and cracking of free fatty acids over acidic catalysts by single step conversion for the production of diesel fuel and fuel blends.* Applied Catalysis B: Environmental, 2015. **174-175**: p. 383-394.
187. Bernas, H., et al., *Deoxygenation of dodecanoic acid under inert atmosphere.* Fuel, 2010. **89**(8): p. 2033-2039.
188. Berenblyum, A.S., et al., *On the mechanism of catalytic conversion of fatty acids into hydrocarbons in the presence of palladium catalysts on alumina.* Petroleum Chemistry, 2011. **51**(5): p. 336.

189. Lestari, S., et al., *Diesel-like Hydrocarbons from Catalytic Deoxygenation of Stearic Acid over Supported Pd Nanoparticles on SBA-15 Catalysts.* Catalysis Letters, 2010. **134**(3): p. 250-257.
190. Chen, J. and Q. Xu, *Hydrodeoxygenation of biodiesel-related fatty acid methyl esters to diesel-range alkanes over zeolite-supported ruthenium catalysts.* Catalysis Science & Technology, 2016. **6**(19): p. 7239-7251.
191. Lestari, S., et al., *Catalytic Deoxygenation of Stearic Acid and Palmitic Acid in Semibatch Mode.* Catalysis Letters, 2009. **130**(1): p. 48-51.
192. Murata, K., et al., *Production of Synthetic Diesel by Hydrotreatment of Jatropha Oils Using Pt−Re/H-ZSM-5 Catalyst.* Energy & Fuels, 2010. **24**(4): p. 2404-2409.
193. Kwon, K.C., et al., *Catalytic deoxygenation of liquid biomass for hydrocarbon fuels.* Renewable Energy, 2011. **36**(3): p. 907-915.
194. Zhang, H., et al., *Hydroprocessing of waste cooking oil over a dispersed nano catalyst: Kinetics study and temperature effect.* Applied Catalysis B: Environmental, 2014. **150-151**: p. 238-248.
195. Liu, Y., et al., *Hydrotreatment of Vegetable Oils to Produce Bio-Hydrogenated Diesel and Liquefied Petroleum Gas Fuel over Catalysts Containing Sulfided Ni–Mo and Solid Acids.* Energy & Fuels, 2011. **25**(10): p. 4675-4685.
196. Tiwari, R., et al., *Hydrotreating and hydrocracking catalysts for processing of waste soya-oil and refinery-oil mixtures.* Catalysis Communications, 2011. **12**(6): p. 559-562.
197. Mikulec, J., et al., *Second generation diesel fuel from renewable sources.* Journal of Cleaner Production, 2010. **18**(9): p. 917-926.
198. Ahmaruzzaman, M., *A review on the utilization of fly ash.* Progress in Energy and Combustion Science, 2010. **36**(3): p. 327-363.
199. Mostafa Hosseini Asl, S., et al., *Porous catalysts fabricated from coal fly ash as cost-effective alternatives for industrial applications: A review.* Fuel, 2018. **217**: p. 320-342.
200. Chakraborty, R., S. Bepari, and A. Banerjee, *Transesterification of soybean oil catalyzed by fly ash and egg shell derived solid catalysts.* Chemical Engineering Journal, 2010. **165**(3): p. 798-805.
201. Fomenko, E.V., et al. *Fly ash cenospheres: composition, morphology, structure, and helium permeability*. in *World of Coal Ash (WOCA) Conference*. 2011.
202. Jain, D., C. Khatri, and A. Rani, *Fly ash supported calcium oxide as recyclable solid base catalyst for Knoevenagel condensation reaction.* Fuel Processing Technology, 2010. **91**(9): p. 1015-1021.
203. Zhang, A., et al., *Heterogeneous Fenton-like catalytic removal of p-nitrophenol in water using acid-activated fly ash.* Journal of Hazardous Materials, 2012. **201-202**: p. 68-73.
204. Song, Y., et al., *Catalytic applications of layered double hydroxides in biomass valorisation.* Current Opinion in Green and Sustainable Chemistry, 2020. **22**: p. 29-38.
205. Thao, N.T., N.D. Trung, and D. Van Long, *Activity of Molybdate-Intercalated Layered Double Hydroxides in the Oxidation of Styrene with Air.* Catalysis Letters, 2016. **146**(5): p. 918-928.
206. Nejati, K., et al., *A highly active oxygen evolution electrocatalyst: Ni-Fe-layered double hydroxide intercalated with the Molybdate and Vanadate anions.* International Journal of Hydrogen Energy, 2019. **44**(29): p. 14842-14852.
207. Song, Y., et al., *Co-Fe-Mo mixed metal oxides derived from layered double hydroxides for deep aerobic oxidative desulfurization.* Fuel, 2021. **306**: p. 121751.

208. Liao, C., et al., *Catalytic deoxygenation of vanillin over layered double hydroxide supported Pd catalyst.* Journal of Industrial and Engineering Chemistry, 2018. **68**: p. 380-386.
209. Zhang, Z., et al., *LDH derived Co-Al nanosheet for lipid hydrotreatment to produce green diesel.* Fuel, 2023. **333**: p. 126341.
210. Arias, S., et al., *Hydrogen-free deoxygenation of industrial vegetable oil waste using Ce, Zr-NiAl catalysts for second-generation biofuels production.* Molecular Catalysis, 2022. **529**: p. 112554.
211. Zhu, H., et al., *Ni-Fe-Al LDH derived NiFe nanosheet for green diesel production from lipid hydrotreatment.* Fuel Processing Technology, 2023. **239**: p. 107537.
212. Oh, J.-M., T.T. Biswick, and J.-H. Choy, *Layered nanomaterials for green materials.* Journal of Materials Chemistry, 2009. **19**(17): p. 2553-2563.
213. Rives, V., M. del Arco, and C. Martín, *Layered double hydroxides as drug carriers and for controlled release of non-steroidal antiinflammatory drugs (NSAIDs): A review.* Journal of Controlled Release, 2013. **169**(1): p. 28-39.
214. Danish, A. and M.A. Mosaberpanah, *Formation mechanism and applications of cenospheres: a review.* Journal of Materials Science, 2020. **55**(11): p. 4539-4557.
215. Ranjbar, N. and C. Kuenzel, *Cenospheres: A review.* Fuel, 2017. **207**: p. 1-12.
216. Danish, A., et al., *Effect of cenospheres on the engineering properties of lightweight cementitious composites: A comprehensive review.* Journal of Building Engineering, 2022. **49**: p. 104016.
217. Bryers, R.W., *Fireside slagging, fouling, and high-temperature corrosion of heat-transfer surface due to impurities in steam-raising fuels.* Progress in Energy and Combustion Science, 1996. **22**(1): p. 29-120.
218. Vassilev, S.V. and C.G. Vassileva, *Methods for Characterization of Composition of Fly Ashes from Coal-Fired Power Stations: A Critical Overview.* Energy & Fuels, 2005. **19**(3): p. 1084-1098.
219. Ju, T., et al., *On the state of the art of crystalline structure reconstruction of coal fly ash: A focus on zeolites.* Chemosphere, 2021. **283**: p. 131010.
220. Vassilev, S.V., et al., *Phase-mineral and chemical composition of coal fly ashes as a basis for their multicomponent utilization. 2. Characterization of ceramic cenosphere and salt concentrates.* Fuel, 2004. **83**(4): p. 585-603.
221. M, K., S. Sindhu Nachiar, and A. S, *A review on fly ash cenosphere as a solid waste in concrete application.* Materials Today: Proceedings, 2022.
222. Lin, S., et al., *Zeolite greenly synthesized from fly ash and its resource utilization: A review.* Science of The Total Environment, 2022. **851**: p. 158182.
223. Visa, M., *Synthesis and characterization of new zeolite materials obtained from fly ash for heavy metals removal in advanced wastewater treatment.* Powder Technology, 2016. **294**: p. 338-347.
224. Sutarno, S. and Y. Arryanto, *Synthesis of faujasite from fly ash and its applications for hydrocracking of petroleum distillates.* Bulletin of Chemical Reaction Engineering & Catalysis, 2007. **2**(2-3): p. 45-51.
225. Sietsma, J.R.A., et al., *Application of ordered mesoporous materials as model supports to study catalyst preparation by impregnation and drying*, in *Studies in Surface Science and Catalysis*, E.M. Gaigneaux, et al., Editors. 2006, Elsevier. p. 95-102.
226. Haukka, S., E.-L. Lakomaa, and T. Suntola, *Adsorption controlled preparation of heterogeneous catalysts*, in *Studies in Surface Science and Catalysis*. 1999, Elsevier. p. 715-750.

227. Wachs, I.E. and C.J. Keturakis, *7.06 - Monolayer Systems*, in *Comprehensive Inorganic Chemistry II (Second Edition)*, J. Reedijk and K. Poeppelmeier, Editors. 2013, Elsevier: Amsterdam. p. 131-151.
228. Brockner, W., C. Ehrhardt, and M. Gjikaj, *Thermal decomposition of nickel nitrate hexahydrate, Ni(NO3)2·6H2O, in comparison to Co(NO3)2·6H2O and Ca(NO3)2·4H2O.* Thermochimica Acta, 2007. **456**(1): p. 64-68.
229. Kovács, T.N., et al., *Thermal decomposition of ammonium molybdates.* Journal of Thermal Analysis and Calorimetry, 2016. **124**(2): p. 1013-1021.
230. Gobichon, A.-E., J.-P. Auffrédic, and D. Louër, *Thermal decomposition of neutral and basic lanthanum nitrates studied with temperature-dependent powder diffraction and thermogravimetric analysis.* Solid State Ionics, 1996. **93**(1): p. 51-64.
231. Hunyadi, D., I. Sajó, and I.M. Szilágyi, *Structure and thermal decomposition of ammonium metatungstate.* Journal of Thermal Analysis and Calorimetry, 2014. **116**(1): p. 329-337.
232. Wendlandt, W.W., *The thermolysis of the rare earth and other metal nitrates.* Analytica Chimica Acta, 1956. **15**: p. 435-439.
233. Karim, A.V., et al., *Nanostructured modified layered double hydroxides (LDHs)-based catalysts: A review on synthesis, characterization, and applications in water remediation by advanced oxidation processes.* Current Opinion in Solid State and Materials Science, 2022. **26**(1): p. 100965.
234. Cavani, F., F. Trifirò, and A. Vaccari, *Hydrotalcite-type anionic clays: Preparation, properties and applications.* Catalysis Today, 1991. **11**(2): p. 173-301.
235. Shin, J., K. Kim, and J. Hong *Zn-Al Layered Double Hydroxide Thin Film Fabricated by the Sputtering Method and Aqueous Solution Treatment*. Coatings, 2020. **10**, DOI: 10.3390/coatings10070669.
236. Constantino, V.R. and T.J. Pinnavaia, *Basic properties of Mg2+ 1-xAl3+ x layered double hydroxides intercalated by carbonate, hydroxide, chloride, and sulfate anions.* Inorganic chemistry, 1995. **34**(4): p. 883-892.
237. P. Newman, S. and W. Jones, *Synthesis, characterization and applications of layered double hydroxides containing organic guests.* New Journal of Chemistry, 1998. **22**(2): p. 105-115.
238. Rives, V. and M.a. Angeles Ulibarri, *Layered double hydroxides (LDH) intercalated with metal coordination compounds and oxometalates.* Coordination Chemistry Reviews, 1999. **181**(1): p. 61-120.
239. Li, F. and X. Duan, *Applications of Layered Double Hydroxides*, in *Layered Double Hydroxides*, X. Duan and D.G. Evans, Editors. 2006, Springer Berlin Heidelberg: Berlin, Heidelberg. p. 193-223.
240. Xie, Z.-H., et al., *Synthesis, application and catalytic performance of layered double hydroxide based catalysts in advanced oxidation processes for wastewater decontamination: A review.* Chemical Engineering Journal, 2021. **414**: p. 128713.
241. Omwoma, S., et al., *Recent advances on polyoxometalates intercalated layered double hydroxides: From synthetic approaches to functional material applications.* Coordination Chemistry Reviews, 2014. **258-259**: p. 58-71.
242. Ng'etich, W.K. and B.S. Martincigh, *A critical review on layered double hydroxides: Their synthesis and application in sunscreen formulations.* Applied Clay Science, 2021. **208**: p. 106095.
243. Yang, L., et al., *Ni-based layered double hydroxide catalysts for oxygen evolution reaction.* Materials Today Physics, 2021. **16**: p. 100292.

244. He, J., et al., *Preparation of Layered Double Hydroxides*, in *Layered Double Hydroxides*, X. Duan and D.G. Evans, Editors. 2006, Springer Berlin Heidelberg: Berlin, Heidelberg. p. 89-119.
245. Arias, S., et al., *Synthesis and characterization of terephthalate-intercalated NiAl layered double hydroxides with high Al content.* Dalton Transactions, 2013. **42**(6): p. 2084-2093.
246. Drezdzon, M.A., *Synthesis of isopolymetalate-pillared hydrotalcite via organic-anion-pillared precursors.* Inorganic Chemistry, 1988. **27**(25): p. 4628-4632.
247. Arias, S., et al., *Unsupported NiMoAl hydrotreating catalysts prepared from NiAl-terephthalate hydrotalcites exchanged with heptamolybdate.* Catalysis Today, 2013. **213**: p. 198-205.
248. Coelho, T., et al., *Influence of the Mg2+ or Mn2+ contents on the structure of NiMnAl and CoMgAl hydrotalcite materials with high aluminum contents.* Catalysis Today, 2015. **250**: p. 87-94.
249. Pancrecious, J.K., et al., *Ni-Al polyvanadate layered double hydroxide with nanoceria decoration for enhanced corrosion protection of aluminium alloy.* Applied Clay Science, 2021. **211**: p. 106199.
250. Aceto, M., *8 - The Use of ICP-MS in Food Traceability*, in *Advances in Food Traceability Techniques and Technologies*, M. Espiñeira and F.J. Santaclara, Editors. 2016, Woodhead Publishing. p. 137-164.
251. Thommes, M., et al., *Physisorption of gases, with special reference to the evaluation of surface area and pore size distribution (IUPAC Technical Report).* Pure and applied chemistry, 2015. **87**(9-10): p. 1051-1069.
252. Bardestani, R., G.S. Patience, and S. Kaliaguine, *Experimental methods in chemical engineering: specific surface area and pore size distribution measurements—BET, BJH, and DFT.* The Canadian Journal of Chemical Engineering, 2019. **97**(11): p. 2781-2791.
253. Voigt, E.M. and R. Tomlinson, *The determination of pore size distribution and surface area from adsorption isotherms.* Canadian Journal of Chemistry, 1955. **33**(2): p. 215-231.
254. Epp, J., *4 - X-ray diffraction (XRD) techniques for materials characterization*, in *Materials Characterization Using Nondestructive Evaluation (NDE) Methods*, G. Hübschen, et al., Editors. 2016, Woodhead Publishing. p. 81-124.
255. Cullity, B. and S. Stock, *Elements of x-ray diffraction, Prentice Hall.* Upper Saddle River, NJ, 2001: p. 388.
256. Kafle, B.P., *Chapter 7 - Infrared (IR) spectroscopy*, in *Chemical Analysis and Material Characterization by Spectrophotometry*, B.P. Kafle, Editor. 2020, Elsevier. p. 199-243.
257. AOAC, A., *Official Method 969.33. Fatty acids in oils and fats.* Official Methods of Analysis of AOAC International, 1998: p. 17.
258. Smith, R., H. Inomata, and C. Peters, *Chapter 2 - Systems, Devices and Processes*, in *Supercritical Fluid Science and Technology*, R. Smith, H. Inomata, and C. Peters, Editors. 2013, Elsevier. p. 55-119.
259. Satyarthi, J.K. and D. Srinivas, *Fourier Transform Infrared Spectroscopic Method for Monitoring Hydroprocessing of Vegetable Oils To Produce Hydrocarbon-Based Biofuel.* Energy & Fuels, 2011. **25**(7): p. 3318-3322.
260. Maryutina, T.A., et al., *Terminology of separation methods (IUPAC Recommendations 2017).* Pure and Applied Chemistry, 2018. **90**(1): p. 181-231.

261. Mohammed, S.T., et al., *Enhancement of stability of Pd/AC deoxygenation catalyst for hydrothermal production of green diesel fuel from waste cooking oil.* Chemical Engineering Science, 2022. **251**: p. 117489.
262. Abdul Razak, N.A., et al., *Production of green diesel via hydrogen-free and solventless deoxygenation reaction of waste cooking oil.* Journal of Cleaner Production, 2022. **366**: p. 132971.
263. Cai, Z., et al., *Improving conversion of methyl palmitate to diesel-like fuel through catalytic deoxygenation with B2O3-modified ZrO2.* Fuel Processing Technology, 2022. **226**: p. 107091.
264. Yang, Y., A. Gilbert, and C. Xu, *Hydrodeoxygenation of bio-crude in supercritical hexane with sulfided CoMo and CoMoP catalysts supported on MgO: A model compound study using phenol.* Applied Catalysis A: General, 2009. **360**(2): p. 242-249.
265. Xu, C., et al., *Upgrading of Athabasca Vacuum Tower Bottoms (VTB) in Supercritical Hydrocarbon Solvents with Activated Carbon-Supported Metallic Catalysts.* Energy & Fuels, 2007. **21**(6): p. 3490-3498.
266. Madsen, A.T., et al., *Step Changes and Deactivation Behavior in the Continuous Decarboxylation of Stearic Acid.* Industrial & Engineering Chemistry Research, 2011. **50**(19): p. 11049-11058.
267. Vitolo, S., et al., *Catalytic upgrading of pyrolytic oils over HZSM-5 zeolite: behaviour of the catalyst when used in repeated upgrading–regenerating cycles.* Fuel, 2001. **80**(1): p. 17-26.
268. Wang, J., et al., *Highly stable Mo-based bimetallic catalysts for selective deoxygenation of oleic acid to fuel-like hydrocarbons.* Journal of Environmental Chemical Engineering, 2023. **11**(1): p. 109104.
269. Li, Y., et al., *Coke Deposition on Ni/HZSM-5 in Bio-oil Hydrodeoxygenation Processing*. Energy & Fuels, 2015. **29**(3): p. 1722-1728.
270. Li, Y., et al., *Coke formation on the surface of Ni/HZSM-5 and Ni-Cu/HZSM-5 catalysts during bio-oil hydrodeoxygenation.* Fuel, 2017. **189**: p. 23-31.
271. Jain, D., C. Khatri, and A. Rani, *Synthesis and characterization of novel solid base catalyst from fly ash.* Fuel, 2011. **90**(6): p. 2083-2088.
272. Chandane, V.S., et al., *Efficient cenosphere supported catalyst for the esterification of n-octanol with acetic acid.* Comptes Rendus Chimie, 2017. **20**(8): p. 818-826.
273. Li, C.J., et al., *Synthesis of fly ash cenospheres-based hollow ABW zeolite for dye removal via the coupling of adsorption and photocatalysis.* Advanced Powder Technology, 2021. **32**(10): p. 3436-3446.
274. Du, Y., et al., *Ionic liquid-based 3DOM meso/macroporous Mo/TiO2 materials with superior oxidation desulfurization performance at room temperature.* Materials Research Bulletin, 2020. **126**: p. 110849.
275. Anggono, J., *Mullite ceramics: its properties structure and synthesis.* Jurnal Teknik Mesin, 2005. **7**(1): p. 1-10.
276. Czuma, N., et al., *Modified fly ash, a waste material from the energy industry, as a catalyst for the CO2 reduction to methane.* Energy, 2022. **243**: p. 122718.
277. Scaccia, S., et al., *Preparation of CaO-based sorbent from coal fly ash cenospheres for calcium looping process.* Journal of Alloys and Compounds, 2019. **801**: p. 123-129.
278. Gao, K., O.A. Sahraei, and M.C. Iliuta, *Development of residue coal fly ash supported nickel catalyst for H2 production via glycerol steam reforming.* Applied Catalysis B: Environmental, 2021. **291**: p. 119958.

279. Kordouli, E., et al., *Probing the synergistic ratio of the NiMo/γ-Al2O3 reduced catalysts for the transformation of natural triglycerides into green diesel.* Applied Catalysis B: Environmental, 2017. **209**: p. 12-22.
280. Ding, S., et al., *Catalytic hydrogenation of stearic acid over reduced NiMo catalysts: Structure–activity relationship and effect of the hydrogen-donor.* Applied Catalysis A: General, 2018. **566**: p. 146-154.
281. Gao, Y., et al., *A novel nickel catalyst supported on activated coal fly ash for syngas production via biogas dry reforming.* Renewable Energy, 2020. **149**: p. 786-793.
282. Samojeden, B., et al. *Novel Nickel- and Magnesium-Modified Cenospheres as Catalysts for Dry Reforming of Methane at Moderate Temperatures*. Catalysts, 2019. **9**, DOI: 10.3390/catal9121066.
283. Deka, B. and K.G. Bhattacharyya, *Using coal fly ash as a support for Mn(II), Co(II) and Ni(II) and utilizing the materials as novel oxidation catalysts for 4-chlorophenol mineralization.* Journal of Environmental Management, 2015. **150**: p. 479-488.
284. Yusuff, A.S., et al., *Synthesis and characterization of coal fly ash supported zinc oxide catalyst for biodiesel production using used cooking oil as feed.* Renewable Energy, 2021. **170**: p. 302-314.
285. Gao, K., O.A. Sahraei, and M.C. Iliuta, *Ni-based catalysts supported on acid/alkali-activated coal fly ash residue for improved glycerol steam reforming.* Applied Catalysis B: Environmental, 2022. **301**: p. 120791.
286. Santillan-Jimenez, E., et al., *Continuous catalytic deoxygenation of model and algal lipids to fuel-like hydrocarbons over Ni–Al layered double hydroxide.* Catalysis Today, 2015. **258**: p. 284-293.
287. Kordulis, C., et al., *Development of nickel based catalysts for the transformation of natural triglycerides and related compounds into green diesel: a critical review.* Applied Catalysis B: Environmental, 2016. **181**: p. 156-196.
288. Monnier, J., et al., *Hydrodeoxygenation of oleic acid and canola oil over alumina-supported metal nitrides.* Applied Catalysis A: General, 2010. **382**(2): p. 176-180.
289. Jitianu, M., et al., *Nanosized Ni–Al layered double hydroxides—Structural characterization.* Materials Research Bulletin, 2013. **48**(5): p. 1864-1873.
290. Kooli, F., et al., *Synthesis and Properties of Terephthalate and Benzoate Intercalates of Mg−Al Layered Double Hydroxides Possessing Varying Layer Charge.* Chemistry of Materials, 1996. **8**(8): p. 1969-1977.
291. Vaysse, C., et al., *Thermal Behavior of Oxometalate (Mo, W)-Intercalated Layered Double Hydroxides: Study of the Grafting Phenomenon.* Journal of Solid State Chemistry, 2002. **167**(1): p. 59-72.
292. Carriazo, D., et al., *Structural and Texture Evolution with Temperature of Layered Double Hydroxides Intercalated with Paramolybdate Anions.* Inorganic Chemistry, 2006. **45**(3): p. 1243-1251.
293. Arias, S., et al., *Mixed NiMo, NiW and NiMoW sulfides obtained from layered double hydroxides as catalysts in simultaneous HDA and HDS reactions.* Catalysis Today, 2017. **296**: p. 187-196.